Composite hollow fiber membranes for ion separation and removal

Composite hollow fiber membranes for ion separation and removal

PROEFSCHRIFT

ter verkrijging van
de graad van doctor aan de Universiteit Twente,
op gezag van de rector magnificus,
Prof. dr. F. A. van Vught,
volgens besluit van het College voor Promoties
in het openbaar te verdedigen
op vrijdag 14 september 2001 te 15.00 uur

Door

Tao He

Geboren op 20 October 1971
te Meishan, P.R. China

Dit proefschrift is goedgekeurd door :

Promotor	Prof. dr. ing. M. Wessling
	Prof. dr. ing. H. Strathmann
Assistant promotor	Prof. dr. ing. M.H.V. Mulder

To Xuemei
and Danny

Acknowledgement

This work described in this thesis was financially supported by EET program (Economy, Ecology and Technology) from the Dutch government.

CIP-GEGEVENS KONINKLIJKE BIBLIOTHEEK, DEN HAAG

He, Tao

Composite hollow fiber membranes for ion separation and removal
Tao He
Thesis Enschede
ISBN 90-365-1624-2
Key words: membranes; supported liquid membranes; co-extrusion; hollow fiber; nanofiltration

Front cover: Cross-section view of a composite hollow fiber membrane with two hydrophilic coating layers and a hydrophobic support.
Back cover: Molecular dynamics simulation of lipid bilayers, similar to the bilayer composite membrane, by Scott Feller at Wabash College.

Preface

In my early twenties, I believed that membranes could be an omnipotent technique to take the place of all the classical separation sections in the production of ammonia and acid/base. At present, in my late twenties, I realize that it is hardly possible for me to be seeing this in my limited lifespan. Membrane is not everything but strong interconnected links giving me precious chance to contact people, to enjoy the life. I would take this opportunity to express my sincere acknowledgments.

My special thanks to Heiner Strathmann for having offered me a Ph.D. position at Membrane Technology Group. It is my honor to discuss my project with you and to have you as my promotor. Marcel Mulder, without your great patience my thesis would never have been finished on time. I enjoyed the freedom in research you gave to me. I value this experience to be of crucial importance for my future. Matthias Wessling, thank you for guiding me into the fantastic world of nanofiltration membranes and for correcting this booklet. I can hardly imagine how my thesis would look like without you. It is my great pleasure to learn from you how to KISS.

Thanks to the people who ever contributed tremendously to the thesis: Claudia's three month work in characterization of ion exchange materials outlined Thoshi's project which is one important part of chapter 4. Meifang's cooperation on solving the dip-coating puzzle initiated my further research on the composite membranes, which finally leaded to the goal of the project. Lydia's excellent technical assistant in the late stage rescued me from laborious experimental work and I had time to write down the main part of the thesis. I owe a debt of gratitude to Maria, whose interesting work is unfortunately not included in my thesis.

I feel grateful to Jianfei, Yutie and Meifang for your scientific support during the stay at Twente. I would like to express my deepest gratitude to my Chinese friends for the wonderful time we had together, especially Zhiyuan, Fenghua, Fahong, Yinjie and Zhiyang.

It is still a fresh memory that Erik Naafs picked me up at Schiphol the first night entering The Netherlands. Thanks Erik. My thanks go to peter, Antoine, Alby, Bernd, Harmen, Herman, Geert-Henk, John and Erik Roevink for your several year earnest help in my life and work. Leo was always punctual at creating my spinnerets. Annemarie spent so much time and effort in my AAS measurement. Clemens helped me a lot with the polymer characterization. Greet has been actively in providing me support both in administration work and many ideas to live with Dutch. Peter, Antoine, Xuemei and Zhiyuan meticulously proof-read this thesis. Fahong and Nico's constructive comments accelerated my speed in finishing the last chapter. Kitty translated the summary into het samenvatting. Many Thanks to the people who took part in my noodle puzzle.

It is impossible to list the other people of the group that I regard as dear colleagues and friends, who have shared with me for four years. Many of you

have left during the times and many have arrived. I treasure the memories of the nice time in conferences, parties, excursions and ping-pong tournaments. Thanks to all of you. Peter and Sybrand, I feel great to have your super heavyweight support at my defense ceremony.

Xuemei and our lovely son Danny are everything that matters to me on earth. Four years ups and downs in research and life, you are the only person who really understands. My parents' continuous encouragement and support contribute immensely to my past and my today.

Tao He

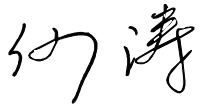

Contents

Chapter 1 Introduction

1.1 Background

Environmentally benign operation of chemical processes have attracted significant attention over the past decades. In removal of heavy metal ions from waste effluents, membrane technology has become increasingly attractive as a low-cost generic separation technique for environmental problems. Membrane processes compete with a variety of processes, such as chemical precipitation, metallic replacement, ion exchange, electrolysis, adsorption, flotation and biological approaches [1]. Among membrane separation techniques such as reverse osmosis, nanofiltration, ultrafiltration, electrodialysis and Donnan dialysis, as well as membrane bioreactor technology and liquid membranes, liquid membranes is extremely versatile, especially for the removal of heavy metals from wastewater down to a very low concentration level. Basically, two different types may be distinguished, supported liquid membranes (SLMs) and emulsion liquid membranes (ELMs) as schematically illustrated in Figure 1.1.

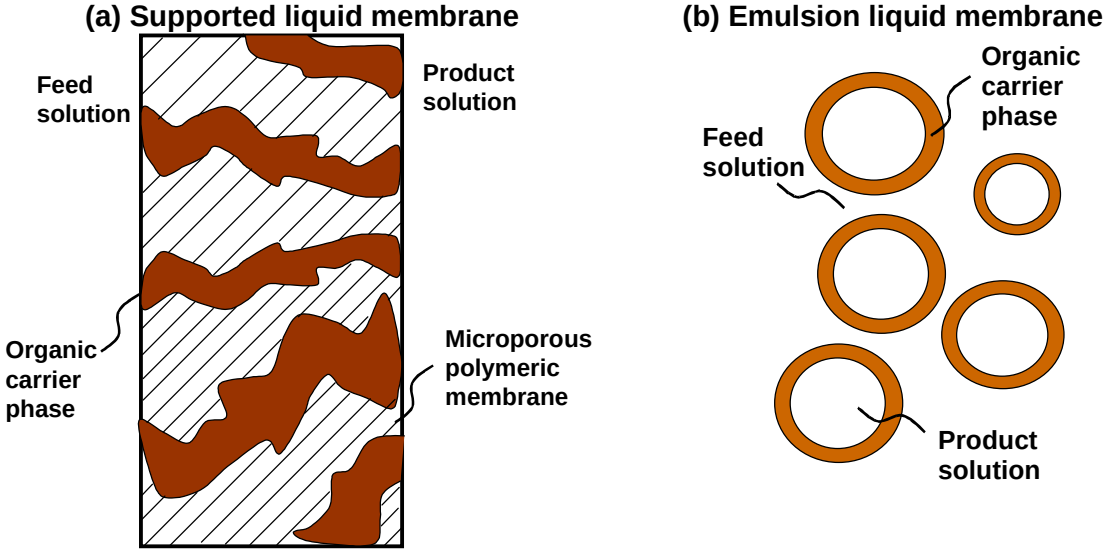

Figure 1.1 *Dfferent types of liquid membranes* [2].

Supported liquid membranes are of particular interest owing to the combination of extraction and stripping into a single step, the reduction of solvent usage and the achievement of very high enrichment factors [3]. However, the industrial application of SLMs is still in the embryonic state due to the short life-time. The long-term performance of SLMs strongly depends on the composition of the organic and the aqueous phases, the type of support membrane, and the operational parameters [3-9]. Although it is complicated, instability is commonly understood as the loss of carrier and/or organic solvent from the liquid membrane phase into the adjacent aqueous phases for either solubility or hydrodynamic reasons [3-16]. The major phenomenon is generally

observed as a decrease in flux, and a subsequent leakage of the stripping liquid [17].

1.2 Stabilization techniques

A time line chart showing the historical development of the stabilization techniques for SLM is given in Figure 1.2. An increase in the viscosity of the organic phase stiffens the aqueous-organic interface and prevents gradual losses [18-21]. This was initially developed by Bloch et al [22-25] and applied in SLMs by Neplenbroek [22-25]. However, this method resulted in a significant decrease in the initial flux. Another method was to apply a thin dense coating layer of polyvinyl chloride (PVC) [22-25]. The hydrophobic polymer PVC can not prevent the direct contact between the organic phase and the aqueous phase, leading to a continuous loss of organic phase because of its solubility in aqueous phase.

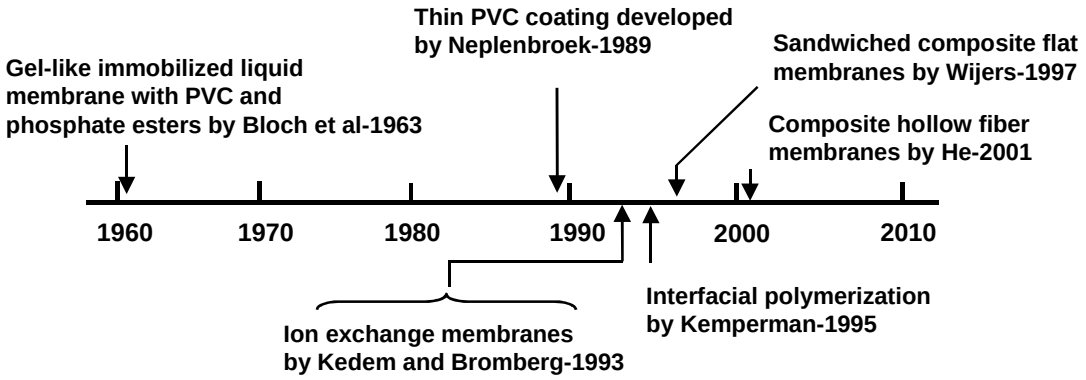

Figure 1.2 *Time line chart representing the development of stabilization of supported liquid membranes.*

Interfacial polymerization (IP) was firstly applied in SLM stabilization by Kemperman [26]. Frequently, a hydrophilic polyamide layer is formed using an amine and acid chloride as monomers [25-28]. An IP layer can only be used for the transport of mono-valent ions but not multi-valent ones [27]. Apart from interfacial polymerization, recently, plasma polymerization [29] was reported to form an ultra-thin skin layer for stabilization of the SLM. Lack of long-term stability showed disadvantage of this technique.

Ion exchange materials were intensively investigated in terms of transport [30-33] in a configuration consisting of two ion exchange membranes and an organic phase in between. In terms of stability, a composite membrane made by lamination of a sulfonated poly (ether ether ketone) (SPEEK) onto a flat polypropylene (PP, Accurel) membrane was investigated [34]. A composite membrane with a “Sandwiched structure" showed improved stability and

moderate fluxes. For the separation of heavy metal ions, ion exchange materials were proven to be a realistic alternative to stabilize SLMs. However, the thickness of a commercial ion exchange membrane as well as the flat-sheet configuration is the disadvantage. A technically viable approach could be a composite hollow fiber membrane with a thin ion exchange layer. This thesis explores the preparation of composite membranes and the application in liquid membranes.

1.3 Structure of the thesis

The objective of this thesis is to develop new membranes with an extended life-time in the application of selective liquid-liquid extraction. The concept is to prepare a composite hollow fiber membrane with an ion exchange coating on a hydrophobic support. Two routes can be distinguished:

(1) A one step process of co-extruding a hydrophilic layer onto a hydrophobic support;
(2) Dip-coating of an ion exchange material onto a tailor-made hydrophobic support.

The thesis describes the application of the new membranes in liquid–liquid extraction and in pressure-driven processes. Schematically, the structure of the thesis is shown in Figure 1.3.

Chapter 2 describes the preparation of a hydrophobic porous support for the supported liquid membrane. An open porous surface is necessary to decrease the transport resistance as much as possible. This chapter reports a new approach to improve the porosity of the outer surface layer of a hollow fiber membrane using a triple-orifice spinneret. With the solvent, N-methylpyrrolidone, as the external fluid, the outer layer of the polysulfone (PSf) solution can be diluted to a polymer concentration close to the critical point. Consequently, a high surface porosity is obtained after immersion precipitation.

Chapter 3 describes a systematic optimization of hollow fiber morphology in terms of maximizing the copper transport in SLMs. A tailor-made porous PSf support membrane is prepared by changing the polymer concentration, the additive concentration and the bore liquid composition. The PSf support shows a similar copper flux as a commercial Accurel polypropylene (PP) membrane Q3/2. The latter is frequently used as a support in SLMs and it has the disadvantage of large surface pores, which thus are difficult to coat. The new PSf support shows a life-time comparable to Accurel and can be coated much easier.

In Chapter 4, the first stabilization technique, co-extrusion of a sulfonated polyether sulfone (SPES) on a polysulfone support is investigated. The mechanical stability of SPES films and the adhesion of SPES to PSf prepared by immersion phase inversion are improved by increasing the SPES concentration in the coating solution. Co-extruded composite membranes show

a rather low permeability towards copper in SLM applications. In the dry state, the coating layer appears to be porous as indicated by no selectivity to gas pairs. However, the co-extruded composite fibers have nanofiltration properties: a low rejection to salts but a high rejection to dyes. The reason for the high resistance to the copper transport in SLMs is the low ion exchange capacity (IEC) of the coating layer. The concept of applying ion exchange materials in co-extrusion seems to be limited to low IEC materials. Another type of ion exchange polymers with high IEC, however, could not be co-extruded owing to their high solubility in a coagulation bath, i.e. water.

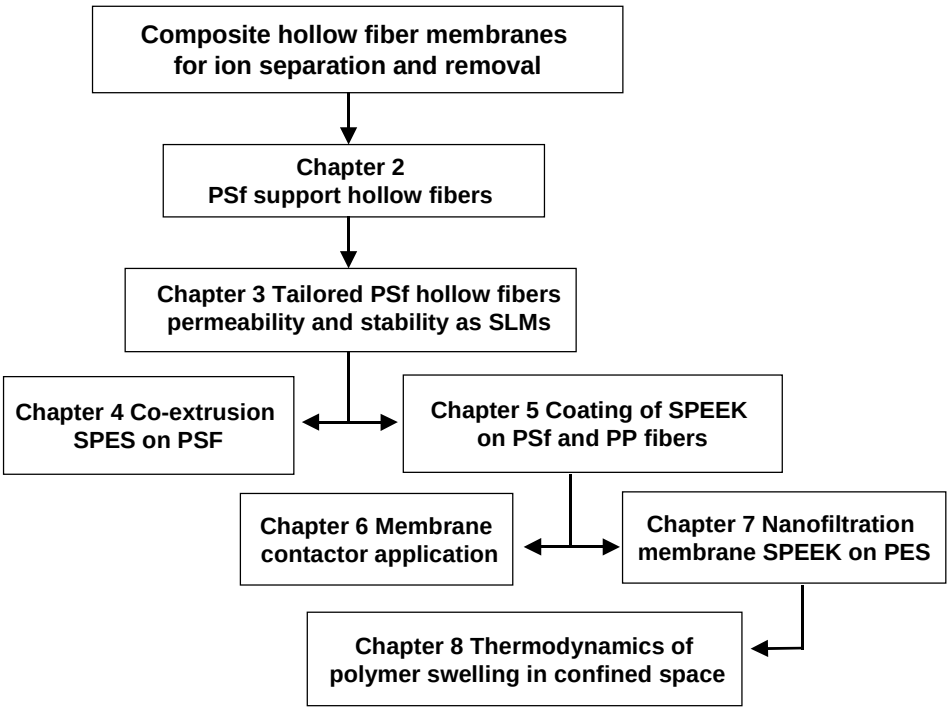

Figure 1.3 *Scheme of the thesis.*

Chapter 5 describes an approach to coat sulfonated poly (ether ether ketone) (SPEEK) layers at the outside of PSf and Accurel PP support hollow fibers. Based on three criteria, volatility, compatibility and spreading, a series of solvents for SPEEK are selected and integral composite membranes have been prepared. In the SLM application, the composite membranes show an improved stability, but still being instable due to the un-coated inner surface of the fiber.

To obtain a SLM with even longer life-time, the best method in theory is to use a double coated composite membrane, or an encapsulated membrane. Technically, this is very difficult to realize on a hollow fiber membrane. An alternative is to operate modules with the composite membrane in a membrane contactor system. The organic phase circulates through the bore side of the composite hollow fibers and the aqueous phases through the shell side (Chapter 6). In this configuration, the organic phase is essentially confined in a double coating layer system. Long term experiments up to two and half months for both polysulfone and Accurel Q3/2 composite membranes show no flux

decline. A film resistance model predicts the flux of the membrane contactor based on mass transfer coefficients obtained from support liquid membrane experiments.

Since SPEEK is a hydrophilic material which swells extensively in aqueous solutions, it may possess nanofiltration properties according to the Donnan exclusion mechanism. The swelling of the material can be controlled by changing the ion exchange capacity and therefore changing the separation properties. In Chapter 7, a new type of nanofiltration membrane has been developed with a SPEEK coating at the inner surface of a polyethersulfone (PES) support membrane. The membrane shows a low rejection to ions and a high rejection to negatively charged dyes. The high molecular weight cutoff indicates the presence of large water clusters acting as pores to transport large uncharged macromolecules. A support membrane made of PSf with a larger pore size than a support membrane made of PES shows penetration of the coating solution into the support. This penetration results in thinner coating layer with a lower flux. We consider that coating polymer is confined and restricted in swelling, leading to an increase in the fixed charge density which increases rejection values.

Chapter 8 describes a thermodynamic model describing the swelling restraint of pore-penetrated polymers. Based on the equilibrium swelling theory of Flory and Rehner [35] the model describes the swelling behavior of a polymer network in a confined space with a certain elastic strength. The polymeric network is assumed to have a shape of a cylinder characterized by the diameter, the length and the volume. The isotropic and anisotropic swelling (the change in radial direction is different from the longitudinal direction) has been investigated by adding an external energy term to the Flory-Rehner equations. The theory is general and can be used to estimate the reduction in swelling of a confined material. This is important for a membrane morphology where the transporting polymer phase is confined inside a non-transporting support structure.

1.4 References

[1] M. Tels, Advances in treating heavy metals containing wastes, Resources and Conservation, 14 (1987) 71-92.

[2] R. W. Baker, Membrane Technology and Applications, McGraw-Hill, New York, 2000.

[3] P. R. Danesi, Separation of metal species by supported liquid membranes, Sep. Sci. Technol., 19 (1984-1985) 857-894.

[4] F. F. Zha, A. G. Fane, C. J. D. Fell, and R. W. Schofield, Critical displacement pressure of a supported liquid membrane, J. Membrane Sci., 75 (1992) 69-80.

[5] P. R. Danesi, L. Reichley-Yinger, and P. G. Rickert, Life time of supported liquid membrane: the influence of interfacial properties, chemical composition, water transport on the long term stability of the membrane, J. Membrane Sci., 31 (1987) 117-145.

[6] T. Shinbo, T. Yamaguchi, H. Yanagishita, K. Sakaki, D. Kitamoto, and M. Sugiura, Supported liquid membranes for enantioselective transport of amino acid mediated by chiral crown ether- effect of membrane solvent on transport rate and membrane stability, J. Membrane Sci., 84 (1993) 241-248.
[7] A. M. Neplenbroek, D. Bargeman, and C. A. Smolders, Supported liquid membranes: instability effects, J. Membrane Sci., 67 (1992) 121-132.
[8] H. Takeuchi, K. Takahashi, and W. Goto, Some observations on the stablility of supported liquid membranes, J. Membrane Sci., 34 (1987) 19-31.
[9] R. Molinari, E. Drioli, and G. Pantano, Stability and effect of diluents in supported liquid membranes for Cr(III), Cr(VI) and Cd(II) recovery, Sep. Sci. Technol., 24 (1989) 1015-1032.
[10] J. F. Dozol, J. Casas, and A. Sastre, Stability of flat sheet supported liquid membranes in the transport of radionuclides from reprocessing concentrate solutions, J. Membrane Sci., 82 (1993) 237-246.
[11] F. F. Zha, A. G. Fane, and C. J. D. Fell, Instability mechanisms of supported liquid membranes in phenol transport process, J. Membrane Sci., 107 (1995) 59-74.
[12] H. Takeuchi and M. Nakano, Progressive wetting of supported liquid membranes by aqueous solutions, J. Membrane Sci., 42 (1989) 183-188.
[13] A. M. Neplenbroek, D. Bargeman, and C. A. Smolders, Mechanism of supported liquid membrane degradation: emulsion formation, J. Membrane Sci., 67 (1992) 133-148.
[14] F. F. Zha, A. G. Fane, and C. J. D. Fell, Effect of surface tension gradients on stability of supported liquid membranes, J. Membrane Sci., 107 (1995) 75-86.
[15] F. F. Zha, Stability and application of supported liquid membranes, Ph.D Thesis, The University of New South Wales, , 1993.
[16] R. W. Baker and I. Blume, Coupled transport membranes, in M. C. Porter, ed., Handbook of industrial membrane technology, Noyes Publication, New Jersey, 1990.
[17] A. J. B. Kemperman, D. Bargeman, T. van den Boomgaard, and H. Strathmann, Stability of supported liquid membranes: state of the art, Sep. Sci. Technol., 31 (1996) 2733-2762.
[18] R. Bloch, O. Kedem, and D. Vofsi, Ion specific polymer membrane, Nature, 199 (1963) 802-803.
[19] A. M. Neplenbroek, D. Bargeman, and C. A. Smolders, Supported liquid membranes: stabilization by gelation, J. Membrane Sci., 67 (1992) 149-165.
[20] L. Bromberg, G. Levin, and O. Kedem, Transport of metals through gelled supported liquid membranes containing carrier, J. Membrane Sci., 71 (1992) 41-50.
[21] G. Levin and L. Bromberg, Gelled membrane composed of dioctyldithiocarbamate substituted on poly(vinylchloride) and di(2-

ethylhexyl) dithiophosphoric acid, J. Appl. Polym. Sci., 48 (1993) 335-341.
[22] A. M. Neplenbroek, Stability of supported liquid membranes, Ph.D Thesis, University of Twente, Enschede, 1989.
[23] A. J. B. Kemperman, B. Damink, T. van den Boomgaard, and H. Strathmann, Stablization of supported liquid membranes by gelation with PVC, J. Appl. Polym. Sci., (1997) 1205-1215.
[24] C. Wijers, Supported liquid membranes for removal of heavy metals: permeability, selectivity and stability, Ph.D Thesis, University of Twente, Enschede, 1996.
[25] C. Clement and M. M. Hossain, Stability of a supported liquid membrane for removing hydrophobic solutes from casein hydrolysate solution, Sep. Sci. Technol., 32 (1997) 2685-2703.
[26] A. J. B. Kemperman, H. H. M. Rolevink, T. van den Boomgaard, and H. Strathmann, Stabilization of supported liquid membranes by interfacial polymerization top layers, J. Membrane Sci., 138 (1998) 43-55.
[27] M. C. Wijers, M. Wessling, and H. Strathmann, Limitation of the lifetime stabilization of supported liquid membrane by polyamides layers, Sep. Purif. Technol., 17 (1999) 147-157.
[28] Y. Wang, Y. S. Thio, and F. M. Doyle, Formation of semi-permeable polyamide skin layers on the surface of supported liquid membranes, J. Membrane Sci., 147 (1998) 109-116.
[29] X. J. Yang, A. G. Fane, J. Bi, and H. J. Griesser, Stabilization of supported liquid membranes by plasma polymerization surface coating, J. Membrane Sci., 168 (2000) 29-37.
[30] O. Kedem and L. Bromberg, Ion-exchange membranes in extraction processes, J. Membrane Sci., 78 (1993) 255-264.
[31] V. S. Kislik and A. M. Eyal, Hybrid liquid membrane (HLM) and supported liquid membrane (SLM) based transport of titanium, J. Membrane Sci., 111 (1996) 271-281.
[32] V. S. Kislik and A. M. Eyal, Hybrid liquid membrane (HLM) system in separation technologies, J. Membrane Sci., 111 (1996) 259-272.
[33] R. Wodzki and G. Sionkowski, Recovery and concentration of metal ions. II multimembrane hybrid system, Sep. Sci. Technol., 30 (1995) 2763-2778.
[34] M. C. Wijers, M. Jin, M. Wessling, and H. Strathmann, Supported liquid membranes modification with sulphonated poly(ether ether ketone): permeability, selectivity and stability, J. Membrane Sci., 147 (1998) 117-130.
[35] P. J. Flory, Principles of Polymer Chemistry, Cornell University Press, New York, 1953.

In the history of scientific and technological endeavor, there are few if any cases in which the end was exactly what was intended at the first beginning. (Chapter 4 of this thesis and discovery of Ultrafiltration membrane), Times, December 4, 2001, p 57.

An entity with certain constraint is stable.

Chapter 2 Preparation of porous hollow fiber membranes with a triple-orifice spinneret

Abstract

A triple-orifice spinneret has been applied for the preparation of hollow fiber microfiltration membranes with a high surface porosity. Considering the general rules of diffusion induced phase separation, a low polymer concentration is required at the outer layer to obtain a highly interconnected open-porous structure. By using N-methylpyrrolidone (NMP) as the external liquid at the outside orifice of the spinneret, a highly porous surface is obtained. For a polymer solution containing a low molecular weight additive and with an initial concentration close to the cloud point, this technique slightly improves the pure water and gas fluxes since the major resistance of the membrane is located at the substructure and the inner skin. However, for a solution containing a high molecular weight additive and with an initial concentration far from the cloud point, a porous shell surface is obtained resulting in a significant improvement in water flux. The effect of various external liquids on the morphology has been investigated as well.

2.1 Introduction

In a dry-wet spinning process, a polymer solution is extruded through a spinneret together with either a bore liquid or gas, followed by an air gap and immersed into a nonsolvent bath which most of the time is water. During the fabrication process, three parameters control the morphology of the hollow fibers to a great extent: composition of the polymer solution, bore liquid composition and air gap conditions. Other parameters, such as composition and temperature of the coagulation bath, spinning speed and post-treatment are important as well.

Frequently, additives are added to the polymer solutions to control the membrane morphology. Two types of additives can be used: a compatible high molecular weight additive, e.g. polyvinylpyrrolidone, PVP [1-4]; or a small molecular weight nonsolvent additive, e.g. water, ethylene glycol or diethylene glycol [5-9]. The inner surface morphology is mostly determined by the composition of the bore liquid. The shell surface morphology can be adjusted by various approaches such as a high temperature bath [4] or a coagulation bath consisting of a mixture of solvent and nonsolvent (e.g. water) [10]. These approaches have several drawbacks: a large amount of solvent is needed which is environmentally unfavorable and capital intensive; raising the bath temperature requires precise control of the manufacturing section to guarantee high reproducibility.

In recent years, a triple-orifice spinneret has been developed, in which a polymer solution, a bore liquid, and an external liquid are simultaneously extruded. By variation of this external liquid, different types of morphologies were prepared such as dense membranes for gas separation [11], pervaporation [12] and porous membranes for ultrafiltration [13]. This chapter describes the use of this spinneret with a solvent as the external liquid to prepare hollow fiber membranes with an open outer skin layer with pore sizes in the micrometer range.

2.2 Concept to prepare porous membranes

During an immersion phase separation, the composition path at the top of the polymer solution may follow three different routes as shown schematically in a phase diagram for a ternary system of polymer/NMP/non-solvent (Figure 2.1). For a solution with a high enough polymer concentration and a high ratio of the outflow of the solvent to the inflow of the nonsolvent, the composition of the top part of the solution follows the first route up to the vitrification region. Consequently, the solution vitrifies and forms an asymmetric membrane with a dense toplayer. In a case where the ratio of the outflow of the solvent to the inflow of the nonsolvent is relatively low, the composition of the solution at the top layer could follow the second path towards the binodal region. Immediately, the top layer solution demixes,

resulting in a porous membrane with ultrafiltration properties. The third composition path follows a direction where the polymer concentration decreases, which could be achieved by applying a coagulation bath composing of solvent and nonsolvent. Consequently, the phase separation occurs at a region close to the critical point, resulting in an open porous membrane [14].

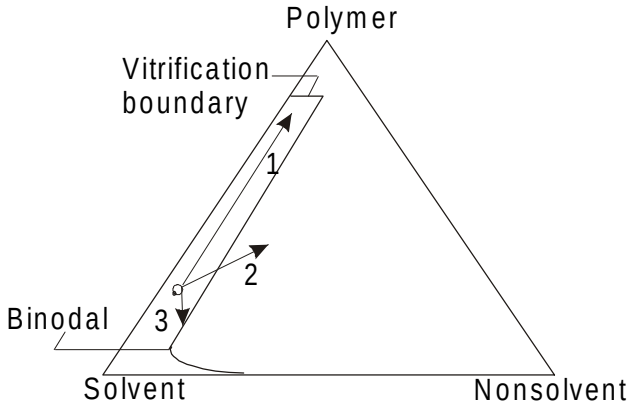

Figure 2.1 *Phase diagram for a ternary system: polymer/solvent/nonsolvent, showing schematically three different composition paths.*

Following the arguments given above, the polymer concentration at the top layer just before demixing needs to be low enough to obtain an open porous toplayer. One may start with a very low polymer concentration [15, 16], but it is hardly possible to spin fibers at such a low viscosity. However, if we increase the polymer concentration to improve the spinning conditions and use water as a coagulant, the polymer content at the top layer of the polymer solution increases as a result of a relatively large outflow of the solvent with respect to the inflow of water [17, 18]. Thus, a membrane with low porosity and small pores is obtained. In order to obtain a highly porous toplayer, the polymer concentration should be low before the occurrence of precipitation. Figure 2.2 shows a two-step process to solve this problem. To spin hollow fibers according to this process, one needs to employ a triple-orifice spinneret where the outer layer contains the solvent. During the contact of the solvent with the polymer solution, solvent diffuses into the polymer solution decreasing the outer layer polymer concentration (representing route A to B in Figure 2.2). The bulk polymer solution however remains the initial high polymer concentration. The fiber is then immersed into a water bath at room temperature in which a precipitation occurs, as indicated by route B to C (Figure 2.2).

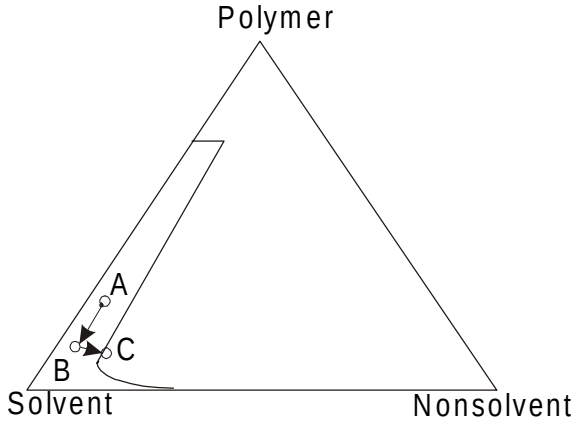

Figure 2.2 *Schematic of the composition change at the top layer of the polymer solution during a two step immersion precipitation process. A-B: contact with solvent; B-C: immersion in water.*

This concept mainly aims to influence the morphology of the skin layer, not the fiber matrix morphology. The fiber matrix morphology needs to be open enough to minimize the transport resistance as well. Two kinds of additive can realize this: diethylene glycol [5] and polyvinyl pyrrolidone [4]. Once the matrix has a minimized resistance, the resistance of the skin layer can be clearly identified and decreased as indicated above.

2.3 Experimental

2.3.1 Materials

Polysulfone (PSf, Udel P3500) was purchased from Amoco. Polyvinyl pyrrolidone (PVP, K90, Mw 360,000 $g.mol^{-1}$) was from Janssen Chimica. N-methylpyrrolidone (NMP), diethylene glycol (DegOH) and acetone were purchased from Merck. The solvents are of analytical grade and used without further purification. Tap water was used as a coagulation bath.

2.3.2 Solution preparation

Pre-dried polysulfone (one week in an oven at 120^{o}C) was dissolved in NMP with a third component: diethylene glycol or PVP K90. The exact compositions are listed in Table 2.1. Polymer solutions were filtered with a metal filter of 15 μm and degassed before use. The viscosity of the polymer solutions at 25^{o}C were measured with a rotation viscometer (Brabender® viscotron, system E17 with spring constant 1699.9). The viscosity was recorded at different rotation speeds or shear rates and extrapolated to zero shear rate.

Table 2.1 *Specifications of spinning solutions.*

Terms	Solution 1 [a]	Solution 2 [b]
w_{PSf} (wt%)	17.0	15
w_{NMP} (wt%)	52.4	70
$w_{additive}$ (wt%)	30.6	15
Viscosity (poise)	53	1100
Cloud Point (^oC)	47±1, LCST [c]	-

[a] PSf/NMP/diethylene glycol; [b] PSf/NMP/PVPK90, no cloud point in the range between 0 to 80 ^oC; [c] LCST: lower critical solution temperature.

2.3.3 Cloud point determination

The cloud point of a polymer solution was measured by a device developed at the Membrane Technology Group, University of Twente. A polymer solution at certain composition was stored in a standard NMR tube and the light transmission was measured as a function of the temperature. When phase separation occurs, a steep light transmission change can be observed. The transition temperature is defined as the cloud point of the polymer solution.

2.3.4 Light transmission

The delay time of the spinning solutions before the phase separation occurs was determined by preparing of a flat membrane and monitoring the light transmission [18]. The delay time is defined as the time between the immersion of the polymer film and the start of turbidity. The turbidity indicates the onset of phase separation and is detected by a decrease in light transmittance through a polymer solution. The light source was located above the coagulation bath and a light detector below. The signal from the light detector was transferred and recorded by a computer. Delayed demixing is a process taking place during an extended period of time after the moment of immersion of the polymer solution in the nonsolvent bath. Instantaneous demixing is a process in which liquid-liquid demixing immediately occurs upon immersion of the polymer solution in the nonsolvent bath. With this measurement, the kinetics of the immersion phase separation process can be quantified.

2.3.5 Spinning process

A triple-orifice spinneret was used for spinning hollow fibers. As shown in Figure 2.3, a polymer solution, an external liquid and a bore liquid simultaneously flow out of the spinneret, passing through an air gap of 50 mm and then immerse into a water bath at room temperature. The spinning speed was set at 6.0 $m.min^{-1}$. The contact time of the first coagulant and the polymer solution in the air gap was 0.5 second. Water forms the coagulation bath, but can not immediately replace the solvent layer ending therefore in much longer

actual contact time [11]. The flow rate of the first coagulant was controlled at 0.43 $cm^3.min^{-1}$. The bore liquid was a mixture of NMP and water with a weight ratio of 3:1 for polymer solution 1 and 4:1 for solution 2. The fibers were cut into pieces of 60 cm and rinsed with tap water for 48 hours. Then the fibers were immersed in a 20 wt% glycerol/water solution for another 24 hour and allowed to dry in ambient environment. Membranes from polymer solution 2 were treated with the standard procedure according to literature [4, 19] using a solution of sodium hypochloride solution of 4000 ppm for 48 hours to wash out the PVP residue and increase the membrane flux.

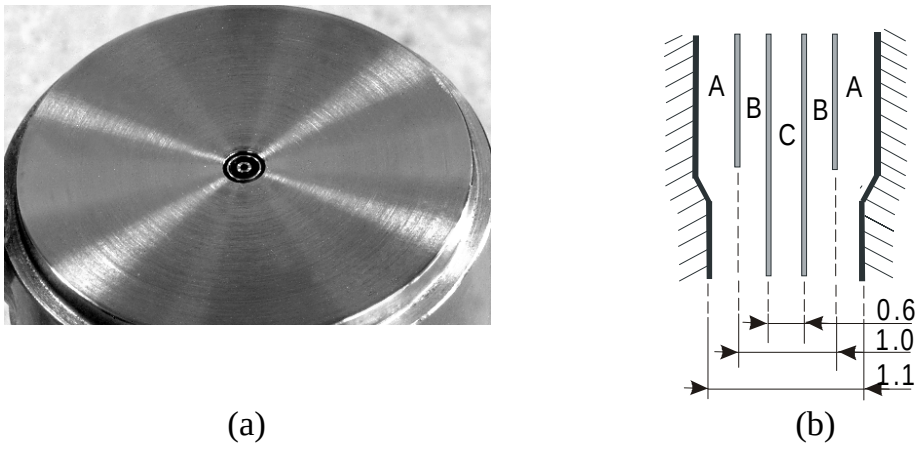

Figure 2.3 *Photograph and schematic of a triple orifice spinneret. Dimension values are in millimeter. (a) Bottom view of a spinneret; (b) Cross-section view. A, external fluid; B, polymer solution; C, bore liquid.*

2.3.6 Characterization of hollow fiber membranes

Four wet hollow fibers were cut into pieces of 20 cm and potted at the both ends with a Nylon tube of 6 mm. The pure water permeability was measured at a pressure of 2.0 bar absolute. The permeation was recorded after one hour pre-pressurizing. The membrane pore size was measured with Coulter Porometer II for pores larger than 0.05 μm. Pores less than 0.05 μm were characterized by permporometry [20].

2.3.7 Scanning electron microscopy

Samples for scanning electron microscopy (SEM, JEOL JSM-T220S) were made by cryogenic breaking of the freshly prepared wet fibers. The samples were allowed to dry under vacuum at 30^oC overnight and coated with a thin gold layer.

2.4 Results and discussion

2.4.1 Characterization of spinning solutions

The solution properties are listed in Table 2.1. The two solutions clearly show different phase separation behaviors. Solution 1 contains 30.6% DegOH and is located close to the cloud point, which is 47±1 ^{o}C. This means that by increasing the solution temperature above 47 ^{o}C, the solution phase separates, as can be seen in Figure 2.4. It also indicates that diethylene glycol attributes PSf/NMP solution a lower critical solution temperature (LCST). Solution 2 contains PVP K90 which is miscible with polysulfone in NMP, and shows no phase separation behavior in the range of 0 to 80 ^{o}C. PVP as an additive increases the solution viscosity, which is 1100 poise at 25 ^{o}C, 20 times higher than that of solution 1 as can be seen in Table 2.1, even though the polysulfone concentration is much higher in solution 1.

A solution close to the cloud point (solution 1) may result in an open substructure and an increase in pore interconnectivity in the membrane. The morphology of the surface may have a tremendous effect on the permeation property. The second solution may also give a highly porous substructure due to the presence of a high molecular weight hydrophilic polymer, PVP [1-4, 21]. However, associated with this open substructure, a dense and thick skin layer may be formed as well giving a high resistance to transport [3].

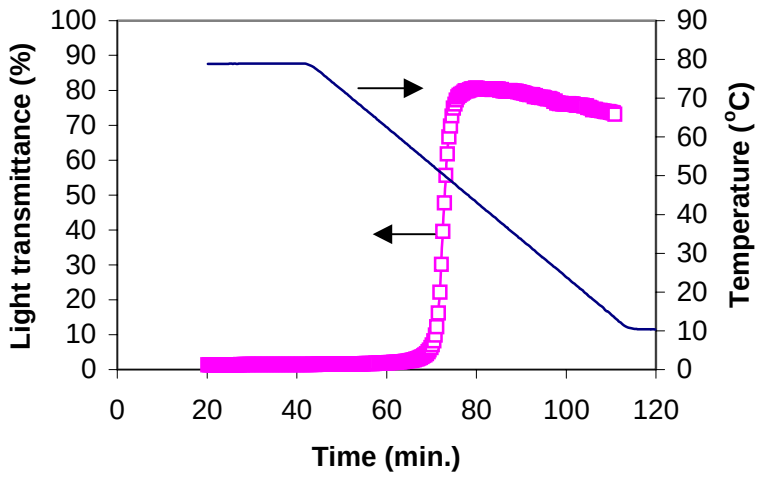

Figure 2.4 *Cloud point curve of polymer solution 1.*

2.4.2 Kinetics of phase separation

Table 2.2 lists the delay time before demixing for different coagulation baths having different solvency. The composition of the coagulation bath strongly influences the delay time. NMP is a good solvent for the polymer and thus gradually dissolves both polymer solutions. Since water is the strongest

nonsolvent, both polymer solutions show instantaneous demixing. An ambient environment with humidity of 55% has a different effect on the delay time. For solution 1, the delay time is 1 second, while it is 39 seconds for solution 2.

For solution 1, a mixture of NMP and acetone still shows a good solvency up to 50wt% acetone. However, pure acetone is a mild nonsolvent for polysulfone and it causes instantaneous demixing of solution 1 since it is located close to the cloud point. In the later discussion, we will show the effect of the solvency of the first coagulants on the porosity and pore interconnectivity of the outside surfaces of membranes obtained from solution 1. Unfortunately, no correlation could be established between morphology and the delay time. The experiments however demonstrate the sensitivity of two polymer solutions to different phase separation conditions. Moreover, the infinite delay time of NMP to both solutions confirms that NMP is an excellent dilution solvent. Therefore, NMP is used to alter the polymer solution towards lower polymer concentration from A to B (Figure 2.2).

Table 2.2 *Delayed time of solution 1 and solution 2 using different first coagulants.*

First coagulant	**Delay time before demixing**	
	Solution 1 (sec.)	**Solution 2 (sec.)**
NMP	∞	∞
NMP/Acetone 50/50	∞	-
Acetone	0	-
Air, humidity 55%	~1	39
Water	0	0

2.4.3 Structure and permeation properties of membranes prepared from solution 1

Solution 1 is located so close to the cloud point that demixing occurs immediately after extruding from the spinneret due to the water vapor presented in the air gap. An open porous structure is obtained with a high porosity as can be seen in Figure 2.5 (A). When NMP is used in the outer orifice, an extremely open surface with a lacy structure is obtained as can be seen in Figure 2.5 (B). We reason that the polymer concentration at the outlayer is diluted by NMP and becomes probably low enough to pass the binodal curve close to the critical point, forming an open and loose structure.

Adding acetone to NMP, therefore decreasing the solvency, results in a much denser surface structure, as shown in Figure 2.5 (C) and (D). A less open surface is obtained using a solution of NMP/acetone at a ratio of 50/50wt%. Moreover, a rather dense surface is obtained by using acetone alone. The results indicate that with decreasing in the solvency of the liquid from the outer orifice, a denser skin is obtained. The morphology is confirmed by the cross-section of various structures as can be seen in Figure 2.6. The hollow fiber spun

using acetone shows a dense surface at the outside as shown in Figure 2.6 (A) (B). Below the top layer a finger-like structure about 3/5 of the total thickness is observed. In the toplayer, a dense skin of about 0.5 μm consists of closed cells. In contrast, the membrane prepared from NMP as the liquid in the outer orifice shows a porous, finger-free and interconnected structure (see Figure 2.6 (C) (D)).

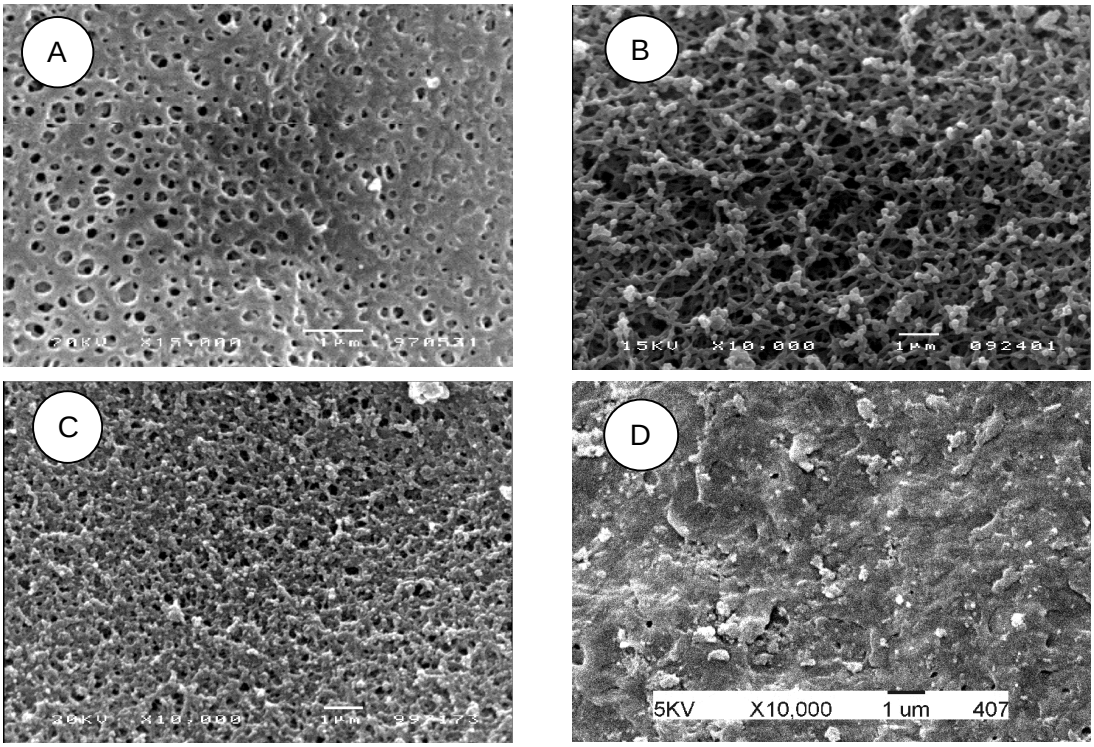

Figure 2.5 *Surfaces of PSf hollow fibers spun under different external conditions. (A) air; (B) NMP; (C) NMP/Acetone 50/50wt%; (D) Acetone.*

Figure 2.7 shows that the permeation properties correspond fairly well to the observed morphology. The membrane using acetone as external liquid has the lowest gas and water permeation, indicating the highest resistance. Slightly higher fluxes are obtained for the membrane prepared with NMP as the external fluid, compared to the membrane prepared either with the NMP/acetone mixture or without external fluids at all. Probably, the outer surface is open enough even without external fluid. The total resistance in this case mainly originates from the substructure and the inner skin layer.

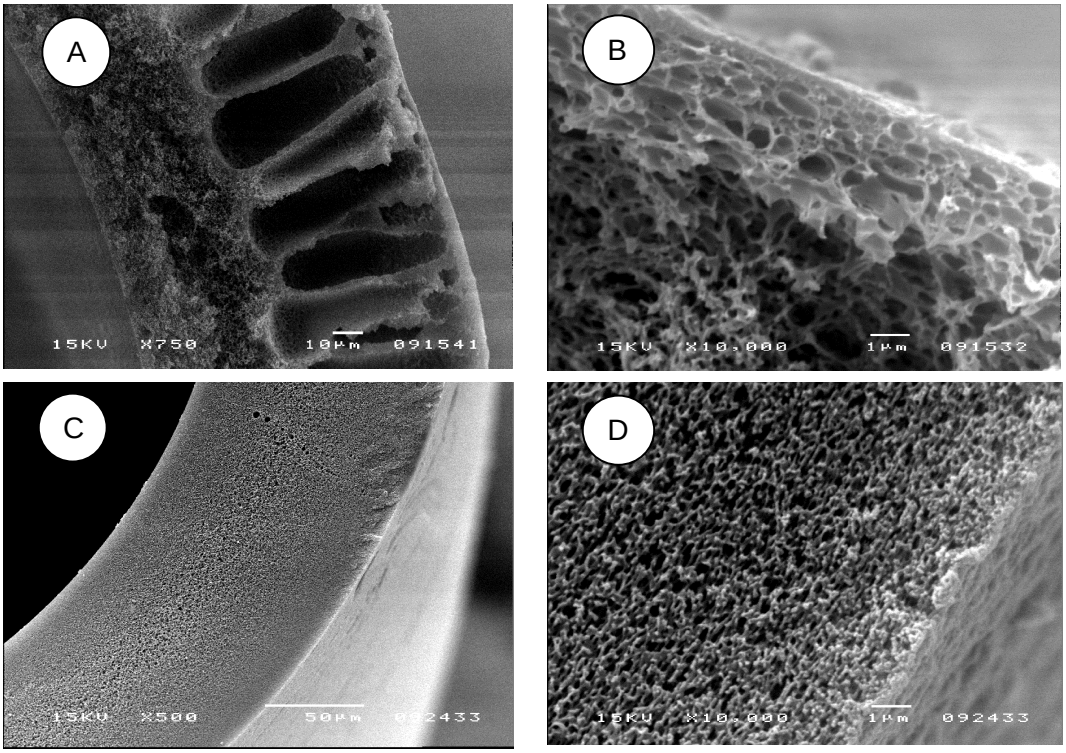

Figure 2.6 *Cross-section of the hollow fibers spun with an external liquid from the outside orifice channel.(A) (B) Acetone; (C) (D) NMP.*

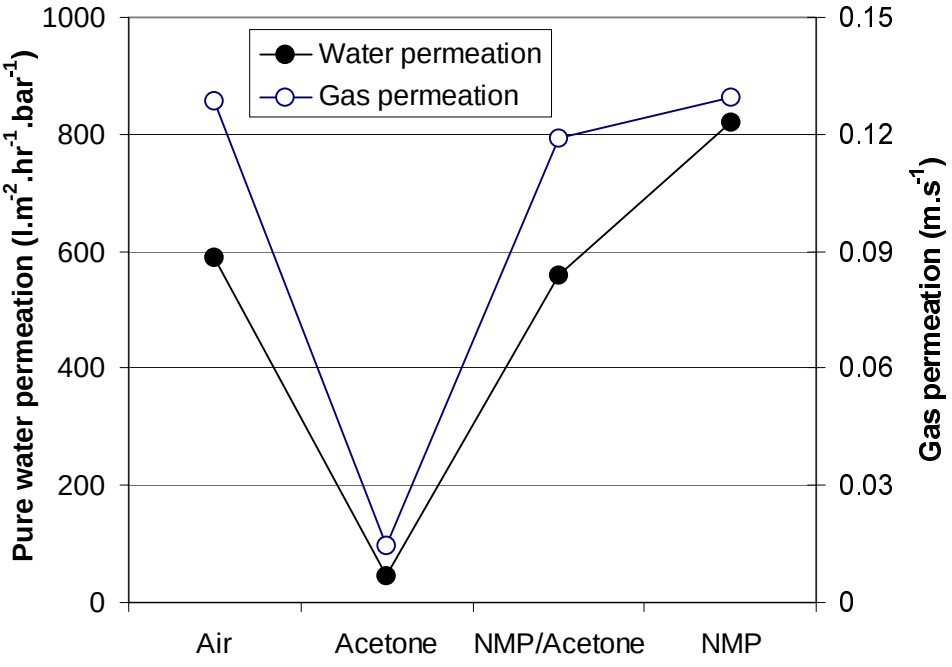

Figure 2.7 *Effect of different external compounds on the permeation of hollow fiber membranes.*

Further improvement of the flux can be achieved either by using a solution which forms far more open substructure (for example solution 2) or by using a demixed solution [22] which may generate defects. Moreover, increase of the pore size at the inner surface layer improves fluxes. Figure 2.8 shows a more open inner surface of the membrane prepared with 80wt% NMP in bore liquid compared to the membrane prepared with 75wt% solvent. Consequently, the pore size is bigger and slightly higher water and gas permeation (as can be seen in Figure 2.8 (C)) are obtained.

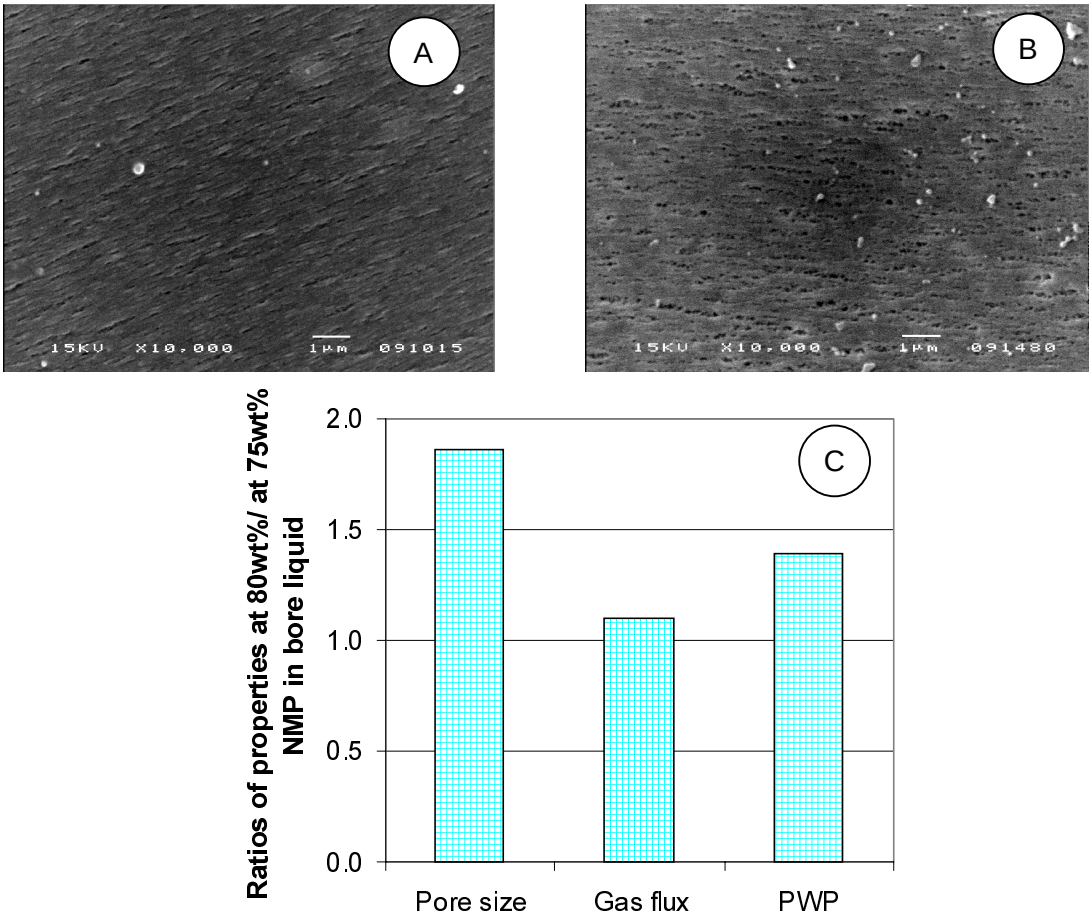

Figure 2.8 *Morphology of the inner surface for membranes prepared with 75wt% (A) and 80wt% (B) NMP in bore liquid and ratios of properties (C) (pore size, gas and pure water permeation, PWP) of two membranes prepared from solution 1. The pore size of membrane (A) is 52 nm and of membrane (B) 97 nm.*

2.4.4 Structure and permeation properties of membranes prepared from solution 2

Figure 2.9 (A) shows the hollow fiber membranes obtained from solution 2 having an extremely dense skin layer, which was also mentioned by

Munari et al. [3]. This dense top layer was obtained by using a polymer solution containing 5 to 10wt% PVP, having a pronounced negative effect on the flux.

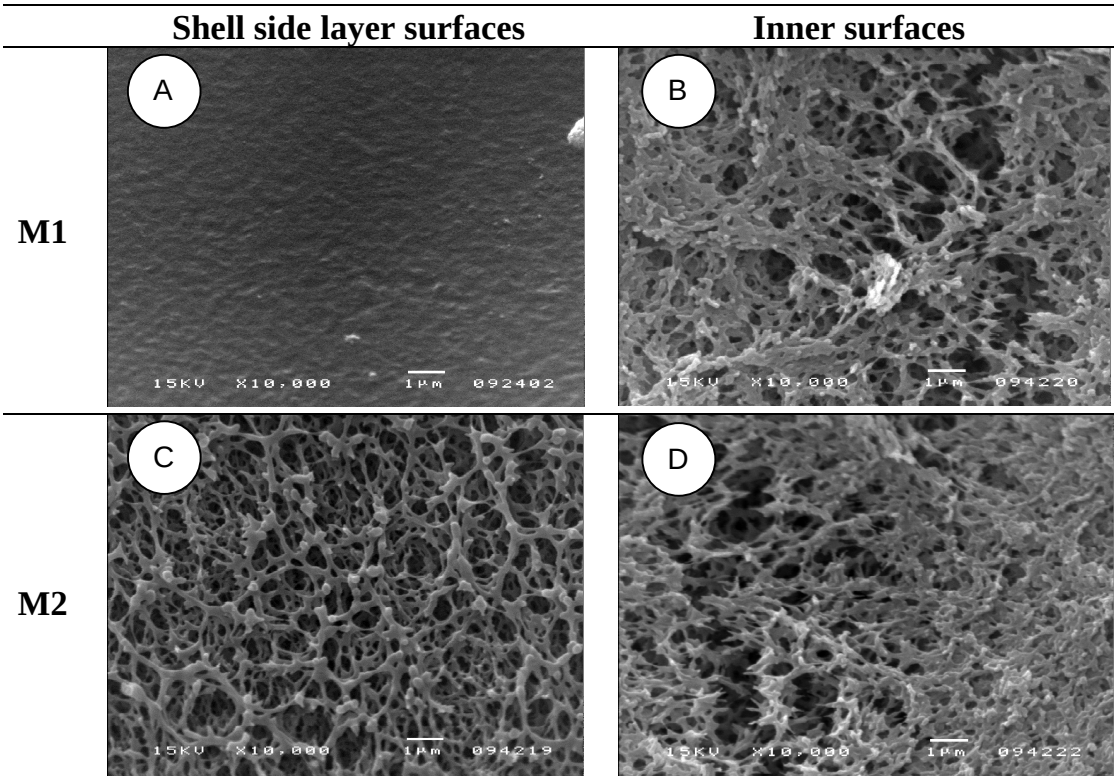

Figure 2.9 *Structure of the shell side surfaces and inner surfaces of hollow fiber membranes prepared from solution 2. M1, membrane made without NMP at the shell side; M2, membrane made with NMP as the external liquid. Bore liquid, 80wt% NMP in water.*

Table 2.3 *Effect of NMP on the properties of a PSf/PVP blend membrane prepared from solution 2.*

No	External liquid	PWP [a] ($l.m^{-2}.hr^{-1}.bar^{-1}$)	Pore size (μm)
M1 [b]	N/A	18	Dense layer
M2 [c]	NMP	4700	1.2-1.3

[a] pure water permeation; [b] prepared by passing through a short air gap, and the pore size was measured by permporometry; [c] prepared by using NMP as the external liquid, and the pore size is measured by Coulter Porometer II.

According to the proposed concept, a highly porous surface can be obtained using NMP as the external liquid and Figure 2.9 (C) indeed confirms this. The whole surface consists of a lacy interconnected porous structure and an extremely low transport resistance of the outside skin is expected. This lacy structure is an indication of a rather low polymer concentration at the outer layer before phase separation occurs. Again, NMP dilutes the polymer solution at the top layer during the short period of contact which results in a loose structure. These membranes also show quite open inner surfaces as seen in Figure 2.9 (B) and (D), since NMP content in the bore liquid is high, up to 80wt%. As listed in Table 2.3, the membrane with a dense skin layer shows a water permeability of only 18 $l.m^{-2}.hr^{-1}.bar^{-1}$ because of its dense surface at the shell side. However, the membrane prepared using NMP as external liquid has a water permeability of 4700 $l.m^{-2}.hr^{-1}.bar^{-1}$ and the average pore size of 1.2 to 1.3 microns.

2.5 Conclusions

This work describes the application of the triple-orifice spinneret in the preparation of microfiltration membranes with a highly porous surface. Dilution solvents, i.e. NMP and NMP/acetone (50/50 wt%), can be used as the external liquids during spinning, but not acetone, a mild nonsolvent for polysulfone. A simple way to obtain a highly porous toplayer independent of polymer solution in the spinning process is to apply a good solvent as the external liquid using a triple-orifice spinneret. A polymer solution close to the cloud point does not show significant improvement in permeability since the surface pores are open enough and not the controlling parameter for transport. However, a porous surface can be obtained for a blending solution of PSf and PVP far from cloud point, forming a dense skin layer and an open substructure.

2.6 References

[1] I. Cabasso, E. Klein, and J. K. Smith, Polysulfone hollow fibers. I. Spinning and properties, J. Appl. Polym. Sci., 20 (1976) 2337-2394.
[2] I. Cabasso, E. Klein, and J. K. Smith, Polysulfone hollow fibers. II. Morphology, J. Appl. Polym. Sci., 21 (1977) 165-180.
[3] S. Munari, A. Bottino, G. Capannelli, P. Moretti, and P. P. Bon, Preparation and characterization of polysulfone-polyvinylpyrrolidone based membranes, Desalination, 70 (1988) 265-275.
[4] H. D. W. Roesink, C. A. Smolders, M. H. V. Mulder, and D. M. Koenhen, USP 4798847, 1989.
[5] T. He and C. Z. Jiang, PES microfiltration membranes: effect of different additives, Mo Kexue Yu Jishu (in Chinese) (CA abstract number 129: 217549), 18 (1998) 43-48.

[6] H. Zhang, W. W. Y. Lau, and S. Sourirajan, Factors influence the production of polyethersulfone microfiltration membranes by immersion phase inversion process, Sep. Sci. Technol., 30 (1995) 33-52.
[7] T. P. Hou, S. H. Dong, and L. Y. Zheng, The study of mechanism of organic additives action in the polysulfone membrane casting solution, Desalination, 83 (1991) 343-360.
[8] G. H. Fan, C. J. Zhang, and L. Y. Zheng, The study of action of organic additives in polysulfone UF membranes, Desalination, 56 (1985) 325-332.
[9] W. F. C. Kools, Membrane Formation by phase inversion in multicomponent polymer systems. Mechanisms and morphologies, Ph.D Thesis, University of Twente, Enschede, 1998.
[10] J. G. Wijmans, J. P. B. Baaij, and C. A. Smolders, The mechanism of formation of microporous or skinned membranes produced by immersion precipitation, J. Membrane Sci., 14 (1983) 263-274.
[11] S.-G. Li, G. H. Koops, M. H. V. Mulder, T. van den Boomgaard, and C. A. Smolders, Wet spinning of integrally skinned hollow fiber membranes by a modified dual-bath coagulation method using a triple orifice spinneret, J. Membrane Sci., 94 (1994) 329-340.
[12] G. H. Koops, J. A. M. Nolten, M. H. V. Mulder, and C. A. Smolders, Integrally skinned polysulfone hollow fiber membranes for pervaporation, J. Appl. Polym. Sci., 54 (1994) 385-404.
[13] I. M. Wienk, H. A. Teunis, T. v. d. Boomgaard, and C. A. Smolders, A new spinning technique for hollow fiber ultrafiltration membranes, J. Membrane Sci., 78 (1993) 93-100.
[14] K. Kimmerle and H. Strathmann, Analysis of the structure-determining process of phase inversion membranes, Desalination, 79 (1990) 283-302.
[15] I. F. Wang, USP 5869174, 1999.
[16] W. J. Wrasidlo, USP 4629563, 1986.
[17] A. J. Reuvers, J. W. A. van den Berg, and C. A. Smolders, Formation of membranes by means of immersion precipitation. part I. a model to describe mass transfer during immersion precipitation, J. Membrane Sci., 34 (1987) 45-65.
[18] A. J. Reuvers and C. A. Smolders, Formation of membranes by means of immersion precipitation. part II. The mechanism of formation of membranes prepared from the system CA/acetone/water, J. Membrane Sci., 34 (1987) 67-86.
[19] H. D. W. Roesink, D. M. Koenhen, M. H. V. Mulder, and C. A. Smolders, USP 5076925, 1991.
[20] Y. Liu, G. H. Koops, and H. Strathmann, Morphology controlled PES hollow fibers by the addition of PEG in dope and lumen solutions, Sep. Purif. Technol., To be published.
[21] R. M. Boom, I. M. Wienk, T. van den Boomgaard, and C. A. Smolders, Microstructures in phase inversion membranes. Part 2. the role of a polymeric additive, J. Membrane Sci., 73 (1992) 277-292.
[22] W. J. Wrasidlo, EP 0036315, 1986.

Chapter 3 Permeation and stability of polysulfone hollow fibers for supported liquid membranes

Abstract

Preparation of composite membranes to stabilize supported liquid membranes (SLMs) is still in the developing stage. A membrane system which shows a lifetime in the scale of at least several months would be a significant achievement. This paper describes the optimization of spinning parameters for the preparation of a new support membrane based on polysulfone. The effect of polymer concentration, amount of additive and the NMP content in the bore liquid are investigated in terms of the copper flux. The membrane is characterized by gas and pure water permeability, porosity and pore size distribution. Suitable support membranes are prepared from solutions of polysulfone content about 17wt%. The amount of diethylene glycol as the additive in the polymer solution should be rather high, i.e 30.6wt%. The NMP concentration in the bore liquid is optimized to be 75wt%. The stability of these polysulfone membranes in SLM is similar to the commercial Accurel polypropylene membrane with a comparable permeability.

3.1 Introduction

Supported liquid membranes (SLMs) have been widely investigated for separation and concentration of various chemical compounds [1] . However, the instability during extended operation hinders the commercial applications of SLMs. Several techniques to stabilize SLMs were reported in literature, i.e. homogenous gelation [2] , gelation coating [3] , interfacial polymerization [4-6], plasma polymerization [7] and a lamination coating of an ion exchange polymer [8] . An extraordinary improvement of SLM stability to at least a few months is necessary to make it a feasible technique for the removal of heavy metal ions such as copper.

The basic idea behind the stabilization of SLMs is to decrease a gradual loss of organic solvent using a hydrophilic ion-permeable coating material on a hydrophobic support [8] . Hollow fiber membranes are chosen as support since compact modules can be prepared. Co-extrusion and dip-coating can be used as simple and reproducible techniques to apply a hydrophilic layer. Both techniques require a support membrane easy to spin or to dip-coat.

In the following, polysulfone (PSf) is used as the membrane support material because of its hydrophobic character and its fairly strong resistance towards concentrated inorganic acids, base solutions, salt solutions and aliphatic hydrocarbons [9] . It is also a versatile polymer for the preparation of porous membranes by an immersion precipitation process. The latter is required to apply co-extrusion technique to prepare a stabilizing layer onto a support membrane. Co-extrusion and dip-coating techniques require a support membrane with adhesion properties better than the commonly used polypropylene based membranes [8] . Polysulfone fulfills this requirement because of its high surface tension. The first research on the use of polysulfone hollow fiber membranes in SLMs was performed by Bend Research in the late 1970s [10-13] . The final product was a membrane with a finger structure, a wall thickness of 70-80 microns and an outside diameter of 800 μm. Hydrophilic additives were used to increase the membrane porosity. However, this alters the membrane hydrophilicity, potentially contributing to an even shorter lifetime. A copper flux of 3.0 $\mu g.cm^{-2}.min^{-1}$ (0.79×10^{-9} $mol.cm^{-2}.s^{-1}$) was found for these membranes, which is only one-fourth of flat Accurel membranes measured by Wijers et al [8] . Moreover, the membranes were instable for metal ion transport.

In the following, we describe the preparation of a new high flux polysulfone hollow fiber membrane to be used as a support for SLMs. The structure of the membrane is optimized systematically in terms of copper flux by varying the polymer concentration and additive concentration in the spinning solution. A low molecular weight additive, diethylene glycol, is chosen to increase the porosity while keeping the hydrophobicity of the material. Diethylene glycol is a small organic molecule and can be easily washed out by water. The copper permeability and stability of polysulfone membranes are compared with a commercial hollow fiber (Accurel Q3/2) membrane.

3.2 Experimental

3.2.1 Materials

N-methylpyrrolidone (NMP), diethylene glycol (DegOH), acetone and dodecane were purchased from Merck and used without further purification. Copper sulfate pentahydrate, $CuSO_4.5H_2O$ (cryst. extra pure) and concentrated sulfuric acid (96-98%, analytical grade) were obtained from Merck. Dodecane (with a purity of 99%） was purchased from Janssen Chimica. LIX84-I, used as carrier in copper transport, was kindly supplied by Henkel KGaA from Germany as a mining chemical grade. Accurel PP Q3/2 membrane was supplied by Membrana, Germany (formerly Akzo Nobel Membrana).

3.2.2 Spinning process

Pre-dried polysulfone (one week at 120^{o}C) was dissolved in a NMP/DegOH mixture at various compositions. The polymer solution was filtered and degassed before spinning. A triple orifice-spinneret and spinning setup were used as described elsewhere [14] , using NMP as the external solution [15] and mixtures of NMP and water as the bore liquid. After a short air gap of 50 mm, the polysulfone hollow fiber was immersed in a water bath at room temperature. The bore liquid was a mixture of NMP and water at different ratios. The fibers were cut into lengths of 60 cm and rinsed with tap water for 48 hours and allowed to dry in ambient environment or stored in 20 wt% glycerol/water solution and then dried in air at room temperature.

3.2.3 Membrane characterization

3.2.3.1 Water and gas permeation measurements

Five glycerol impregnated hollow fibers of 20 cm were potted at both ends with a Nylon tube of 6 mm and cut open. The permeation of ultra pure water (MilliQ, Millipore) was recorded after one hour pre-pressurization using a feed pressure of 2 bar absolute.

Two or four dried fibers without a glycerol impregnation were potted the same way as described before. Nitrogen gas at a pressure of 0.4 bar or 0.2 bar gauge was used for measuring the gas permeability. Stable gas permeation was recorded after 30 minutes with a soap bubble meter.

3.2.3.2 Pore size distribution and porosity

The pore size distribution of the membrane was determined by permporometry [16] . The porosity of the fibers as well as the density of the polymer were determined using a Pycnometer (Accupyc 1330, from Micromeritics® Instrument Corporation). By combining the nominal density of

the hollow fiber, ρ_{nom} , obtained by the mass and the volume of the fiber, the porosity of the fiber ϕ is expressed as

$$\phi = (1 - \frac{\rho_{nom}}{\rho_{PSf}}) \times 100 \quad (1)$$

3.2.3.3 Scanning electron microscopy

Samples for scanning electron microscopy (SEM, JEOL JSM-T220A) were prepared by cryogenic breaking of the fresh wet fibers. Samples were dried in vacuum at 30°C overnight and sputtering coated with a thin gold layer before examination.

3.2.4 Copper permeation

Two polysulfone fibers with the ends potted into Nylon tubes of 8 mm diameter were cut open at both ends. Potted fibers were fixed into a glass housing (inner diameter 10.5 mm) with an effective length of about 40 cm. The module was dried in a vacuum oven at 30 °C for at least 48 hours before a permeation test.

The module was mounted into a permeation set-up as schematically shown in Figure 3.1. An organic solution of 20vol% LIX84-I in dodecane was impregnated into the support fibers by contact for 30 minutes. A feed ($CuSO_4$, 0.025 M) and strip solution (H_2SO_4, 2 M), both of 200 ml, were stored in the reservoirs and the temperature was kept at 25°C. The membranes contacted the feed and strip for 30 minutes before starting circulating aqueous phases with peristaltic pumps (Masterflex 7521-25, Cole-Parmer Instrument Company, Niles, Illinois, USA). The feed solution circulates through the bore side of the hollow fiber and the strip circulates through the shell side. Samples of about 0.5 ml were taken from the feed and strip phases at certain time intervals. In total, seven samples were taken in 7 to 8 hours. For stability tests, feed and strip were refreshed before the next sampling series.

The copper concentrations were determined by atomic absorption spectrometry (Spectra 10, Varian, Houten, The Netherlands). A linear relationship of the initial copper concentration versus time was obtained. From the slope, the flux *J* for copper ions was calculated using Equation 2:

$$J = \frac{V}{A}\left|\frac{dC}{dt}\right| \quad (2)$$

C is the concentration of copper ions; *A* is the membrane area in contact with the aqueous phase and *V* is the volume of the feed or strip phase.

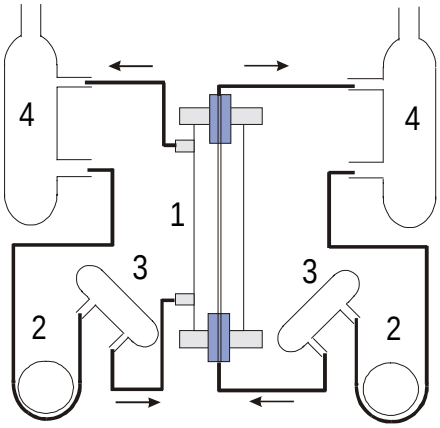

Figure 3.1 *Schematic of the permeation set-up for copper transport with hollow fiber SLMs. (1) Hollow fiber module; (2) Peristaltic pump; (3) Buffer vessel; (4) Feed or strip reservoir.*

3.3 Results and discussion

3.3.1 Structure of support hollow fiber

A porous, asymmetric, macrovoid-free hollow fiber has been prepared with a wall thickness of 120±10 μm. The cross-section of a sample used in the experiment is shown in Figure 3.2. The outside surface shows an interconnected network structure with a high porosity. The inner surface consists of much smaller pores compared to the outside. The nominal pore size at the inside as obtained from the SEM picture is about 0.08 μm.

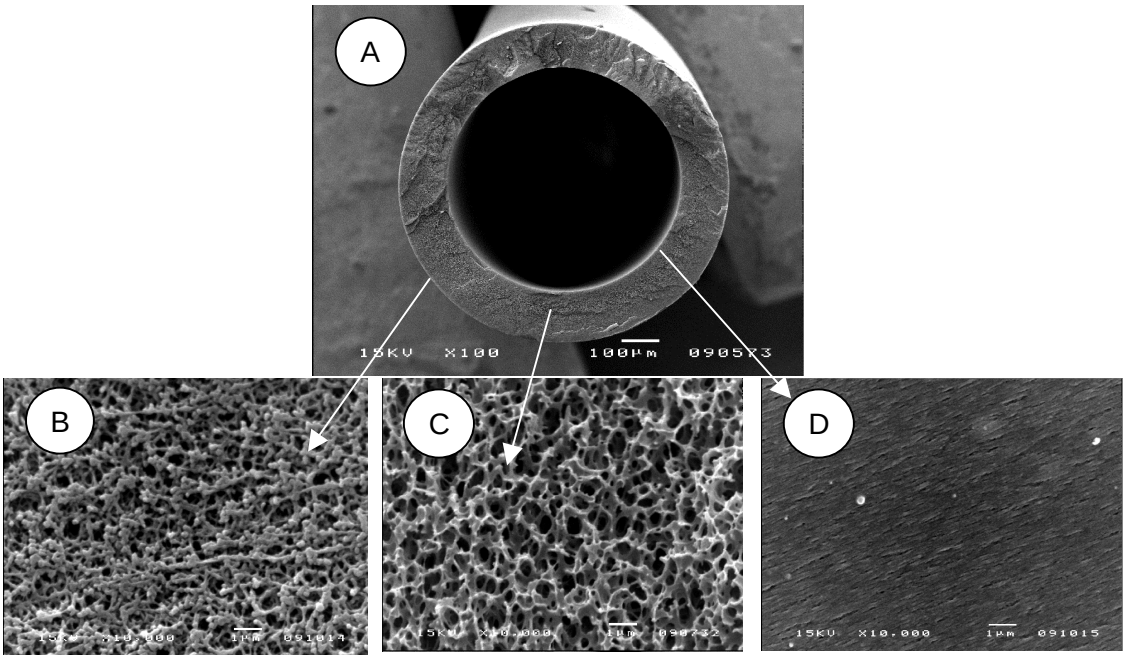

Figure 3.2 *SEM photos of polysulfone hollow fiber. (A) Cross-section of the fiber; (B) Outside surface of the fiber; (C) Middle part of the fiber wall; (D) Inner side surface of the fiber.*

3.3.2 Optimization of operational parameters

Equation 2 is used to calculate the overall flux through the membranes which results is a combined contribution of the membrane resistance and the laminar boundary layer resistance. Membrane fluxes typically depend on the circulation rates of the solutions. A high shear rate of the fluids tends to reduce the thickness of the boundary layer adjacent to the membranes. Without adequate circulation, the boundary layers would cause an additional resistance resulting in a lower flux. At an optimal circulation speed, the feed concentration has been optimized to be in the range of 0.025 M at a pH value of 2.5 to 2.7, which is about the copper concentration in hydrometallurgical applications [13] . The sulfuric acid concentration is 100 $g.l^{-1}$ (about 2 M) to obtain a sufficiently fast extraction [17] . The LIX84-I as a carrier needs to be diluted because of its relatively high viscosity, which generates a high diffusion resistance.

Finally, the optimized parameters are listed in Table 3.1 at a feed concentration of 0.025 M $CuSO_4$, a strip concentration of 2 M H_2SO_4, and a LIX84-I concentration in dodecane of 20vol%. The flow rates are 1.86 $m.s^{-1}$ at the feed side and 0.094 $m.s^{-1}$ at the strip side.

Table 3.1 *Optimal parameters for copper transport with hollow fiber supported liquid membranes.*

Parameters	Values	Units
Feed, $CuSO_4$	0.025	M
Strip, H_2SO_4	2.0	M
LIX84-I in dodecane	20	vol%
Feed flow rate	1.86	$m.s^{-1}$
Strip flow rate	0.094	$m.s^{-1}$

3.3.3 Relation between membrane structure and permeability

3.3.3.1 Effect of polymer concentration

The polymer concentration in the spinning solution is crucial in adjusting the transport properties. Figure 3.3 (A-C) shows the inner surfaces of the hollow fibers at different polysulfone concentration. From the surface images, it is observed that the pore size is more open at a polysulfone concentration of 22wt% than that at 17wt%. No obvious difference can be distinguished from the structure at the central part of the hollow fibers. In order to quantify the difference among these membranes, various permeation experiments were carried out as listed in Table 3.2. A membrane made from 22wt% PSf shows only one-fourth gas flux compared to that of a membrane made from 14wt% PSf. A membrane made from 17wt% PSf showed a gas flux

in between the other two membranes. The pure water permeability decreases with an increase in the polymer concentration, although not as pronounced as for the gas flux.

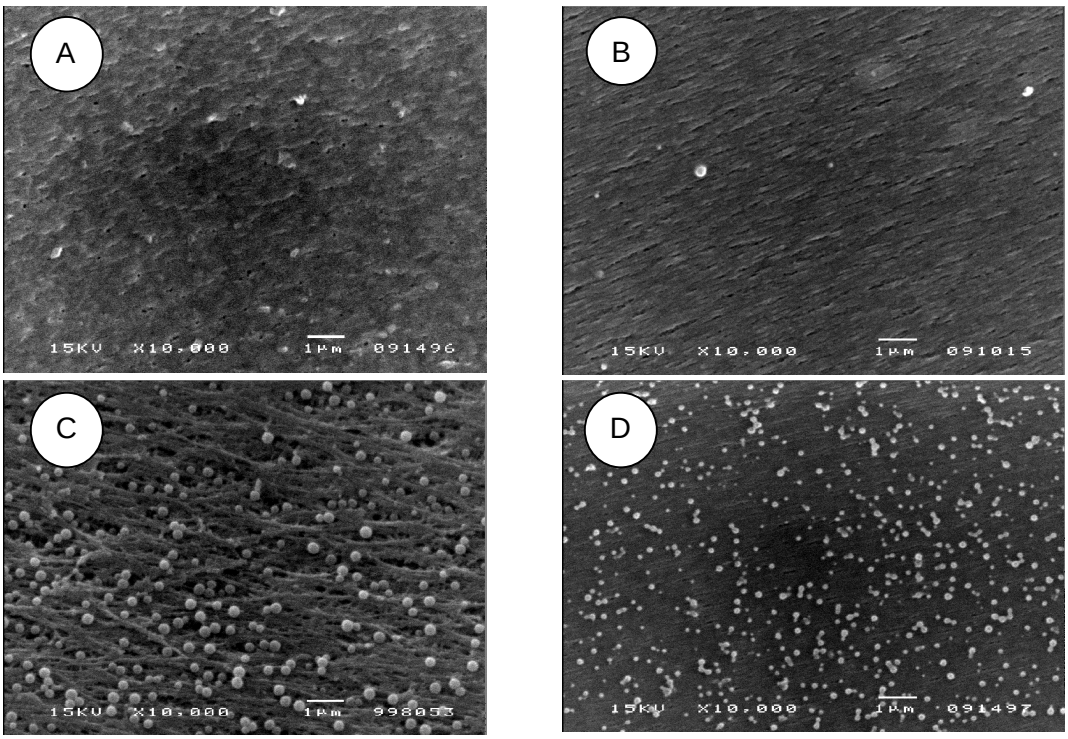

Figure 3.3 *Inner surfaces of PSf hollow fiber membranes from different polymer solutions. Polymer solution compositions are given as wt% PSf/NMP/DegOH:(A) 14.0/54.3/31.7; (B) 17.0/52.4/30.6; (C) 22.0/49.3/28.7; (D) 17.0/55.9/27.1.*

The concentration of the polymer solution affects the porosity of the membrane. As shown in Table 3.2, the membrane made from 22wt% PSf has the lowest porosity 68% while the membrane made from 14wt% PSf has the highest porosity 81%. The copper flux of the membrane made from a 14wt% solution is 4.5 $x10^{-9}$ $mol.cm^{-2}.s^{-1}$, similar to that of membrane made from a 17wt% PSf solution (5.1 $x10^{-9}$ $mol.cm^{-2}.s^{-1}$), which is much higher than that of the membrane made from 22wt% PSf. This indicates that the copper flux of a membrane is not directly related to the overall porosity of the membrane. However, the connectivity of the central and surface porous structure is more important than the overall porosity.

3.3.3.2 Effect of additive concentration

The pure water permeation (PWP) could be improved by increasing the additive concentration in the polymer solution as a result of an increase in the porosity and connectivity of the pores at both the skin layer and substructure [18] .

Table 3.2 *Influence of the structure on the permeation properties of polysulfone hollow fiber.*

No	Polymer solution PSf/NMP/DegOH (wt%)	Gas flux [a] ($l.cm^{-2}.min^{-1}.bar^{-1}$)	PWP [b]	D_{pore} (μm)	Porosity (%)	Copper flux (10^{-9} $mol.cm^{-2}.s^{-1}$)
1	14.0/54.3/31.7	1.05	500	(-)	81	4.5
2	17.0/52.4/30.6	0.776	820	0.052	77	5.1
3	22.0/49.3/28.7	0.236	440	(-)	68	1.6
4	17.0/55.9/27.1	0.077	470	(-)	76	0.77
5	Accurel Q3/2	1.80	(-)	0.2	70	5.3
6	PSf-150 [c]	(-)	5	(-)	73.5	0.79

[a] pressure normalized gas flux;
[b] pure water permeation, $l.m^{-2}.hr^{-1}.bar^{-1}$;
[c] PSf-150, made by Babcock et al [10-13] from Bend Research Inc. Liquid membrane phase: 30% Kelex 100 in Kermac 470B; Feed: 2000 ppm copper sulfate at pH of 2.5; Strip: 100 $g.l^{-1}$ H_2SO_4.

Therefore, besides the polymer concentration, we have investigated the effect of the amount of additive on the membrane permeation. A compact skin layer is obtained for the membrane made of 17 wt% PSf with 27.1 wt% diethylene glycol (membrane No 4 in Table 3.2) as shown in Figure 3.3 (D). However, by adding 30.6 wt% diethylene glycol, a much more porous surface is obtained (membrane No 2) as can be seen in Figure 3 (B). The gas flux of membrane No 4 (as seen in Table 3.2) in only 10% of membrane No 2, although the pure water permeation (470 $l.cm^{-2}.min^{-1}.bar^{-1}$) is at the same order of magnitude as that of membrane No 2 (820 $l.cm^{-2}.min^{-1}.bar^{-1}$). Moreover, the copper flux of membrane No 4 is only 0.77 $x10^{-9}$ $mol.cm^{-2}.s^{-1}$, less than one-fifth of membrane No 2. Only 3.5 wt% increase of additive can improve the gas flux up to 10 times and the copper flux more than 6 times, indicating the importance of the amount of additive in polymer solution.

The membrane from Babcock et al [10-13] (see Table 3.2, membrane No 6) has a rather low copper flux compared to our membrane and Accurel Q3/2 (membrane No 5). Two factors may explain this difference: the extractant system and the membrane structure. Since Kelex100 as a carrier shows always a higher copper flux than LIX64 [10-13] , a similar extractant as LIX84-I, it is argued that the membrane structure has high transport resistance. Further evidence for the high transport resistance is the low water permeability (5 $l.cm^{-2}.min^{-1}.bar^{-1}$). Compared to the Accurel PP Q3/2 membrane, the PSf membrane described in this paper has a comparable copper flux, but a much lower gas flux and smaller pore sizes. This is probably due to the fact that copper flux is a diffusion-controlled process, which depends not only on the skin layer but also on the morphology of the porous structure. However, the convection controlled

process, such as water permeability and gas permeation characterization, is more related to the skin layer, i.e. the pore size and porosity of the skin, once the sub-structure is open enough as in our case.

3.3.3.3 Effect of inner structure

An optimized copper flux is obtained for PSf hollow fiber membranes, which is comparable to that of a flat or hollow fiber Accurel PP membrane. However, it is still a challenge whether the flux of the membranes can be further improved. Since the outside surface is already highly porous with its interconnected structure, we focus on the inner surface structures. The solvent concentration in the bore liquid influences the membrane pore size [19] .

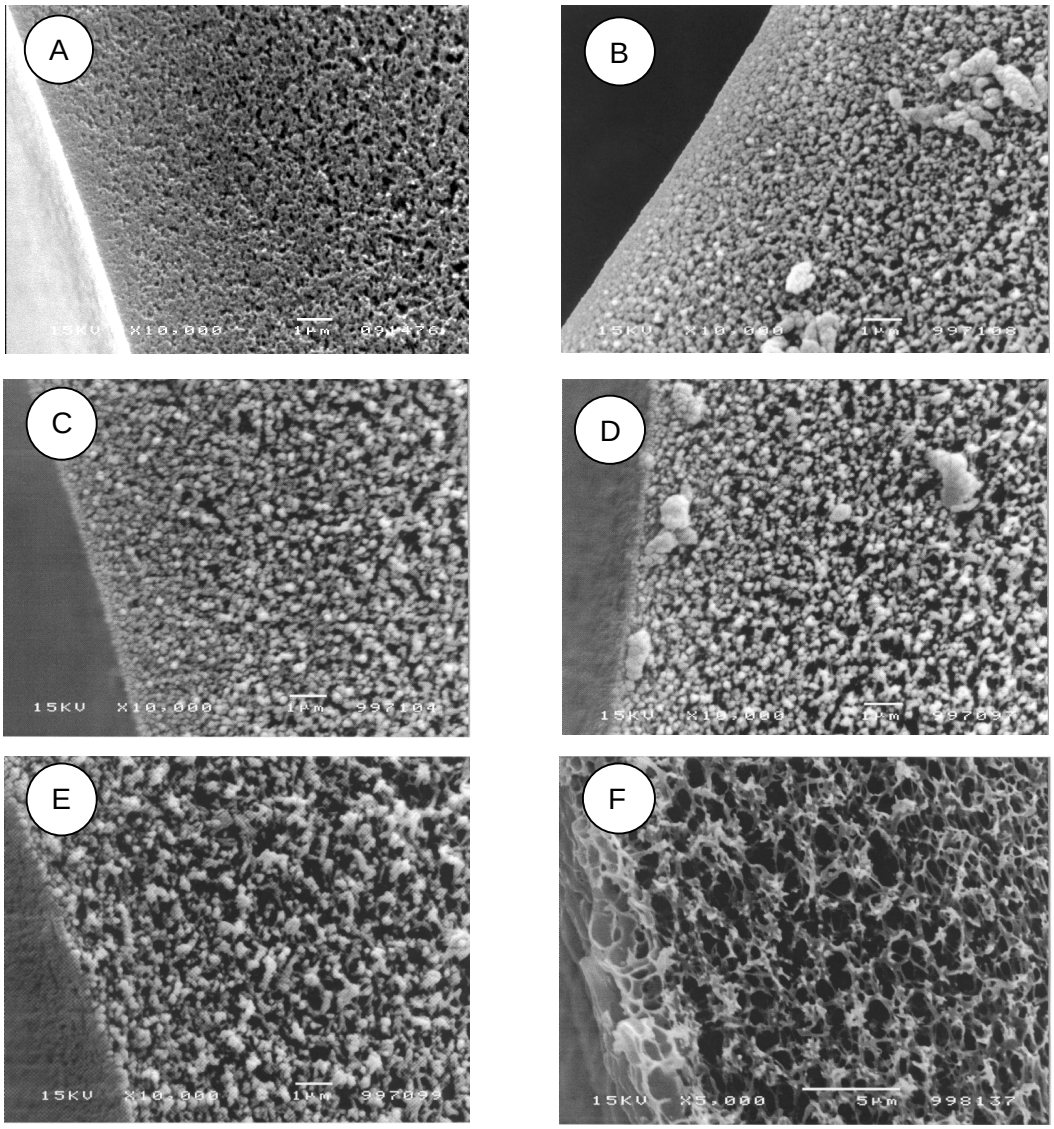

Figure 3.4 *Cross-section view of the bore side of the membranes at various lumen compositions. NMP/H_2O (in wt%): (A) 0/100; (B) 25/75; (C) 50/50; (D) 75/25; (E) 80/20; (F) 90/10.*

Figure 3.4 shows the effect of NMP concentration in the bore liquid on the structure of the hollow fiber adjacent to the inner surface. A compact skin layer is obtained when the bore liquid is pure water. The porosity increases gradually from the surface to the substructure, representing a typical asymmetric structure. With an increase of NMP content in the bore liquid, the toplayer becomes more and more open as seen in Figure 3.4 (B) to (F). Some closed cells of 2 to 4 microns appear at 90% NMP.

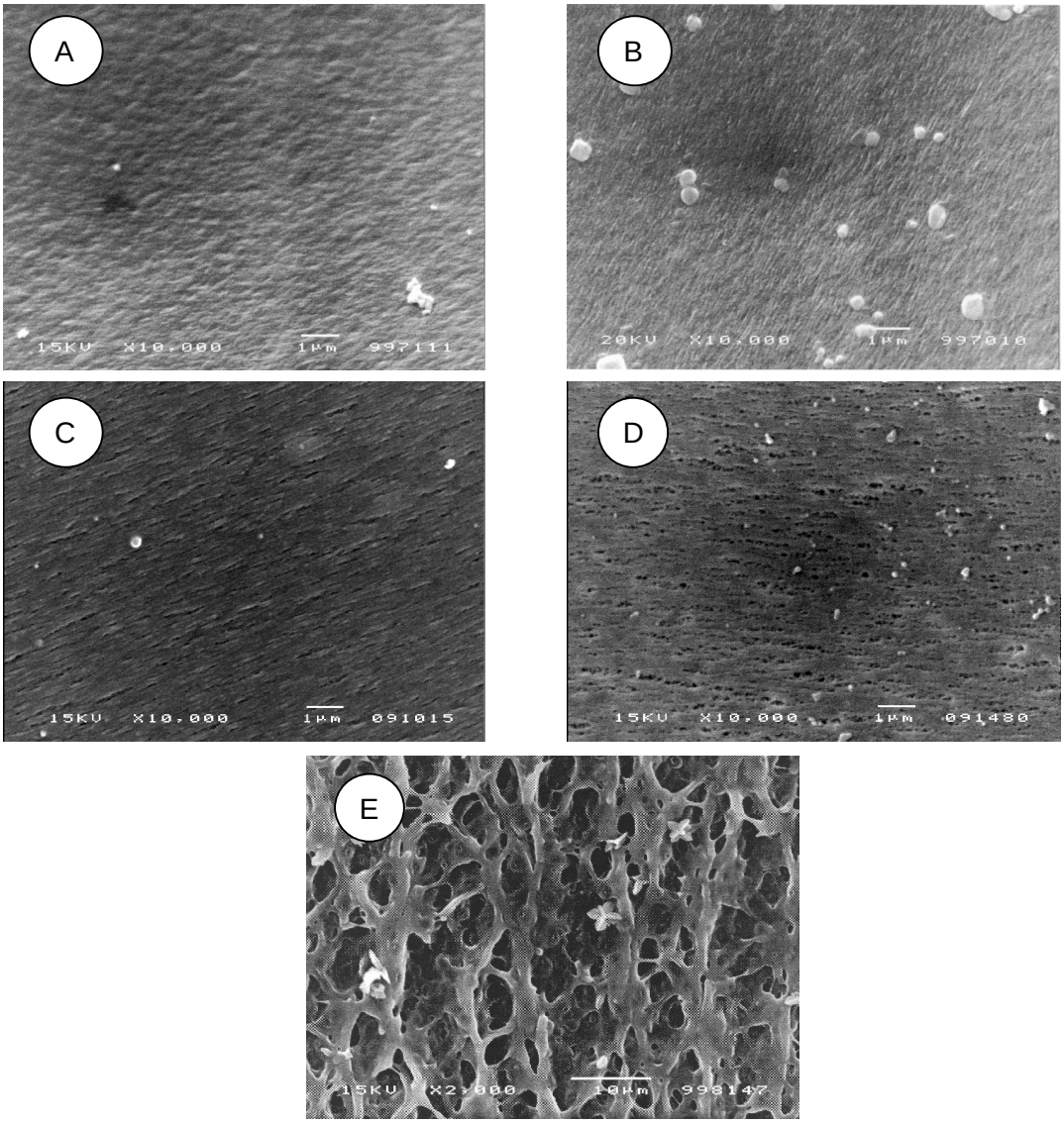

Figure 3.5 *Effect of NMP concentration in the bore liquid on the inner surface structure of the hollow fiber membranes. NMP/H2O ratio (in wt%): (A) 25/75; (B) 50/50; (C) 75/25; (D) 80/20; (E) 90/10.*

The surface view of all membranes is shown in Figure 3.5. A quite dense and smooth surface is obtained when the NMP content in the bore liquid is less than 25wt% (as seen in Figure 3.5 (A)). It is difficult to distinguish pores in the membranes made with less than 50wt% NMP in the bore liquid (as seen in Figure 3.5 (A) and (B)). At higher concentrations, small interstices are

visible at 75wt% NMP and much larger pores are visible by a further increase of the NMP concentration up to 80wt%. At 90wt%, a porous surface is obtained, indicating a structure with a high permeability. However, the cross-section pictures imply that this membrane has a high transport resistance.

Figure 3.5 shows that the pore size and porosity at the inner skin of polysulfone hollow fibers can be adjusted to a certain extent by simply changing the NMP concentration in the bore liquid. In fact, as shown in Table 3.3, the pore radius can be controlled over a broad range from 2.7 nm to 48.5 nm. As seen in the SEM photos, the increase in the pore size is followed by an increase in the porosity at the skin layer.

Table 3.3 *Average pore radius (R) at the bore side.*

NMP content (wt%)	R (nm)
0	2.7
25	4.3
50	5.3
75	26.0
80	48.5

Polymer solution compositions: PSf/NMP/DegOH 17.0/52.4/30.6wt%.

Figure 3.6 shows a combined picture of the influence of the bore liquid composition on the gas, water and copper permeability. The ratios between all fluxes are given with respect to the membrane prepared using a bore liquid NMP concentration of 75wt%. The copper, gas and water permeation decrease when the solvent content in the bore liquid decreases. However, above 75wt%, a significant drop of the copper permeability is observed without a decrease in gas and water permeability. When the NMP content is above 80wt%, a drastic decrease of all permeation rates is observed. This can be explained by the fact that the pore connectivity of the inner layer decreases with solvent increase in the bore liquid at above 80wt% (see the structure of the membrane made from 90wt% NMP). The transition region to lower fluxes is equally sharp for all permeation characteristics. Currently, we do not have an explanation at hand.

3.3.4 Stability of PSf hollow fibers

3.3.4.1 Reproducibility and effect of reimpregnation of liquid membrane phase

To detect the reproducibility of the polysulfone hollow fiber, two modules with the fibers from the same batch are operated at exactly the same

conditions as listed in Table 3.1. Figure 3.7 clearly shows that two modules have a comparable copper flux as well as the flux decline dynamics.

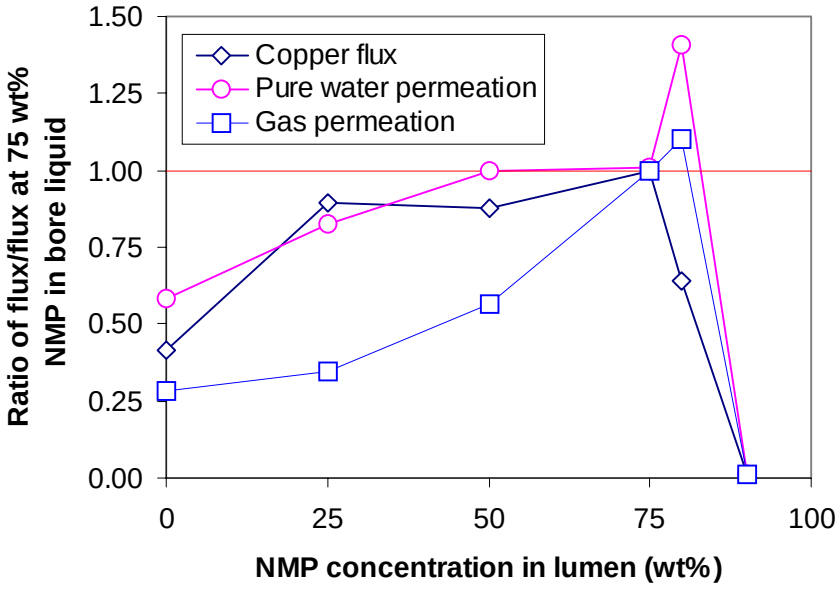

Figure 3.6 *Influence of NMP concentration in the bore liquid on water, gas (nitrogen) and copper permeation. Spinning solution: PSf/NMP/DegOH 17.0/52.4/30.6wt%.*

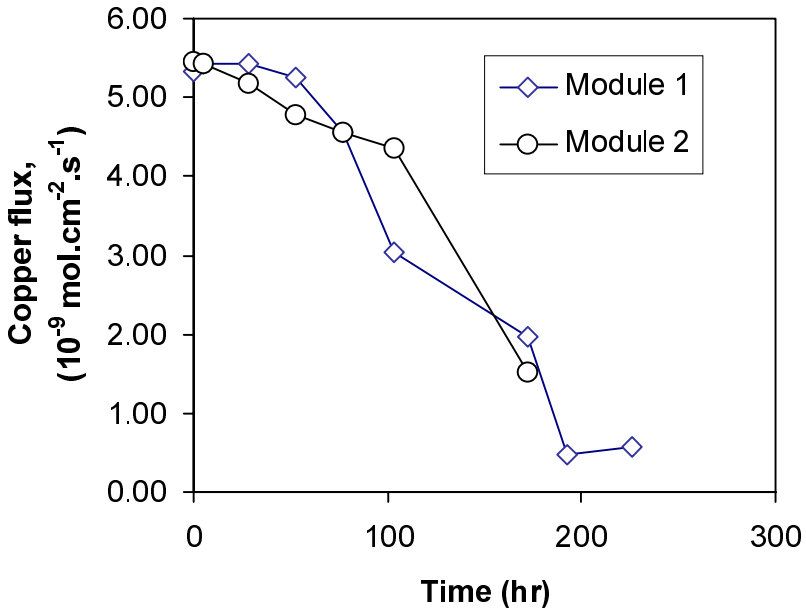

Figure 3.7 *Stability of two polysulfone hollow fiber membranes from the same batch (No 2 in Table 3.2) for transport of copper ions.*

A second concern with respect to this new support fiber is the chemical stability of the material. A reimpregnation test has been performed to determine whether the flux decline is related to a potential degradation of the polymeric

support, either by the organic solvents or by the feed and strip solutions. The instable membrane was reloaded with a fresh organic liquid, assuming that the flux would return to its initial value if the polymeric support remains intact. Figure 3.8 shows that, within the experimental error, the same initial copper fluxes are obtained after each reimpregnation, verifying the integrity of polysulfone in a harsh environment. A further investigation on the structure with SEM indicates that the porous structure is intact as well (not shown here).

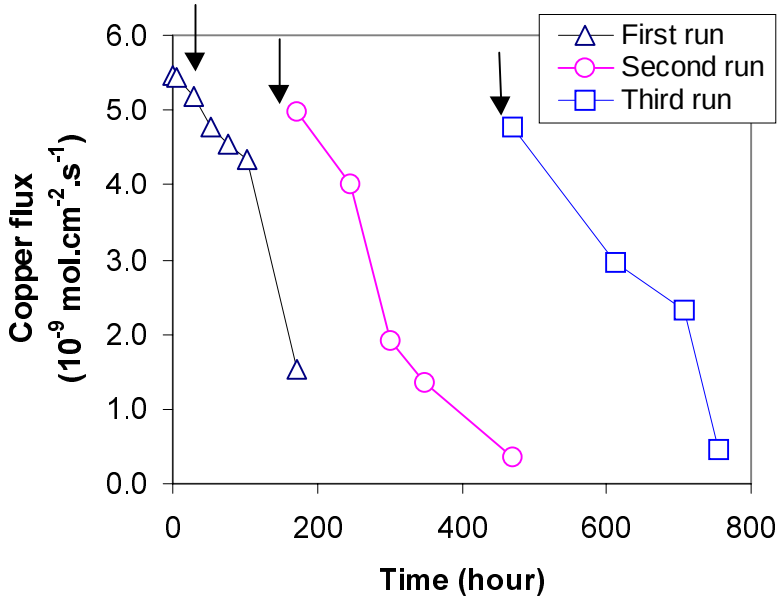

Figure 3.8 *Effect of reimpregnation on stability of the polysulfone hollow fiber membranes in transport of copper ions. Arrows refer to the impregnation point.*

3.3.4.2 Effect of polymer concentration

The lifetime of the SLM, i.e. the dynamics by which the flux declines, may be influenced by the membrane morphology. Figure 3.9 compares the dynamics of flux decline for the support membranes listed in Table 3.2. Within an experimental error, the copper permeability of membranes made from 14wt% and 17wt% of PSf are identical until 300 hours of operation. The structure of both hollow fibers is quite similar in terms of the inner surface and the porous sub-structure. This might explain the comparable copper flux and stability of both membranes.

A different stability curve can be observed for a hollow fiber made from 22wt% PSf. The initial flux, 1.64 x10^{-9} mol.cm^{-2}.s^{-1}, is about one-third of the other two membranes. Moreover, a quite stable flux profile is obtained which decays very fast after about two weeks. Probably, the support structure is more compact at higher PSf concentration, hence, lower copper fluxes.

Since a relatively high initial flux is the goal of the research, a support fiber made of 22wt% PSf solution is not a suitable candidate. Concerning both

14wt% and 17wt% solutions, a 17wt% solution has priority in terms of the spinnability for its high solution viscosity.

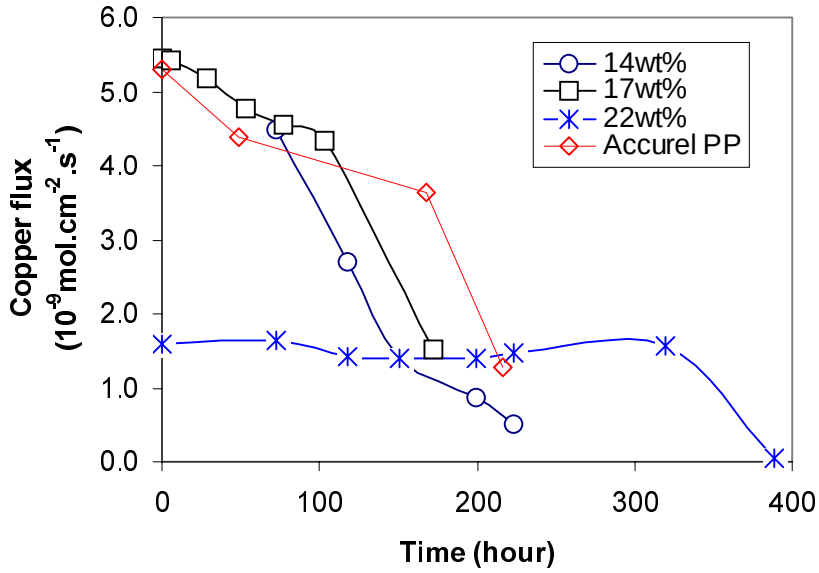

Figure 3.9 *Effect of polymer concentration on the stability of the supported liquid membrane for copper transport.*

3.3.4.3 Effect of additive concentration

Less additive in the polymer solution results in a membrane with lower water and gas permeation [18] . This correlates to a low copper flux in a supported liquid membrane application as can be seen in Figure 3.10. The membranes made with 27.1wt% diethylene glycol as additive shows a much lower copper flux during the whole stability test. However, the copper flux remains quite stable compared with membranes made with 30.6 wt% DegOH. Therefore, in terms of both flux and stability, DegOH concentration of 30.6wt% is preferred.

3.4 Conclusions

` A new type of polysulfone hollow fiber was prepared which can be used as the support for SLM. The effect of polymer concentration, amount of the additive and the NMP content in the bore liquid were investigated in terms of copper flux. Gas and pure water permeation, the porosity and pore size of the membrane were used as characterization methods. To prepare a suitable support membrane, the polysulfone content should be less than 22wt% PSf. The amount of additive in the solution is preferably high, up to 30.6wt%. It has been shown that a further decrease of the polymer content does not increase the porosity of the substructure and therefore does not increase the copper

permeability. The amount of NMP in the bore liquid was optimized at 75wt%. A higher NMP content does not show a higher flux.

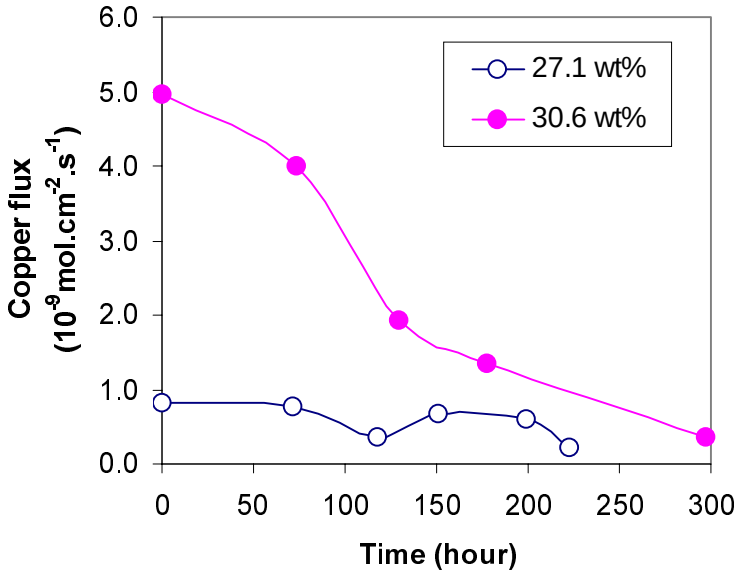

Figure 3.10 *Effect of amount of additive on the stability of the PSf hollow fiber membrane. Polymer concentration in the solution is 17wt%.*

The stability of the polysulfone membranes is similar to the commercial Accurel PP membrane. At high initial copper flux, the membrane is always less stable than a membrane with a low initial copper flux.

The membrane made from a 17wt% PSf and 30.6wt% additive will be used as the support membrane for co-extrusion [14] or dip-coating [20] to apply a hydrophilic layer in order to stabilize the SLM.

3.5 References

[1] J. de Gyves and E. R. de San Rodriguez, Metal ion separations by supported liquid membranes, Ind. Eng. Chem. Res., 38 (1999) 2182-2202.

[2] A. M. Neplenbroek, D. Bargeman, and C. A. Smolders, Supported liquid membranes: stabilization by gelation, J. Membrane Sci., 67 (1992) 149-165.

[3] A. M. Neplenbroek, Stability of supported liquid membranes, Ph.D Thesis, University of Twente, Enschede, 1989.

[4] A. J. B. Kemperman, H. H. M. Rolevink, T. van den Boomgaard, and H. Strathmann, Stabilization of supported liquid membranes by interfacial polymerization top layers, J. Membrane Sci., 138 (1998) 43-55.

[5] C. Clement and M. M. Hossain, Stability of a supported liquid membrane for removing hydrophobic solutes from casein hydrolysate solution, Sep. Sci. Technol., 32 (1997) 2685-2703.

[6] Y. Wang, Y. S. Thio, and F. M. Doyle, Formation of semi-permeable polyamide skin layers on the surface of supported liquid membranes, J. Membrane Sci., 147 (1998) 109-116.
[7] X. J. Yang, A. G. Fane, J. Bi, and H. J. Griesser, Stabilization of supported liquid membranes by plasma polymerization surface coating, J. Membrane Sci., 168 (2000) 29-37.
[8] M. C. Wijers, M. Jin, M. Wessling, and H. Strathmann, Supported liquid membranes modification with sulphonated poly(ether ether ketone): permeability, selectivity and stability, J. Membrane Sci., 147 (1998) 117-130.
[9] G. H. Koops, J. A. M. Nolten, M. H. V. Mulder, and C. A. Smolders, Integrally skinned polysulfone hollow fiber membranes for pervaporation, J. Appl. Polym. Sci., 54 (1994) 385-404.
[10] W. C. Babcock, R. W. Baker, D. J. Kelly, and H. K. Lonsdale, Coupled transport membranes for metal separation. Final Report, Phase III, NTIS PB79-293029, Bend Research, Inc., Bend, Oregon, 1979.
[11] W. C. Babcock, R. W. Baker, D. J. Kelly, H. Kleiber, and E. LaChapelle, Coupled transport membranes for metal separation. Final Report, Phase IV, NTIS PB 81-214843, Bend Research, Inc., Bend, Oregon, 1981.
[12] W. C. Babcock, R. W. Baker, J. W. Brooke, D. J. Kelly, and L. E.D., Coupled transport membranes for metal recovery. Final Report, Phase II, NTIS PB 81-179947, Bend Research, Inc., Bend, Oregon, 1980.
[13] W. C. Babcock, R. W. Baker, J. W. Brooke, D. J. Kelly, and E. D. LaChapelle, Industrial water resuse with coupled transport membranes, NTIS PB 80-206014, Bend Research, Inc., Bend, Oregon, 1979.
[14] T. He, M. H. V. Mulder, M. Wessling, and H. Strathmann, Preparation of composite hollow fiber membranes. Co-extrusion of dense hydrophilic coating onto porous hydrophobic support structures, Chapter 4, submitted to J. Membrane Sci.
[15] T. He, M. H. V. Mulder, and M. Wessling, Preparation of porous hollow fiber with a triple-orifice spinneret, Chapter 2.
[16] Y. Liu, G. H. Koops, and H. Strathmann, Morphology controlled PES hollow fibers by the addition of PEG in dope and lumen solutions, Sep. Purif. Technol., To be published.
[17] , Henkel Corporation, MID Redbook on the chemistry of metals recovery using LIX Reagents., , Tucson, Arizona, 1997.
[18] H. Zhang, W. W. Y. Lau, and S. Sourirajan, Factors influence the production of polyethersulfone microfiltration membranes by immersion phase inversion process, Sep. Sci. Technol., 30 (1995) 33-52.
[19] J. G. Wijmans, J. P. B. Baaij, and C. A. Smolders, The mechanism of formation of microporous or skinned membranes produced by immersion precipitation, J. Membrane Sci., 14 (1983) 263-274.
[20] T. He, M. H. V. Mulder, and M. Wessling, Composite hollow fiber membranes as supported liquid membranes, Chapter 5.

Chapter 4 Preparation of composite hollow fiber membranes: Co-extrusion of dense hydrophilic coatings onto porous hydrophobic support structures

Abstract

Surface functionalization of membranes can be performed by coating a polymer layer onto a support membrane. Frequently, this procedure is a two-step process. In this paper, we describe a one step membrane preparation process in which a coating layer forms in-situ onto a support membrane by a co-extrusion technique. Our aim is to apply a thin ion exchange layer (sulfonated polyethersulfone, SPES) onto a polysulfone support. The mechanical stability and adhesion of the ion exchange material to the hydrophobic support membrane (polysulfone) has been studied by a systematic approach of initial proof-of-principle experiments, followed by single-layer and double-layer flat sheet casting. Critical parameters quantified by the latter experiments are translated into the co-extrusion spinning process. The composite hollow fiber membrane has a low flux as a supported liquid membrane for the copper removal due to the low ion exchange capacity of the SPES. The coating layer of the composite membrane is porous as indicated by gas pair selectivity close to unity. However, our new composite membrane has nanofiltration properties: it passes mono and bivalent inorganic salts but rejects larger charged organic molecules. The experimental work demonstrates that co-extrusion can be a viable process to continuously prepare surface tailored hollow fiber membranes in a one step process, even if the support and coating material differ significantly in hydrophilicity.

4.1 Introduction

Composite membranes emerged right after the discovery of asymmetric RO membranes [1]. This development opened the door for tailor-made membranes to a much wider range of applications. Several methods can be used to prepare composite membranes [2, 3]: lamination of a pre-formed film, interfacial polymerization, in-situ polymerization, dip coating, plasma deposition and dynamic membrane formation. In general, fabrication of such a composite membrane consists of at least two separate steps: manufacturing of the support and subsequent coating. The advantage of this sequential processing includes flexibility in adjusting a variety of parameters and immense knowledge available. However, such multi-step fabrication processes are more expensive and time consuming. In addition, the composite membranes produced by these processes can experience failure and poor performance due to an increasing risk of introducing defects in the substrate and separating layer with the increasing number of processing steps involved.

Co-extrusion is a high potential fabrication method to make a multi-layer configuration in the form of film, sheet, or fiber by simultaneous extrusion of two or more polymers through a single die [4]. Co-extrusion avoids many of the manufacturing steps required by conventional lamination and coating processes, such as making and handling of individual films, application of coating primers, and solvent drying. Because of these economic and technical advantages, the application of co-extrusion is growing rapidly [5-10].

Co-extrusion in membrane technology is novel and challenging, with only a few patents and publications [11-24]. Basically, co-extruded membranes include two types: dense and porous. Co-extruded dense membranes include dialysers [15] and gas separation membranes [11-14, 17]. Most of the work published deals with the similar polymers for both the coating and support membranes. Porous membranes, both for ultrafiltration and microfiltration, are made from the same polymers, i.e. polypropylene [20, 21], polysulfone (PSf) [22, 23] and polytetrafluoroethylene [24]. To our knowledge, there are only two patents describing the spinning of sulfonated polymers on polysulfone or polyethersulfone (PES) [18, 19]. Sulfonated polysulfone (SPSf) with an ion exchange capacity of about 0.8 meq.g^{-1} is coated on a polysulfone solution [18]; and this is used as an anti-fouling membrane in the separation of an emulsion solution. The other patent [19] describes the use of blends of SPSf and PSf or PES to hydrophilize the membrane surface.

In this paper, a systematic approach is described to prepare a co-extruded composite membrane with a dense coating layer of SPES onto a polysulfone support. The sulfonated polymer itself will be investigated in terms of mechanical properties as well as adhesion onto the PSf support. A concept of critical polymer concentration is introduced for preparation of an integral composite hollow fiber membrane of SPES on PSf (see Figure 4.1). Initial screening and proof-of-principle experiments are carried out determining the

critical process parameters in the co-extrusion process. The fiber integrity is characterized by scanning electron microscopy (SEM). Based on these experiments, detailed characterization of the coagulation behavior of the coating material is performed and the obtained membranes are characterized by field emission scanning electron microscopy (FESEM). Co-casting of flat-sheet membranes addresses the critical issue of layer adhesion in order to identify recipes that can be further applied during co-extrusion. Finally, co-extruded membranes are tested with respect to their gas separation, ion retention and liquid membrane extraction performances.

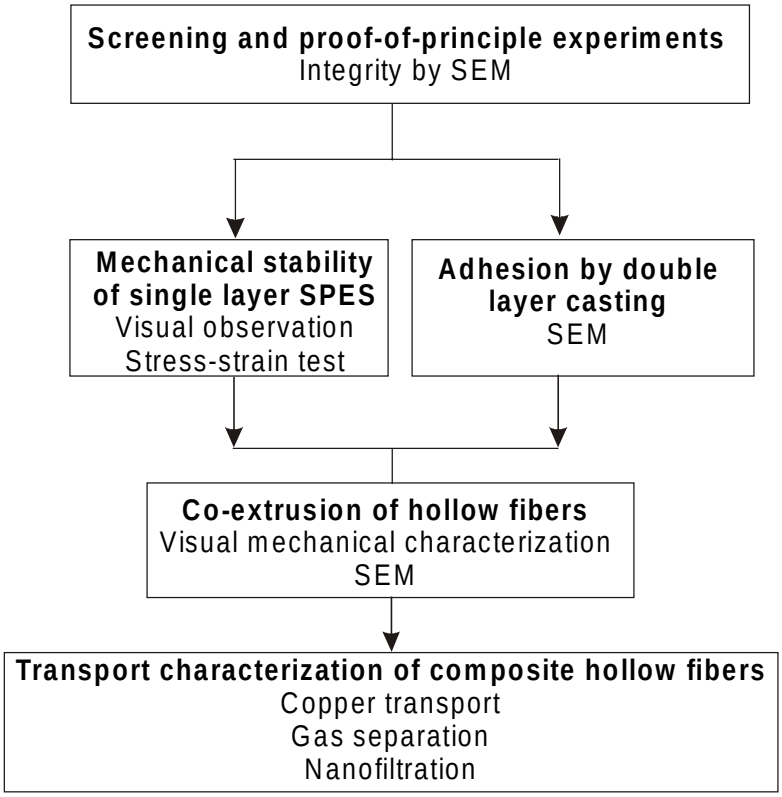

Figure 4.1 *Working procedure for the preparation of a hydrophilic SPES coating onto a hydrophobic support by a co-extrusion spinning process.*

4.2 Experimental

4.2.1 Materials

Polysulfone (PSf, Udel P3500) was purchased from Amoco. Sulfonated polyethersulfone (SPES) was kindly provided by AKZO Nobel. Solvents, N-methylpyrrolidone (NMP), Diethylene glycol (DegOH) and acetone were purchased from Merck. The solvents were of analytical grade and used without further purification. Sodium sulfate (Na_2SO_4), copper sulfate pentahydrate ($CuSO_4.5H_2O$, cryst. extra pure) and concentrated sulfuric acid (96-98%, analytical grade) were purchased from Merck. Dodecane with a purity of 99% was purchased from Janssen Chimica. The solvents are of analytical grade and

used without further purification. LIX84-I, as carrier in copper transport, was purchased from Henkel KgaA, Germany as a mining chemical grade. Three dyes were used: procion blue (Mw 840.12, negative charged, λ_{max} 607 nm, from Chimica), sunset yellow (Mw 452.38, negative charged, λ_{max} 482 nm, from Aldrich) and methyl green (Mw 472.51, positive charged, λ_{max} 629 (423) nm from Merck).

4.2.2 Characterization of SPES

The ion exchange capacity (IEC) is defined as the number of equivalents per gram of dried polymer. It was determined by elemental analysis. The water sorption was measured by soaking a piece of SPES dense films in pure water at 25 ^{o}C for 7 days. The swollen films were weighed and then dried in vacuum oven at 30 ^{o}C for another 7 days. The degree of swelling (DS) was determined from the difference in weight (W) between dry and swollen films according to:

$$DS = \frac{\left(W_{swollen} - W_{dry}\right)}{W_{dry}} \times 100\ \%$$

Duplicate samples were examined. The degree of swelling and the IEC of SPES are listed in Figure 4.1. The properties of PES are listed as well for comparison. SPES has an ion exchange capacity of 0.36 meq.g^{-1}, which is low compared to other ion exchange materials. SPES shows a water uptake of 9.1wt%, which is significantly higher than that of PES (3.1wt%).

Table 4.1 *Properties of sulfonated poylethersulfone.*

Polymer	Ion exchange capacity meq.g^{-1} dry polymer	Degree of Swelling DS (%)
PES	-	3.1
SPES	0.36	9.1

Swelling is determined at 25^{o}C in pure water.

4.2.3 Single film casting

Before solution preparation, SPES was pre-dried in an oven at 80^{o}C for one week and in a vacuum oven at 30^{o}C for another week. SPES solutions were prepared by dissolving a certain amount of polymer in NMP or acetone and NMP mixtures at room temperature. After filtering by a 15 microns metal filter, the solutions were allowed to degas for at least 24 hours, and then cast onto pre-cleaned glass plates using a casting knife of a 50 μm thickness. After 2 seconds of exposure to ambient air with a relative humidity of 45-55%, the initial films were immersed into an aqueous coagulation bath. The prepared films were

stored in ultra-pure water (MilliQ, Millipore) to rinse residual solvent for 24 hours at room temperature.

4.2.4 Stress-tensile test

Mechanical stress-strain experiments were performed on a Zwick Tensile Machine (Materialprufung Z020) made in Germany. Pre-dried SPES films were initially cut into standard dumb-bell test pieces. And then two ends of the film were clasped onto the tensile machine. Because of film shrinkage, a certain force, 0.25N, was pre-applied to avoid contribution of the force acting on flattening the crumbled films.

4.2.5 Double-layer casting

A special casting knife was used to co-cast double layer membranes as shown in Figure 4.2. The settings of the casting knives were 200 μm and 250 μm respectively, resulting in films with a coating thickness of 50 μm and a sublayer thickness of 200 μm. The polymer solutions were cast on a glass plate and the precipitation starts from the top side. When the support solution contains additives, such as diethylene glycol, a nitrogen gas flushed box with a relative humidity between 10 to 15% was used for casting. The films were rinsed in tap water for at least 24 hours before analysis. The adhesion of the top layer to sublayer was examined visually both in wet state and dry state.

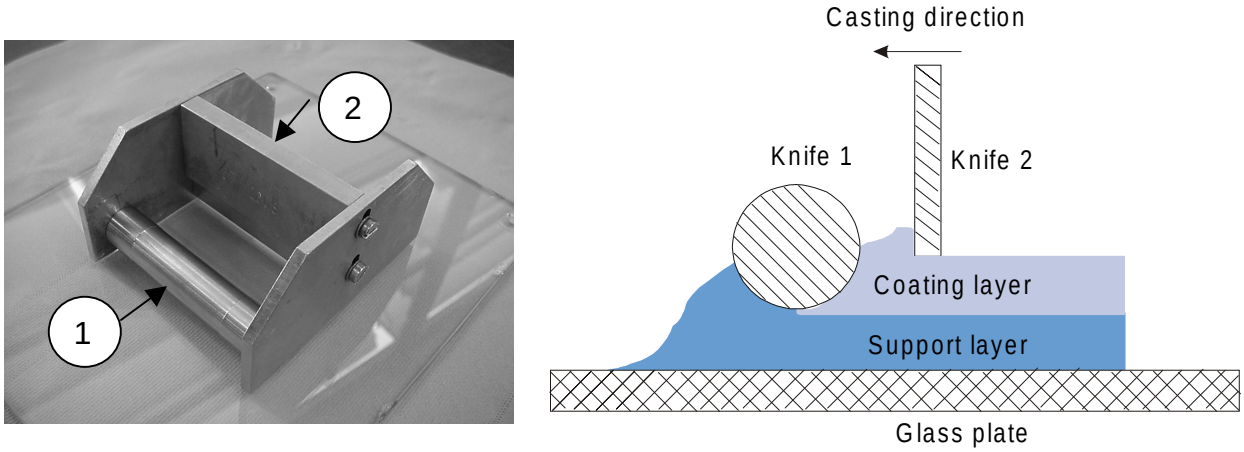

(a) (b)

Figure 4.2 *(a) Co-casting knife; (b) Schematic description of casting knife for double layer membranes. Number 1 and 2 represent the casting knife 1 and 2.*

4.2.6. Co-extrusion hollow fiber spinning

Pre-dried polysulfone (one week in 120^{o}C oven) was dissolved in a mixture of NMP and diethylene glycol (PSf/NMP/DegOH, 17/52.4/30.6wt%).

The polymer solution was filtered and degassed before spinning. The coating solutions were prepared as described above.

In order to prepare a composite hollow fiber, a spinneret with a tube and two orifices was used as shown in Figure 4.3 (b) and (c) [25]. The SPES coating solution was extruded through the outer orifice A, whereas the polysulfone solution was extruded simultaneously through channel B. Channel C was used for the bore liquid. Two gear pumps were used to control the flow velocity of both polymer solutions. After a short contact inside the spinneret, the solutions entered the air gap between the spinneret and coagulation bath followed by solidification in the coagulation bath. In the air gap, heat enhanced drying might be applied as well. A convective drying chimney or infra-red (IR) radiation were used as the drying techniques as seen in Figure 4.3 The chimney was kept at constant temperature by a silicon oil bath. At the same time, pre-heated nitrogen gas flushed through the inside of the chimney with a laminar flow. A mixture of NMP and water with weight ratio of 3:1 was used as the bore liquid. The fibers were cut into pieces of 60 cm and rinsed with tap water for 48 hours. The fibers then were immersed in 20wt% glycerol/water solution for another 24 hour and then allowed to dry in the air.

4.2.7. Characterization of permeation properties

All permeation properties were measured for two membrane samples. For gas permeation characterization, six co-extruded hollow fibers were dried in air and potted at the end with one side open at a length of 20 cm. Helium, nitrogen and carbon dioxide permeation were measured at room temperature (22^oC) at a pressure of 0.4 to 1.0 bar gauge.

For ion retention permeation experiments, two wet fibers of 38 cm were potted into a glass housing. Test solutions were circulated through the lumen of the fiber and the permeation was collected from the outside. The solutions were sodium sulfate, copper sulfate, methyl green, sunset yellow, and procion blue at a concentration of 500 ppm.

To perform the supported liquid membrane experiment (setup is described in detail in [26]), two dried hollow fibers of 38 cm were potted into a glass housing. LIX84-I diluted in dodecane at 20vol% was used as organic extractant. A 0.025 M $CuSO_4$ solution was used as the feed and a 2 M H_2SO_4 solution as the strip. The volume of both feed and strip was 200 ml. The aqueous phases flowed parallel along the fiber with the strip solution at the shell side and the feed at the bore side. The flow velocity of feed and strip was 1.86 $m.s^{-1}$ and 0.094 $m.s^{-1}$, respectively. The temperature was kept at 25^oC. The concentration of the feed and strip was determined by taking 7 samples in 7 or 8 hours interval and analyzed by atomic absorption spectrometry (Spectra 10, Varian, Houten, The Netherlands). The copper flux was calculated from the slope of the copper concentration versus time.

4.2.8. Scanning electron microscopy

Samples for scanning electron microscopy (SEM, JEOL JSM-T220A) were prepared by cryogenic breaking of the fresh wet films or fibers. Samples were allowed to dry under vacuum at 30°C for overnight and then coated with a thin gold layer. Samples for field emission scanning electron microscopy (FESEM, Hitachi S800) were coated with an Au/Pd layer at a thickness of approximately 4 nm.

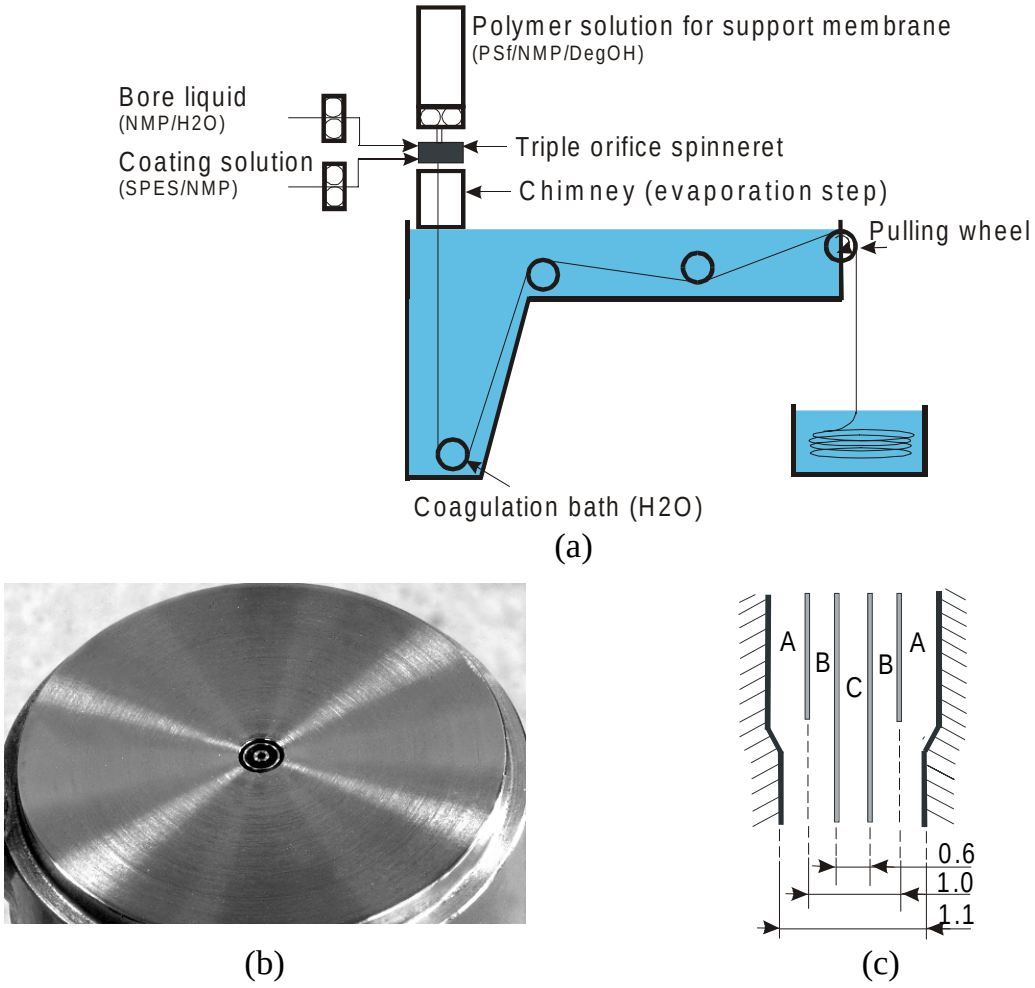

Figure 4.3 *Schematic of the spinning set-up and spinneret. (a) spinning set-up; (b) bottom view of a real spinneret; (c) schematic description of the spinneret. A, coating solution channel (1.1 mm); B, support solution channel (1.0 mm); C, bore liquid channel (0.6 mm).*

4.3 Results and discussion

4.3.1. Screening and proof-of-principle experiments

The initial concept of preparing the SPES coated polysulfone hollow fiber membrane was based on accelerated drying of a low concentration solution of

SPES using a convective evaporation chimney or infra red light. During drying, the polymer concentration in the polymer solution increases, resulting in a thin, dense coating layer. Table 4.2 summarizes a variety of experiments performed based on this concept. Major problems are the integrity of the coating layer and the adhesion of the coating layer onto the support. Several conclusions can be drawn from these spinning experiments:

- Increasing the chimney temperature results in a coating layer with less mechanical defects;
- Infra-red radiation results in an improved layer, but the surface smoothness is still insufficient;
- Addition of volatile solvent (acetone) improves the surface integrity;
- Increase of the SPES concentration improves adhesion and integrity of the coating layer, however, the fiber becomes brittle upon drying.

Table 4.2 *Screening and proof-of-principle experiments.*

SPES (wt%)	Drying method		Outside surface	Adhesion
	Process	**Temp (^{o}C)**		
4	IR radiation	(-)	Uneven surface, holes	Separated
6	Chimney	52	Numerous holes	Separated
		70	Cracks, dispersed holes	Separated
		90	Uneven, less cracks	Separated
	IR radiation	(-)	Uneven, less cracks	Separated
		(-) [a]	Big cracks and holes	Separated
	(-)	(-)	Numerous holes	Separated
10	IR radiation	(-)	Holes, small cracks	Small part attached
16	IR radiation	(-)[b]	Smooth with dispersed holes	partly separated

[a] without acetone; [b] the membrane became brittle after drying. All other membranes showed brittle coating layers but tough hollow fibers.
Spinning parameters: coating solution: SPES/NMP/Acetone, NMP/Acetone ratio: 50/50; coating solution flow rate: 1.3 ml.min^{-1}; air gap: 200 mm; spinning rate: 6 m.min^{-1}; chimney length: 200 mm; IR radiation: infra-red lamp.

From these screening experiments, we encounter two major problems related to co-extrusion of SPES onto PSf solution: (a) the mechanical property and integrity of the SPES thin coating layer; and (b) the insufficient adhesion between the coating layer and the support. The first problem is related to cracks and holes on the outer fiber surface (SPES). For the second problem, the thin layer tends to separate from the support layer in some cases. In the following parts, we address both problems separately. Firstly, the mechanical

properties of the SPES film are investigated to find a relationship between mechanical properties and casting solution composition. Secondly, adhesion of SPES layer onto the PSf layer is investigated with a co-casting process. Finally, co-extrusion experiments are carried out based on the knowledge gained from the experimental series.

4.3.2. Mechanical stability of SPES films

In general, the hydrophilic SPES films coagulated in a water bath show mechanical instability upon drying. Initially, the films are soft because of the gel-like structure containing water. Upon drying, water slowly evaporates from the membrane resulting in a brittle structure. Visual observation of these films gives qualitative information (see Table 4.3). In the wet state, the films cast from a solution with a concentration less than 20wt% are opalescent and extremely soft. It is rather difficult to remove these films from the glass plate without breaking. Upon drying in an ambient environment, these films become so brittle that they break into small pieces upon a gentle touch. By increasing the polymer content above 20wt%, tough and flexible films are obtained when the films remain wet. However, at dry state, a SPES concentration up to 35wt% is necessary to obtain a tough film. This information is significant for the spinning process: the coating is located on the outside of the fiber and it therefore should be strong enough to withstand the friction from conducting rollers and possible stretching. On the other hand, it is required that the composite fiber should be mechanically stable at dry state. As indicated by the initial experiments, the composite fibers become brittle when the coating layers are brittle and show good adhesion to the support. Therefore, the coating layer itself needs mechanical stability. These experimental considerations indicate that a high SPES content is required.

Table 4.3 *Observation of SPES films in wet and dry state.*

SPES conc. (wt%)	Wet state	Dry state
10	Opalescent, soft	Clear, brittle
15	Opalescent, soft	Clear, brittle
20	Opalescent, flexible	Clear, brittle
25	Opaque, flexible	Clear with droplets, rigid
30	Opaque, tough	Clear with droplets, rigid
35	Opaque, tough	Clear with droplets, tough

To quantify the mechanical properties, the single cast SPES films are dried in air and their stress-strain behavior is tested. Figure 4.4 shows the stress-strain behavior of two SPES films at the concentration of 30 and 35 wt%, respectively. It can be seen that a 5wt% increase of SPES concentration influences the mechanical failure behavior significantly. Films from a 30wt% solution show a lower fracture stress, of about 24.1 MPa compared to 32.0 MPa for the films from a 35wt% solution. Moreover, the maximum strain before film

rupture increases from 1.23% to 3.56%. The initial stress for the 30wt% film is higher than that of the 35wt% film because of difference in thickness. The significant change of mechanical properties indicates that concentration increase transforms an extremely brittle film to a more flexile one.

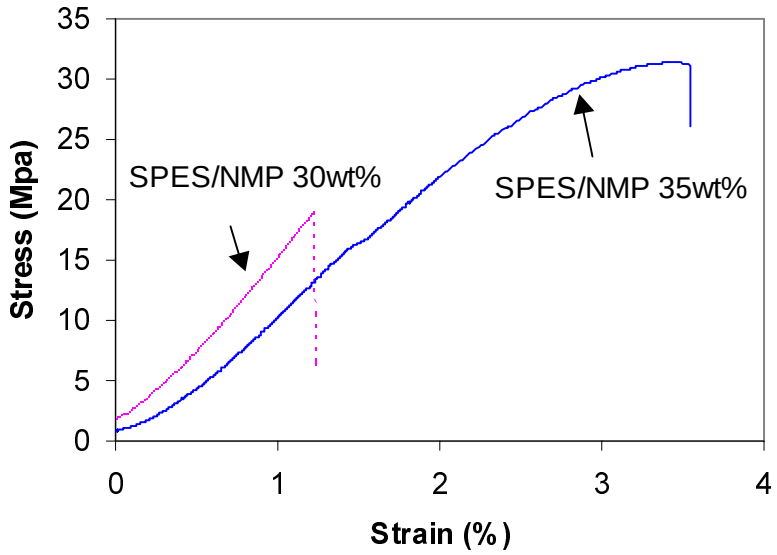

Figure 4.4 *Tensile test of SPES/NMP films made from SPES/NMP solutions coagulated in water.*

Figure 4.5 shows the micro-structure in the central part of SPES films coagulated in water with different SPES concentrations in the solution. Films from a 20wt% solution (Figure 4.5 (A)) show a nodular structure with only weak bridges between the nodules. The nodule size is about 40-60 nm (including about 4 nm platinum coating). Films cast from a 30wt% solution have a similar structure with more interconnections between the nodules having the appearance of local melting upon contact. With a SPES concentration of 35wt%, an interconnected cellular structure is obtained which is completely different from the other two. A further proof of improved mechanical toughness is the bright and fluffy structure observed in the photo, probably caused by the plastic deformation of the cell walls upon breaking. We interpret the transition from the nodular to cellular structure to be responsible for the mechanical strength increase with the increase of polymer concentration. Unfortunately, the solutions with a concentration above 30wt% SPES cannot be used for double-film casting or co-extrusion spinning due to its high viscosity. With this in mind, we proceed to experiments with the highest SPES concentration of 30wt% as the coating solution, which forms a mechanically stable film at wet state with sufficient mechanical strength at dry state.

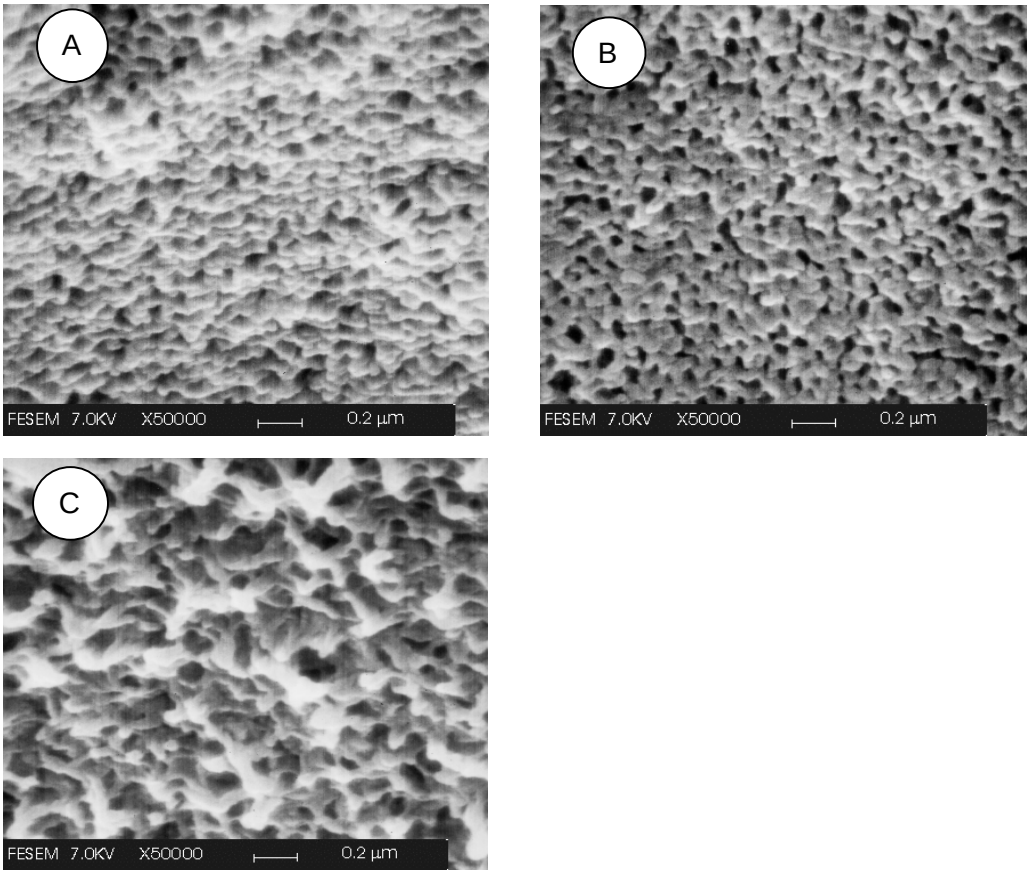

Figure 4.5 *FESEM pictures of SPES films prepared from immersion of SPES/NMP (A) 20wt%; (B) 30wt%; (C) 35wt%, solution in a tap water at room temperature. Casting thickness: 50 µm.*

4.3.3 Adhesion of SPES layer onto PSf layer

The previous section discussed the first problem encountered in the co-extrusion of dense hydrophilic materials onto porous hydrophobic support membranes. The second problem, interlayer adhesion, is addressed below by performing a systematic study in double-layer casting of flat membranes. The support membrane is a polysulfone/NMP solution of 25wt%. Furthermore, the influence of the additive (diethylene glycol) will be investigated. The additive acts as a non-solvent and results in a more rapid demixing of the support membrane [27], which may influence the adhesion.

4.3.3.1 Effect of polymer concentration and volatile co-solvent in coating solution

Figure 4.6 and Table 4.4 summarize the results of a systematic parameter study. At a low concentration of SPES in the coating solution, the coating layers completely separate from the PSf support. In fact, the coating layers are already separated even in the wet state. By using coating solutions of 25wt% SPES, the adhesion improves considerably. The SPES film partly separates but

the area with good adhesion is larger than the delaminated area. We attribute this to a lateral heterogeneity in the phase separation kinetics. With a further increase of SPES concentration to 30wt%, an excellent adhesion of SPES to PSf is obtained. The phenomena can be qualitatively understood by a decrease of water diffusion into the interface between SPES and PSf solution. As listed in Table 4.5, a SPES 30wt% solution in NMP has viscosity at zero shear rate of 22000 cP; whereas the viscosity at 25wt% is 6300 cP, less than one third of the former; an extremely low viscosity of a 20wt% solution is found being 380 cP. For a simplified estimation, the Stokes-Einstein equation gives an inverse relationship between diffusion coefficient D and viscosity. Therefore, the approximate ratios of water diffusion coefficients in a 30wt% and a 25wt% solution are 1.7% and 6.0% of that in a 20wt% solution, respectively. We hypothesize that the polymer chains can diffuse freely resulting in an entangled “interdiffusion” layer as long as no water reaches the interface. This "interdiffusion" stops when the non-solvent (water) reaches the solution forming the porous support membrane. Hence, the longer time available for the diffusion results in better adhesion. SPES/NMP solution of 30wt% is the most viscous solution resulting in the slowest water inflow and the best adhesion for the final double layers. The authors are aware that the same argument of slow diffusion with increasing polymer concentration holds for the polymer interdiffusion. However, this extremely complex phenomenon is beyond the purpose of this paper and requires more work.

Table 4.4 *Adhesion and mechanical properties of double layer films cast from SPES solutions on PSf solutions.*

Support	Coating solution (wt%)			Wet state	Dry state
	SPES	NMP	Acetone		
A	20	80	(-)	Separated	Separated, SPES film brittle
	25	75	(-)	Good adhesion	Good adhesion, brittle
	30	70	(-)	Good adhesion	not brittle, neither flexible
	20	40	40	Separated	Separated
	30	35	35	Good adhesion	Good adhesion, not brittle
B	20	80	(-)	Separated	Separated, brittle
	30	70	(-) [a]	Good adhesion	Good adhesion, not brittle
	30	70	(-) [b]	Separated	Separated
	20	40	40	Separated	Separated
	30	35	35 [a]	Good adhesion	Partly separated
	30	35	35 [b]	Separated	Separated

[a] In a controlled condition with humidity of 15%. Support solution was still clear; [b] In the ambient condition. Support solution was already demixed before casting the second layer. Solution A: PSf/NMP 25/75wt%. Support solution B: PSf/NMP/DEG 17/52.4/30.6wt%.

SPES conc. (wt%)	Solvents	
	NMP	NMP/Acetone, 50/50
20	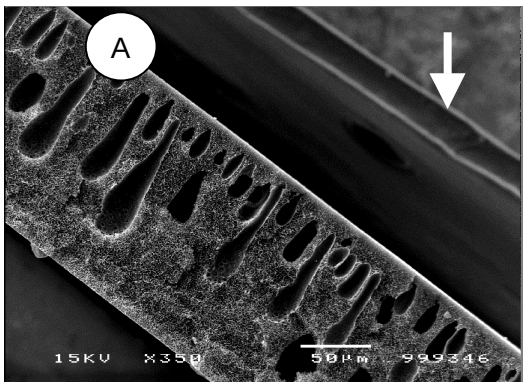	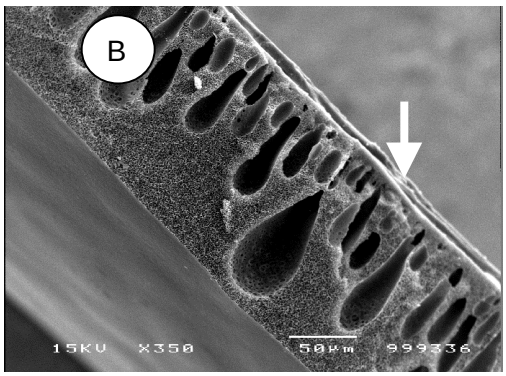
25	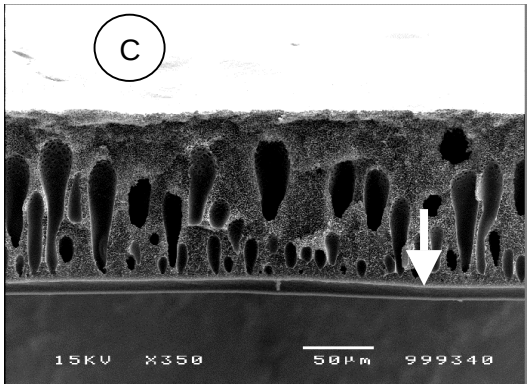	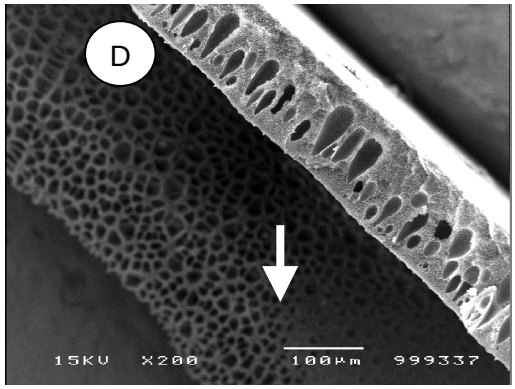
30	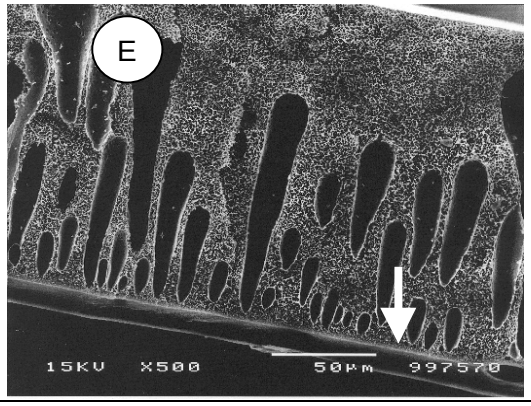	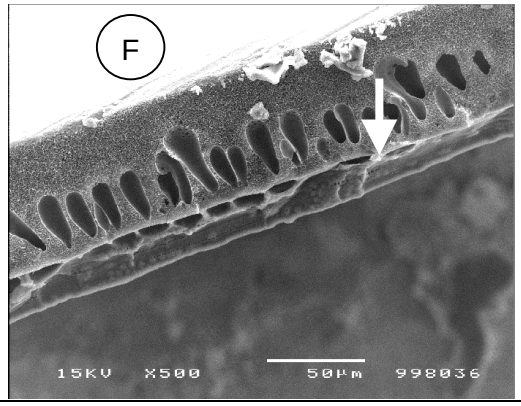

Figure 4.6 *Adhesion of SPES/NMP solutions and SPES/NMP/Acetone solutions on PSf/NMP 25wt% solution. Arrow refers to the coating layer. A, C, E: SPES/NMP solution at 20, 25, 30wt%; B, D, F: SPES/NMP/Acetone solution at 20, 25, 30wt%; NMP/acetone ratio: 50/50.*

When acetone is added to the coating solution, only the 30wt% solution shows good adhesion to the support. The coating layer prepared from a 20wt% solution is brittle and damaged by sample preparation. For a coating solution of

25wt%, the coating layer delaminates from the support and thus, only the bottom side of the SPES layer is observable. Nevertheless, an increase in the SPES concentration results in a better adhesion.

Table 4.5 *Viscosity at zero shear rate and estimated diffusion coefficients of SPES solutions.*

SPES conc. (wt%)	Viscosity (cP)	Ratio of estimated diffusion coefficients
20	380	1.0
25	6300	0.06
30	22000	0.017

Solvent: NMP. Temperature: 25^{o}C.

4.3.3.2 Effect of solvent in support solutions

A casting solution of PSf/NMP forms a relatively dense layer indicated by finger structures and closed cells. Non-solvent additives can make the support open by decreasing the "solvent power" of the support solution [28]. However, this change in support solution may affect the adhesion between the coating layer and the support membrane.

A rapidly demixing polysulfone/NMP solution can be achieved by adding diethylene glycol up to 30.6wt%. Within less than two seconds, the solution becomes white only being in contact with ambient air having a humidity of about 55%. As seen in Table 4.4, after exposing this solution to air for 10 seconds, the coating solution of PES/NMP 30wt% does not adhere to PSf. However, under controlled environment with humidity less than 15%, this coating solution shows a good adhesion to the support layer. Quite similar results are shown for the adhesion property between the additive-doped support and the original PSf solution. Both SPES/NMP and SPES/NMP/Acetone solutions at 30wt% show very good adhesion to the PSf/NMP/DegOH layers as can be seen in Figure 4.7 (A). Moreover, a much more porous support structure is obtained compared to the original solution without loss in adhesion property.

The double-layer casting of flat sheet membranes reveals that an increase of the SPES concentration results in a mechanically stable and good adhering coating layer. Adhesion is not influenced by the additive inside the support solution if the environmental humidity is at a low level. The next paragraph describes the co-extrusion of composite hollow fibers based on these observations. Diethylene glycol is added to the support dope to prepare an open support membrane.

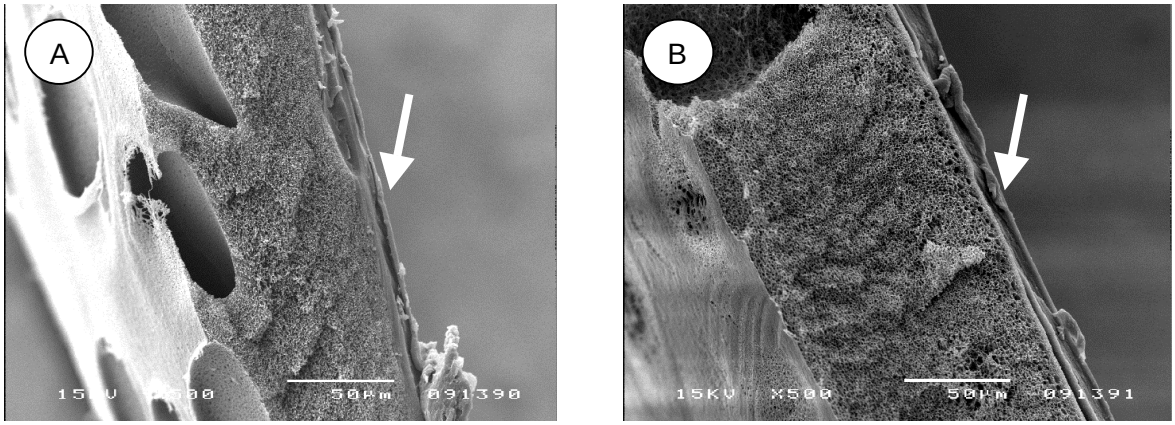

Figure 4.7 *SEM photos of double layer films from A, SPES/NMP 30wt%; B, SPES/NMP/Acetone, 30/35/35wt%. Support solution: PSf/NMP/Diethylene glycol, 17.0/52.4/30.6 wt%. Arrow refers to the coating layer.*

4.3.4 Spinning of double-layer membranes

As can be seen in Figure 4.8, six membranes are prepared from a SPES/NMP and SPES/NMP/acetone solution, respectively, and at a SPES concentration of 20, 25, 30wt%. With respect to the SPES/NMP coating solution, a concentration increase from 20wt% to 30wt% shows a large improvement in adhesion. With an air gap of 30 mm, the contact time between coating and support solutions is about 0.3 seconds at a spinning speed of 6 $m.min^{-1}$. In such a short time interval, the concentration effect is a predominant factor. The lowest SPES concentration results in a separated coating layer as shown in Figure 4.8 (A). A SPES concentration of 25 and 30 wt% results in composite membranes with good adhering layers. The coating solutions containing acetone give also very good adhesion. However, a concentration as low as 20wt% appears to be sufficient.

Composite hollow fiber membranes show high flexibility in both wet and dry state after immersion in glycerol. However, without any glycerol addition, the membranes become brittle upon drying when the coating concentration is lower than 25wt%. Mechanically stable composite membranes are obtained when the SPES concentration is 30wt% as shown in Table 4.6. In the dry state, the composite membrane shows similar mechanical properties as the coating layer itself and the fiber no longer maintains the flexibility of the support structure. We therefore conclude a similarity in mechanical behavior between the coating layer material (see single layer experiments) and the composite structure.

SPES conc. (wt%)	Solvents	
	NMP	NMP/Acetone, 50/50
20	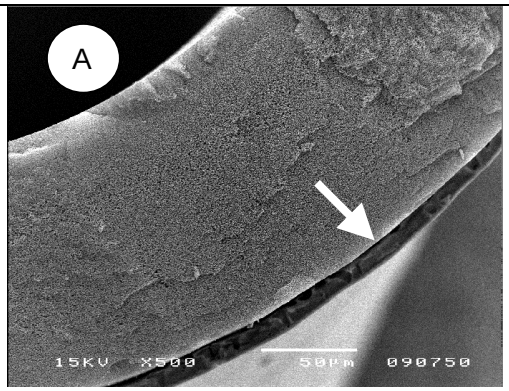	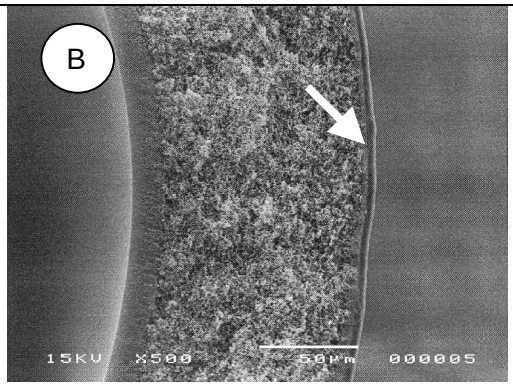
25	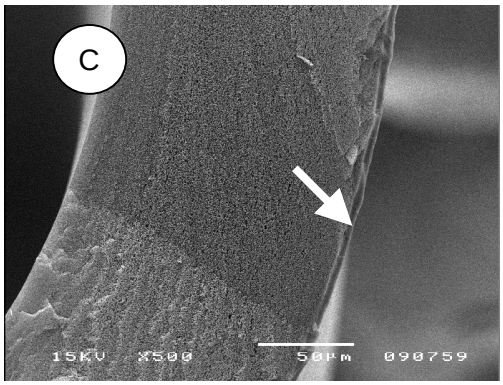	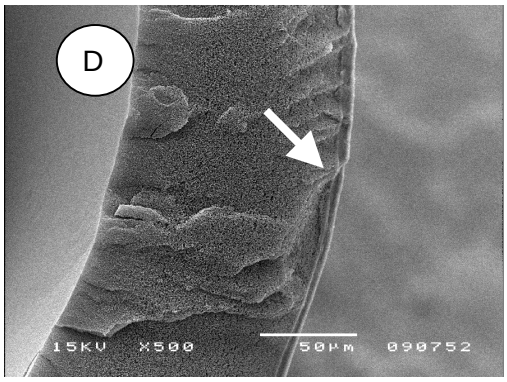
30	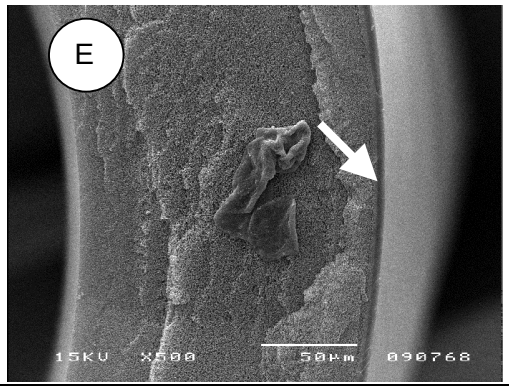	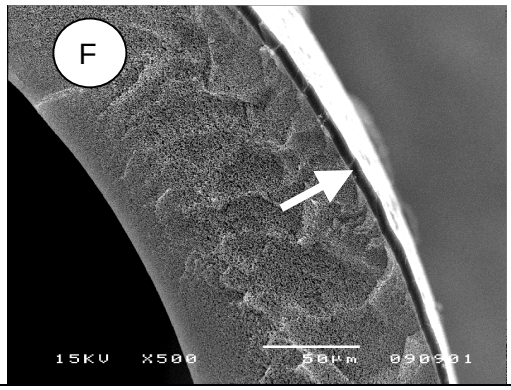

Figure 4.8 *SEM photos of SPES/NMP and SPES/NMP/Acetone coatings. A, C, E: SPES/NMP coating layers with a polymer content of 20, 25, 30wt% respectively; B, D, F: SPES/NMP/Acetone coating layers with a polymer content of 20, 25, 30wt% respectively. Arrow refers to the coating layer. Spinning speed: 6 m.min^{-1}. Air gap: 30 mm. Flow rate: 0.43 ml.min^{-1}. Temperature: 21± 0.5 ^{o}C.*

Table 4.6 *Mechanical behavior of the composite hollow fiber membranes.*

Coating solution composition (wt%)			Wet	Dry	Glycerol
SPES	**NMP**	**Acetone**			
(-)	100	(-)	Flexible	Flexible	Flexible
20	80	(-)	Flexible	Brittle	Flexible
25	75	(-)	Flexible	Brittle	Flexible
30	70	(-)	Flexible	Rigid	Flexible
20	40	40	Flexible	Brittle	Flexible
25	37.5	37.5	Flexible	Rigid	Flexible
30	35	35	Flexible	Rigid	Flexible

Support solution: PSf/NMP/DegOH, 17.0/52.4/30.6wt%. Wet state: stored in water; Dry state: dried in air. Glycerol: immersed in 20wt% glycerol solution for 48 hours, then dried in air. Spinning speed, 6 $m.min^{-1}$; air gap: 30 mm; coating flow rate: 0.43 $ml.min^{-1}$.

4.3.5 Separation performance of composite hollow fibers

The composite fibers are used as supported liquid membranes for copper transport. We anticipate the co-extruded membrane to have improved life-time performance as a stabilized supported liquid membrane as well as a relatively high flux. The polysulfone support membrane without the coating has a flux of 5.1 $x10^{-9}$ $mol.cm^{-2}.s^{-1}$, which is comparable to porous microfiltration membranes such as Accurel or Celgard [26]. However, an extremely low flux for Cu^{2+} is obtained (0.15 $x10^{-9}$ $mol.cm^{-2}.s^{-1}$) for the composite membrane made from a coating solution of 30wt% (with a coating layer thickness of 2 μm). This low copper flux for the composite membrane is caused by the low ion exchange capacity of the SPES top layer, which exhibits a high resistance towards the transport of copper ions.

Gas permeation experiments are performed with the composite hollow fibers using helium, nitrogen and carbon dioxide (see Table 4.7). Because the experimentally observed selectivity is even lower than the Knudsen selectivity, it is suggested that the SPES coating is a porous layer having pores larger the free path length of the gases. This is in agreement with FESEM analysis performed on the single-cast SPES layers described earlier.

Finally, the membranes are characterized with respect to their retention and aqueous flux characteristics in pressure-driven applications. Table 4.8 summarizes the permeation experiments for a variety of solutes. All experiments are carried out as single component experiments and the membranes remained in the wet state. HT-SPES-25 is a composite membrane made from a coating solution of SPES/NMP /acetone solution at 25wt%. It is more porous than HT-SPES-30, thus all retention values for this membrane are

lower than for the second membrane. Almost all copper sulfate and sodium sulfate pass through this membrane. However, retentions of 6.3% for $CuSO_4$ and 20.7% for Na_2SO_4 are obtained for HT-SPES-30. In addition, charged dye molecules are also used as model compounds. Methyl green is a positive charged dye with a molecule weight of 472.51 $g.mol^{-1}$. Although it is large in size, its retention is low, 10% and 34% for both membranes respectively. For sunset yellow, a negatively charged dye of molecular weight of 450.38 $g.mol^{-1}$, a higher retention is obtained, 12% for HT-SPES-25, but 87% for HT-SPES-30. Moreover, the retention for a negatively charged procion blue of molecular weight of 840.12 $g.mol^{-1}$ is even higher; 28% for the first membrane and 92% for the second membrane.

Table 4.7 *Gas permeation results for SPES composite hollow fiber membranes.*

SPES conc. (wt%)	**Gas pair selectivity**		
	α (N_2/He)	α (CO_2/He)	α (CO_2/N_2)
	2.6*	3.3*	1.3*
25	1.2	1.3	1.1
30	1.3	1.5	1.2

* Knudsen selectivity.
Coating solutions: SPES/NMP/Acetone, NMP/Acetone 50/50 wt%.

Table 4.8 *Nanofiltration results of SPES composite hollow fiber membranes*.*

Membrane		**HT-SPES-25**	**HT-SPES-30**
Coating solution composition (SPES/NMP/acetone, wt%)		25.0/37.5/37.5	30.0/35.0/35.0
Clean water permeability ($l.m^{-2}.hr^{-1}.bar^{-1}$)		8.9-12.9	0.5-0.8
Solute retention (%)	$CuSO_4$	0.0	6.3
	Na_2SO_4	1.2	21
	Methyl green	10	34
	Sunset yellow	12	87
	Procion blue	28	92

* The hollow fiber membranes are kept wet by immersing in a 20 wt% glycerol water solution.

These results can be explained by two factors: steric (sieving) and Donnan exclusion effects [29-32]. SPES has sulfonic acid groups on the main chain, and therefore it rejects solutes with the same charge, i.e. sunset yellow and procion blue. Moreover, it shows a low rejection for positive charged solute, i.e. methyl green. On the other hand, sieving effect contributes as well. HT-SPES-25 membrane is a rather porous membrane compared with HT-SPES-30. Hence, the retention is much higher for HT-SPES-30 than for HT-SPES-25 when the molecule has a comparable hydrodynamic size as the pore size of the coating layer.

4.4 Conclusions

Integral SPES composite hollow fiber membranes are successfully prepared by co-extrusion of SPES solutions onto polysulfone solutions. In terms of mechanical and adhesion properties, the SPES concentration in the coating solution is of key importance to obtain a good composite membrane. A nodular to cellular structure is observed when the SPES concentration changes from 20 to 35wt% and this corresponds to an improvement in mechanical properties. Adhesion of the coating to the PSf support is also improved by increasing the SPES concentration of the coating solutions.

The composite hollow fiber shows an extremely low copper ion transport in supported liquid membrane system and no selectivity for He/N_2, He/CO_2 and N_2/CO_2 in gas separation. The membrane shows low inorganic salt retention and high retention for charged organic dye molecules. The concept of a co-extruded membrane with ion exchange functionality in the coating layer shows potential in fabrication of nanofiltration membranes as well as tight hydrophilic ultrafiltration membranes.

4.5 References

[1] S. Loeb and S. Sourirajan, eds., Sea water demineralization by means of an osmotic membrane, Advances in Chemistry Series 38: Saline water conversion-II, American Chemical Society, 1963.

[2] J. E. Cadotte and R. J. Petersen, in Synthetic Membranes, Vol I. Desalination, ACS symp. Ser. No.153 (A. F. Turbak, ed.), American Chemical Society, Washington, DC, 1981.

[3] R. J. Petersen, Composite reverse osmosis and nanofiltration membranes, J. Membrane Sci., 83 (1993) 81-150.

[4] W. J. Schrenk and T. J. Alfrey, Co-extruded multilayer polymer films and sheets, in D. R. Paul and S. Newman, (ed.), Polymer blends, Vol. 2, Academic Press, Inc., New York, 1978, pp.129.

[5] W. C. Chen, J. H. Chen, S. Y. Yang, J. Y. Cherng, Y. H. Chang, and B. C. Ho, Preparation of gradient-index(GRIN) polymer fibers for imaging applications, J. Appl. Polym. Sci., 60 (1996) 1379-1383.

[6] B.-T. Liu, W.-C. Chen, and J.-P. Hsu, Mathematical modeling of a co-extrusion process for preparing gradient-index polymer optical fibers, Polymer, 40 (1999) 1451-1457.
[7] C.-C. Tsai, T.-J. Liu, Y.-H. Chang, and W. T. W. Tseng, Numerical Simulation of an optical fiber-forming process, Chem. Engr. Sci., 52 (1997) 221-223.
[8] J.-Y. Chiou, P.-Y. Wu, C.-C. Tsai, and T.-J. Liu, An integral analysis for a co-extrusion process, Polym. Eng. Sci., 38 (1998) 49-59.
[9] W. A. Gifford, A three-dimensional analysis of co-extrusion, Polym. Eng. Sci., 37 (1997) 315-320.
[10] C.-C. Ji, J.-C. Yang, and W.-S. Lee, Mechanics of steady flow in coextrusion fiber spinning, Polym. Eng. Sci., 36 (1996) 1399-1409.
[11] O. M. Ekiner, R. A. Hayes, and P. Manos, USP 5,085,676, 1992.
[12] Y. Kusuki, T. Yoshinaga, and H. Shimazaki, USP 5,141,642, 1992.
[13] Y. Kusuki, K. Nakagawa, and T. Yoshinaga, Preparation of asymmetric polyimide hollow fiber membrane, International Congress on Membrane and Membrane Processes, Chicago, USA, 1990.
[14] H. Suzuki, K. Tanaka, H. Kita, K. Okamoto, H. Hoshino, T. Yoshinaga, and Y. Kusuki, Preparation of composite hollow fiber membranes of poly(ethylene oxide)-containing polyimide and their CO_2/N_2 separation properties, J. Membrane Sci., 146 (1998) 31-37.
[15] W. Henne, G. Dunwey, W. Schmitz, R. Rohle, and F. Lawitzki, USP 4,267,047, 1981.
[16] K. Li, D. L. Wang, D. F. Li, and W. K. Teo, Internally staged permeator prepared from annular hollow fibers for gas separation, AIChE, 44 (1998) 849-858.
[17] M. Sakashita, T. Sakamoto, and Y. Harada, JP63-218213, 1988.
[18] T. Yanamoto, JP6219205, 1987.
[19] S. Li and Z. Liu, CN 1103814A, 1995.
[20] S. Nago and Y. Mizutani, Microporous polypropylene hollow fiber with double layers, J. Appl. Polym. Sci., 56 (1995) 253-261.
[21] S. Nago and Y. Mizutani, Microporous polypropylene hollw fiber with double layers, J. Membrane Sci., 116 (1996) 1-7.
[22] K. Komatsu and N. Okamoto, JP4-45830, 1992.
[23] U. Holzki, H. J. Muller, and T. Renner, USP 5,620,790, 1997.
[24] S. Tamaru, K. Yamamoto, O. Tanaka, H. Nishibayashi, and O. Inoue, USP 5,225,131, 1993.
[25] S.-G. Li, G. H. Koops, M. H. V. Mulder, T. v. d. Boomgaard, and C. A. Smolders, Wet spinning of integrally skinned hollow fiber membranes by a modified dual-bath coagulation method using a triple orifice spinneret, J. Membrane Sci., 94 (1994) 329-340.
[26] M. C. Wijers, M. Jin, M. Wessling, and H. Strathmann, Supported liquid membranes modification with sulphonated poly(ether ether ketone): permeability, selectivity and stability, J. Membrane Sci., 147 (1998) 117-130.

[27] T. He, PES microfiltration membranes: Effect of small organic molecules in membrane formation, Master Thesis, Dalian Institute of Chemical Physics, Dalian, 1997.
[28] T. P. Hou, S. H. Dong, and L. Y. Zheng, The study of mechanism of organic additives action in the polysulfone membrane casting solution, Desalination, 83 (1991) 343-360.
[29] L. P. Raman, M. Cheryan, and N. Rajagopalan, Consider nanofiltration for membrane separations, Chem. Eng. Prog., 90 (1994) 68-74.
[30] T. Tsuru, S. Nakao, and S. Kimura, Calculation of ion rejection by extended Nernst-Planck equation with charged reverse osmosis membranes for single and mixed electrolyte solutions, J. Chem. Eng. Japan, 24 (1991) 511-517.
[31] W. R. Bowen and H. Mukhtar, Characterization and prediction of separation performance of nanofiltration membranes, J. Membrane Sci., 112 (1996) 263-274.
[32] J. M. M. Peeters, J. P. Boom, M. H. V. Mulder and H. Strathmann, Retention measurements of nanofiltration membranes with electrolyte solutions, J. Membrane Sci., 145 (1998) 199-209.

Appendix to Chapter 4 Characterization of ion exchange membranes for ion transport

Abstract

Several cation ion exchange polymers and blend materials have been investigated in terms of swelling, ion permeability and water permeability. Sulfonated poly (ether ether ketone) (SPEEK) is found to have the lowest resistance for ion transport. In terms of equivalent flux, SPEEK membrane has similar fluxes for three different ions, K^+, Cu^{2+} and Al^{3+}. Certain minimum SPEEK concentration in blend of SPEEK and polyethersulfone or sulfonated polyethersulfone is necessary to obtain a high flux. A nonlinear behavior of swelling, ion and water permeation for the blend materials is observed.

A4.1 Introduction

A supported liquid membrane (SLM) is particularly suitable for the removal or recovery of valuable and toxic heavy metal ions from industrial effluents due to its high permeability and selectivity. However, the industrial application of SLMs is still in an embryonic stage because of a short life-time in a practical operation [1]. A concept of improving the life-time of the support liquid membrane had been proposed by using a lamination of an ion exchange coating layer on an Accurel flat porous membrane [2]. An improved life-time indicated that the ion exchange coating layer may be a solution for the stabilization problems.

Ion exchange materials have been applied in liquid membranes [3-8]. In a hybrid liquid membrane (HLM) system, the organic phase is separated from the aqueous phases by two ion exchange membranes (IEMs). A reasonable permeability of copper and silver was found [3]. Moreover, a lower organic concentration in the aqueous phases was found compared to porous support membrane [4, 5], which indicates an improved life-time of SLMs by blocking the diffusion passage of the carrier by ion exchange materials.

It is our aim to prepare a composite hollow fiber membrane with an ion exchange coating layer. However, commercial ion exchange membranes are mostly cross-linked and can not be used for coating purposes such as co-extrusion [9] or dip-coating [10]. In this paper, different materials are selected as the most suitable coating layer and characterized in terms of the ionic transport permeability. The permeability results are also related to the material properties, such as ion exchange capacity (IEC), water uptake, and water permeability.

A4.2 Experimental

A4.2.1 Materials

Copper sulfate pentahydrate ($CuSO_4.5H_2O$, cryst. extra pure), potassium sulfate (K_2SO_4) and aluminum sulfate-18-hydrate ($Al_2(SO_4)_3.18H_2O$) were purchased from Merck. All chemicals are of analytical grade and used without further purification. Sulfuric acid (95-98%) was purchased from Merck as well. Milli-Q (Millipore) ultrapure water was used in all experiments.

Several polymers have been used and their specifications are listed in Table A4.1. Sulfonated polysulfone (SPSf-1 and SPSf-2) were prepared in our lab following the procedure of Quentin [11]. Sulfonated poly (ether ether ketone) (SPEEK) was prepared following the method by Bishop et al [12]. Carboxylated polysulfone (PSfCOOH) was kindly supplied by NRC, Canada. Sulfonated polyethersulfone (SPES) was obtained from AKZO Nobel.

Table A4.1 *Specifications of ion exchange materials.*

Polymer	**IEC (meq.g^{-1})**	**Degree of substitution**
SPSf-1	0.22	0.10
SPSf-2	0.68	0.30
SPES	0.43	0.10
PSf-COOH	-	0.86
SPEEK	2.79	0.99

A4.2.2 Membrane preparation

Polymer solutions were prepared by dissolving the polymers at a concentration of 20wt% in NMP at 21-22^{o}C. After filtration with a 15 μm metal filter, the solutions were degassed for 4 hours and then cast onto a glass plate with a knife of 300 μm in thickness. The films were dried in an oven at 50^{o}C overnight and further dried in a vacuum oven at 30^{o}C for 48 hours. All dried membranes were about 25.0 μm thick within an error of 5%.

Single component membranes consist of substituted polymers, i.e. SPSf-1, SPSf-2, PSfCOOH, SPES, and SPEEK. Blend membranes consist of SPEEK/SPES at ratios of SPEEK and SPES of 9/1, 4/1, 3/2, 5/5. In case of blending SPEEK and PES , the ratios are 9/1, 4/1, 3/2, 5/5 and 1/3 respectively.

A4.2.3 Characterization of sulfonated polymers

The degree of sulfonation and the IEC were determined according to the same procedure as described recently [10]. The degrees of swelling were determined using the following solutions: H_2SO_4 (2.0 M), $CuSO_4$ (0.025M), K_2SO_4 (0.025M) and $Al_2(SO_4)_3$ (0.0083M).

A4.2.4 Ion permeation experiment and water transport

The ion exchange membranes were cut into pieces with the same size as diffusion dialysis cell, as seen in Figure A4.1. They were stored in a H_2SO_4 solution (2 M) before the permeation experiment.

The same setup for determination of ion permeability was used to measure the water transport across the ion-exchange membranes. A $CuSO_4$ solution (0.025M) was in the feed reservoir and a H_2SO_4 solution (2.0 M) in the strip reservoir. A capillary was connected to each reservoir with which the volume of the aqueous phase was recorded as a function of time. The water permeability was estimated from the slope of the curve. The circulation speed was kept at 1.0 $ml.s^{-1}$ to prevent turbulence of the water level in the capillary meter.

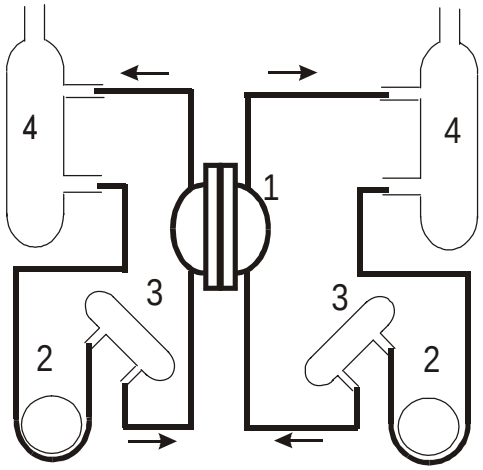

Figure A4.1 *Schematic of permeation set-up for ion transport. 1, Flat membrane cell; 2, Feed or strip reservoir; 3, Buffer vessel; 4, Peristaltic pump.*

A4.3 Results and discussion

A4.3.1 Sulfonation degree and degree of swelling of different materials

Four different types of polymers are used: PSfCOOH with a substitution degree of 0.86; SPES, SPSf-1 and SPSf-2, sulfonated polymers with a low IEC (< 1.0 $meq.g^{-1}$); SPEEK with an IEC higher than 1.0 $meq.g^{-1}$; blend materials from SPEEK and PES or SPEEK and SPES.

Considering the various homopolymers, the swelling values for three kinds of salt solutions fall into two categories: a low swelling degree for PSfCOOH, SPES, SPSf-1 and SPSf-2 and a high swelling degree (SPEEK). The swelling is controlled predominantly by the amount of sulfonated groups inside the polymers as seen in Table A4.1 and A4.2. SPEEK has a water uptake of 440wt% due to its high ion exchange capacity of 2.79 $meq.g^{-1}$, whereas the

other polymers show a water uptake less than 12wt% due to their relatively low degree of sulfonation. Because of the low dissociation coefficient of the -COOH group, carboxylated polysulfone shows only a water uptake of 8.1wt%, even though its degree of substitution is as high as 0.86. A similar trend is obtained for the swelling values in different salt solutions.

An interesting phenomenon is the swelling behavior of SPEEK in different salt solutions. The salt solutions are prepared in terms of the same SO_4^{2-} concentration in order to exclude the effect of the different concentration on swelling and permeation except sulfuric acid. The following sequence is obtained

H_2O > $Al_2(SO_4)_3$ (0.0083 M) > $CuSO_4$ (0.025 M) > K_2SO_4 (0.025 M) > H_2SO_4 (2 M)

A drastic decrease in swelling is observed by addition of salts. After exchanging, SPEEK is transformed from a proton form into the salt form, which substantially decreases the swelling [13]. However, a multi-valent cation can not easily be coupled with the fixed charges of the polymer matrix, which means more active sites are accessible to water compared to mono-valent ions. Furthermore, the concentration of the ions also influences the swelling since the activity of water molecules decreases with increase of the salt or acid concentration. This explains the lowest swelling of SPEEK in a sulfuric acid solution.

Table A4.2 *Swelling of different membranes in several aqueous solutions at 25°C.*

	Swelling (wt%)				
	H_2O	**H_2SO_4**	**$CuSO_4$**	**K_2SO_4**	**$Al_2(SO4)_3$**
SPSf-1	4.9	2.1	4.7	3.5	-
SPSf-2	11.9	11.8	14.3	6.5	12.2
SPES	8.1	3.8	9.5	1.4	4.1
PSfCOOH	6.5	3.4	7.8	2.3	2.1
SPEEK	440	50.0	73.4	56.4	309

In order to find a proper ion exchange value, SPES and PES are blended with SPEEK and an increase of the swelling degree can be observed when increasing the SPEEK content, as seen in Figure A4.2. At approximately 50wt% of SPEEK in the blend, the membranes show a dramatic increase in swelling value in all solutions and a strong nonlinear behavior can be observed. This will be discussed further.

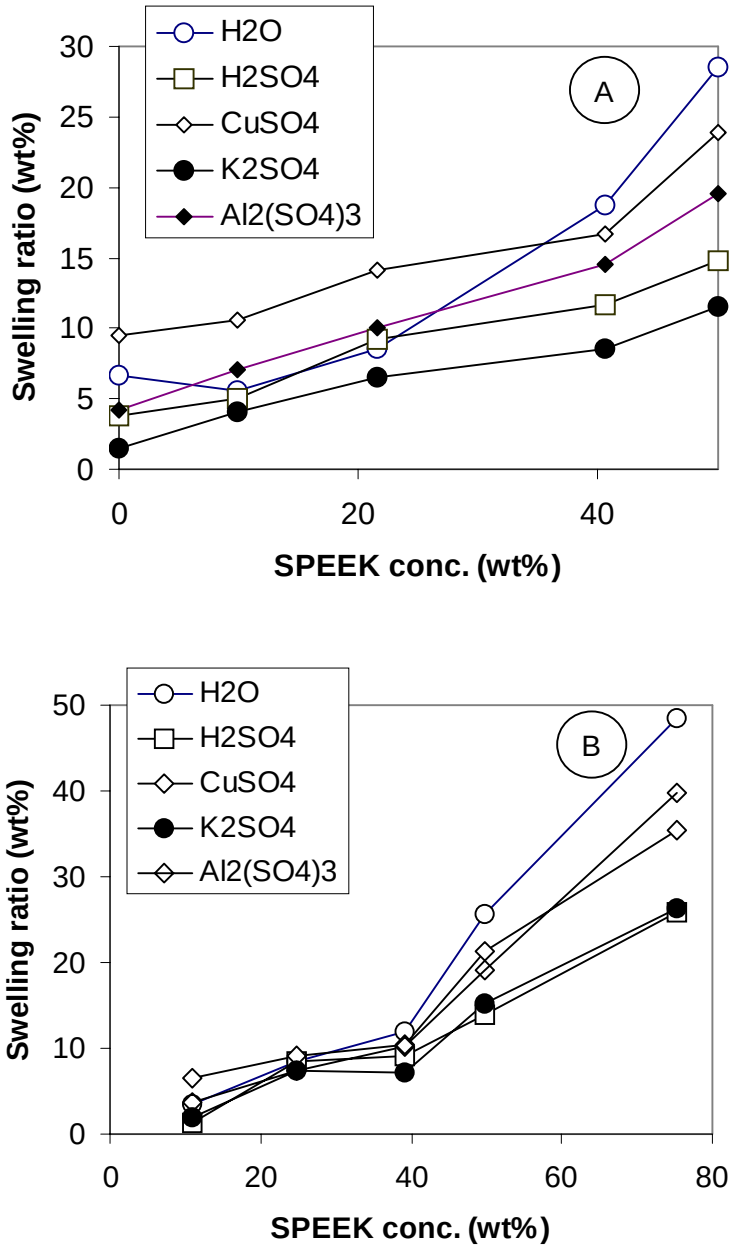

Figure A4.2 *Effect of the SPEEK content on the swelling of blend membranes. (A) SPEEK/SPES; (B) SPEEK/PES.*

A4.3.2 Ion permeability

As can be seen in Table A4.3, the ionic permeability of the homopolymers are low except for SPEEK. Negligible permeability of three ions is obtained for SPES probably because the experimental time is too short. Carboxylated polysulfone shows rather low ion permeability probably due to

the low dissociation coefficient of the carboxylated group. According to the results, SPEEK is the most promising material for ion transport due to its high degree of swelling. It is interesting that the equivalent fluxes for three ions are the same within an experimental error range. Compared to K^+, the equivalent flux of copper ion is 71.4 $x10^{-9}$ $mol.cm^{-2}.s^{-1}$, which is close to that of Al^{3+} of 72.6 $x10^{-9}$ $mol.cm^{-2}.s^{-1}$ and K^+ of 79.5 $x10^{-9}$ $mol.cm^{-2}.s^{-1}$. This can be understood by the fact that the actual transport process is dominated by the diffusion of quite mobile H^+ ions through the cation exchange membrane.

As can be seen in Figure A4.3, the permeability of ions can be manipulated by adjusting the SPEEK concentration in the blends. A clear transition of permeability is obtained at a SPEEK concentration in the range of 40 to 50 wt% for blends of SPEEK/SPES and SPEEK/PES, which is related to the swelling behavior as can be seen in Figure A4.2.

The results can be explained by the physical cross-linking of SPEEK with PES or SPES. Since two blending polymers have a quite different hydrophobicity, they most probably form a microphase separated structure. In this state, the exact structure is dependent on the composition of two polymers: a predominant compound forms a continuous phase and when composition is close to 50:50, a percolated structure, or a bi-continuous one may be obtained.

Table A4.3 *Single ion exchange membrane transport for ions.*

Membranes	**K^+ flux (10^{-9} $mol.cm^{-2}.s^{-1}$)**	**Cu^{2+} flux (10^{-9} $mol.cm^{-2}.s^{-1}$)**	**Al^{3+} flux (10^{-9} $mol.cm^{-2}.s^{-1}$)**
SPSf-1	-	0.74	-
SPSf-2	0.37	0.74	0.09
SPES	0	0	0
PsfCOOH	0.92	1.92	0.92
SPEEK	79.5	35.7	24.2

At a low concentration, SPEEK is dispersed in a continuous hydrophobic phase such as PES or SPES, and is therefore not easily accessible to the aqueous phase. The swelling is controlled by the surrounding hydrophobic phases which suppress the swelling of the isolated SPEEK domains. Only after the percolation of SPEEK and PES occurs, a free swelling of SPEEK is possible and the transport resistance is low. Further increase of SPEEK content does not lead to a decline in transport resistance.

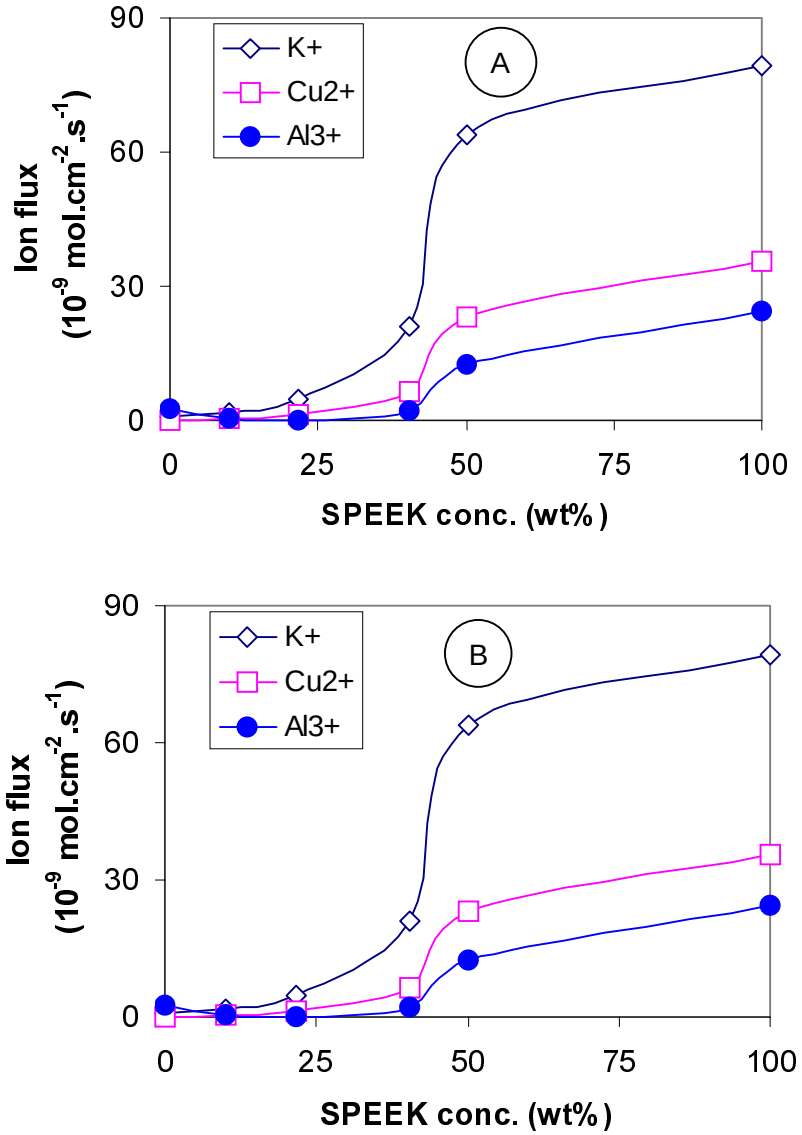

Figure A4.3 *Ionic flux as the function of the SPEEK composition in the blend. (A) SPEEK/SPES; (B) SPEEK/PES.*

A4.3.3 Water transport

The water permeability is an additional transport property of importance. Water molecules may either be transported together with the ions in a hydrated form or diffuse as free molecules once the polymer is in a swollen state. Figure A4.4 shows a similar phenomenon as ion transport with a sudden increase in water permeability at a SPEEK content of about 40 to 50wt%.

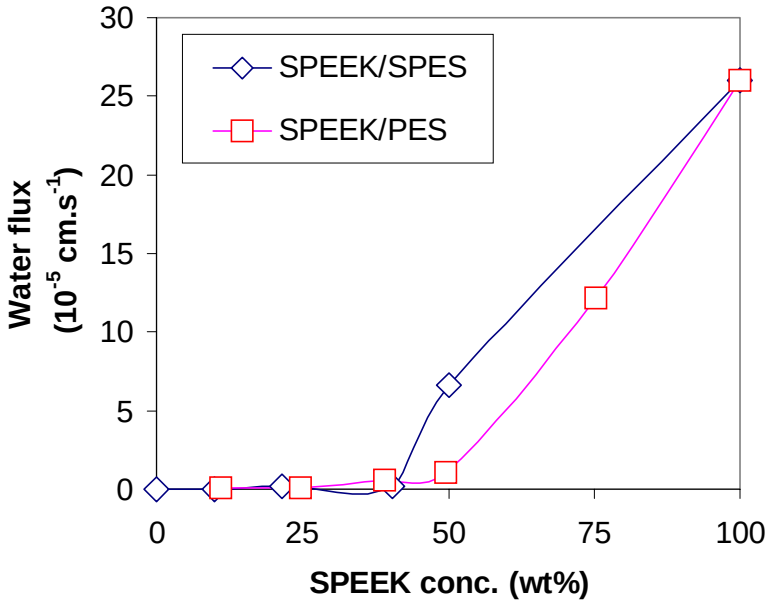

Figure A4.4 *Water flux of SPEEK/SPES and SPEEK/PES blend membranes as a function of the SPEEK concentration.*

A4.4 Conclusions

Several cation ion exchange polymers and blend materials have been investigated in terms of swelling, ion and water permeability. Carboxylated polysulfone as well as the sulfonated polysulfone with an ion exchange capacity lower than 0.7 meq.g^{-1} shows a rather high ion transport resistance. SPEEK shows the highest ion permeability. Properties of the blend membranes of SPEEK with PES or SPES indicate that certain threshold ion exchange capacity is necessary to achieve a low transport resistance.

A4.5 References

[1] A. J. B. Kemperman, D. Bargeman, T. van den Boomgaard, and H. Strathmann, Stability of supported liquid membranes: state of the art, Sep. Sci. Technol., 31 (1996) 2733-2762.

[2] M. C. Wijers, M. Jin, M. Wessling, and H. Strathmann, Supported liquid membranes modification with sulphonated poly(ether ether ketone): permeability, selectivity and stability, J. Membrane Sci., 147 (1998) 117-130.

[3] O. Kedem and L. Bromberg, Ion-exchange membranes in extraction processes, J. Membrane Sci., 78 (1993) 255-264.

[4] V. S. Kislik and A. M. Eyal, Hybrid liquid membrane (HLM) system in separation technologies, J. Membrane Sci., 111 (1996) 259-272.

[5] V. S. Kislik and A. M. Eyal, Hybrid liquid membrane (HLM) and

supported liquid membrane (SLM) based transport of titanium, J. Membrane Sci., 111 (1996) 271-281.
[6] R. Wodzki and G. Sionkowski, Recovery and concentration of metal ions. II multimembrane hybrid system, Sep. Sci. Technol., 30 (1995) 2763-2778.
[7] T. Kojima, S. Furusaki, and K. Satto, A fundamental study on recovery of copper with a cation exchange membrane: part 1. Ion exchange equillibria between cupric and hydrogen ions, Can. J. Chem. Eng., 60 (1982) 642-649.
[8] T. Kojima, S. Furusaki, and K. Satto, A fundamental study on recovery of copper with a cation exchange membrane: part 2. Tranfer rate of copper and hydrogen ion through a cation exchange membrane, The Can. J. Chem. Eng., 60 (1982) 650-658.
[9] T. He, M. H. V. Mulder, M. Wessling, and H. Strathmann, Preparation of composite hollow fiber membranes. Co-extrusion of dense hydrophilic coating onto porous hydrophobic support structures, Chapter 4, submitted to J. Membrane Sci..
[10] T. He, M. H. V. Mulder, and M. Wessling, Composite hollow fiber membranes as supported liquid membranes, Chapter 5.
[11] J. P. Quentin, USP 3,709,841, 1973.
[12] M. T. Bishop, F. E. Karasz, and P. S. Russo, Solubility and properties of a poly(aryl ether ether ketone) in strong acids, Macromolecules, 18 (1985) 86-93.
[13] K. Dorfner, Introduction to ion exchanger and ion exchangers, Walter de Gruyter & Co., Berlin, 1991.

Chapter 5 Composite hollow fiber membranes as supported liquid membranes

Abstract

The instability of supported liquid membranes significantly limits their wide application in industry. Improvement of the life-time can be achieved by applying a hydrophilic coating layer to prevent the leakage of the organic liquid membrane. A SPEEK coating layer is dip-coated onto the outside surface of a polysulfone or an Accurel polypropylene hollow fiber. Investigation on the solvents for SPEEK identifies several potential solvent groups. A defect free SPEEK coating layer has been prepared based on three criteria, volatility, compatibility and spreading. In addition, the polymer concentration in the coating solution and the number of the coating steps have been varied. Copper permeation results show an improvement in the stability compared to an uncoated membrane. An initial research on an encapsulated composite membrane with SPEEK layers demonstrates that it is a potential solution for stability improvement, but further development is necessary.

5.1 Introduction

Supported liquid membrane (SLM) technique is an efficient technique for the extraction of heavy metal ions from industrial effluents. The advantages of SLM are a high ion flux and a high selectivity. However, the continuous loss of organic membrane phase causes a drop of flux and selectivity during a long-term operation, and therefore is hampering the further development of the technology. The instability of SLM is ascribed to the loss of the liquid phase because of several possible mechanisms, such as solubility and emulsion formation [1].

To improve the membrane stability, several solutions have been proposed in literature. The first concept was an increase of the viscosity of the organic phase based on stiffening of the aqueous-organic interface to prevent gradual loss of membrane phase [2-4]. However, this resulted in a significant decrease of the flux. Another method was to apply a dense coating layer of polyvinyl chloride (PVC) [5-8]. The loss of organic phase continues since the hydrophobic polymer PVC, can not prevent the direct contact between the organic phase and the aqueous phase.

Interfacial polymerization (IP) is another often used technique in SLM stabilization. Frequently, a hydrophilic polyamide layer has been formed using multifunctional amines and acid chlorides as monomers [[8-11]. However, IP layer is permeable to mono-valent ions but not multi-valent ions [10]. Apart from interfacial polymerization, recently, plasma polymerization [12] was reported to form an ultra thin skin layer for stabilization of SLM. Although the loss of organic solvent decreases, lack of long term stability hampers further technical implementation.

Ion exchange materials in liquid membranes were investigated intensively in terms of transport [13-16] in a configuration consisting of two ion exchange membranes and an organic phase in between. To investigate the stability, an encapsulated composite membrane was prepared by lamination of two sulfonated poly (ether ether ketone) (SPEEK) layers onto a flat Accurel membrane with an organic phase in between [17]. This membrane demonstrated improved stability and moderate fluxes. However, the composite membrane showed adhesion problems due to the incompatibility of the hydrophilic SPEEK and the hydrophobic polypropylene. Moreover, this technique lacks the potential in terms of scale-up as well as reproducibility. Furthermore, it is difficult to prepare such a coating layer onto a porous Accurel membrane without pretreatment. Former researchers reported that SPEEK could dissolve in a protic high-boiling-point solvent, i.e. dimethyl formamide (DMF). This implicitly indicates that Accurel PP membrane could not be dip-coated with SPEEK without any hydrophilicity treatment. It implies as well that many support membranes, i.e. polysulfone (PSf), polyethersulfone (PES), can not be used as support membrane since the solvents of SPEEK dissolve the membrane material.

In this chapter, we will address a novel approach on dip-coating a SPEEK layer to both PSf and PP support membranes. A systematic selection of suitable solvents for SPEEK results in highly volatile solvents, such as methanol and ethanol. These new composite membranes are characterized with respect to their mass transport properties and their life-time as a supported liquid membrane.

5.2 Experimental

5.2.1 Materials

Poly (ether ether ketone) powder (450PF, Victrex, Mw 102000 $g.mol^{-1}$, specific density 1.34 $kg.l^{-1}$) was purchased from ICI. Two different support membranes were used in this experiment: a tailor-made porous polysulfone hollow fiber prepared as described earlier [18] and Accurel Q3/2 PP hollow fibers provided by Membrana, Germany (formerly AKZO Nobel. Membrana).

AG grade N,N-methylpyrrolidone (NMP), methanol, ethanol and acetone were purchased from Merck. Copper sulfate pentahydrate, $CuSO_4.5H_2O$ (cryst. extra pure) and concentrated sulfuric acid (96-98%, extra pure) were purchased from Merck as well. Dodecane (with a purity of 99%) was obtained from Janssen Chimica. The carrier for copper transport, LIX84-I, a mining chemical grade, was supplied by Henkel KGaA from Germany. Ultrapure water was from a MilliQ (Millipore Corp.).

5.2.2 Preparation and characterization of SPEEK

60 g of PEEK powder was dissolved in 1 liter concentrated H_2SO_4 and stirred at 20 ^oC for a certain reaction time ranging between 48 to 140 hours. The polymer was precipitated drop-wise into about 5 liter of ultrapure water at 5^oC. The residue acid was rinsed away with 15 liters of pure water in three washing steps. The resulting SPEEK was then dried in air for 48 hours before completely drying in a vacuum oven at 30^oC for 7 days. Different batches of SPEEK are named as "S-number", e.g. S-48, in which the number indicates the sulfonation time.

The ion exchange capacity is defined as the equivalent sulfonic group per gram of dried polymer. This value was determined by elemental analysis. The swelling was measured by soaking a piece of SPEEK dense films in pure water, $CuSO_4$ (0.025 M) or H_2SO_4 (2 M) at 25^oC for 7 days. The swollen films were weighed and then dried in a vacuum oven at 30 ^oC for another 7 days. The dry weight was then recorded. The degree of swelling, DS, was determined by the weight difference between the dry and swollen states in comparison to the dry weight as described in the following

$$DS = \frac{\left(W_{swollen} - W_{dry}\right)}{W_{dry}} 100\ \% \qquad (1)$$

Duplicate experiments were performed. The swelling results of S-140 are shown in Table 5.1. This polymer shows 440% water uptake in pure water, 70% in in $CuSO_4$ solution and 48% in H_2SO_4. Any further increase of ion exchange capacity by increasing the sulfonation would render the SPEEK water solubility.

The solubility of SPEEK in different solvents has been investigated by adding a certain amount of polymer at about 10wt% in a solvent and leaving the system for 24 hours at room temperature. A good solvent was characterized by a clear solution and a bad solvent is defined by no visual change of the polymer.

Table 5.1 *Swelling results for SPEEK S-140.*

	Ultrapure water -	**$CuSO_4$ solution** (0.025 M)	**H_2SO_4 solution** (2.0 M)
Swelling degree (%)	440	70	48

5.2.3 Dip-coating and determination of defects by gas permeation

The dry SPEEK (batch S-140) was dissolved in a certain amount of methanol at a concentration of 5wt% or 10wt%. After filtration with 15 μm metal filter, the solution was allowed to degas for one hour before dip-coating. The dip-coating process was carried out with the setup as shown in Figure 5.1. The funnel has a diameter matching the diameter of the fibers. The diameter is 1.0 mm for PSf hollow fibers and 1.1 mm for Accurel PP hollow fibers. Before coating, the fiber was pre-positioned inside the funnel, as shown in Figure 5.1. Subsequently, the coating solution was added in and the fiber was pulled upward, allowing a contact between the fiber and the solution for 3 seconds. Before drying in an oven of 80^{o}C for 12 hours, the initial coated fibers were exposed to air for 5 seconds, allowing the formation of an initial thin film.

To prepare an encapsulated hollow fiber membrane, a three-step procedure “coating-impregnating-coating” was applied. A single-layer composite fiber prepared as above was at first impregnated with the organic phase, followed by a drying step with nitrogen gas for 10 seconds to drain out excessive amount of organic phase. Then, a SPEEK solution of 10wt% was introduced into the fiber bore for two times with a drying procedure with nitrogen gas for 30 seconds in between. At last, the fiber was dried with flowing nitrogen for 12 hours before use.

Two coated fibers with an effective length of 15 cm were glued into a Nylon tube with a hot-melt polyethylene at both ends and then one end was cut open. Nitrogen at 0.4 bar gauge was applied at the open side and the gas permeation was measured by a soap bubble flow meter. Zero permeation was defined as no observable bubble shift in a 1 ml capillary (length of 30 cm) for 5 minutes.

5.2.4 Copper permeation

The detailed experimental procedure was described elsewhere [18]. The membrane used consiseds of one coated fiber with an effective length of 20 cm. LIX84-I diluted in dodecane to 20vol% was used as organic extractant. A 0.025 M $CuSO_4$ solution was used as the feed and a 2 M H_2SO_4 solution as the strip. The volume of both feed and strip was 200 ml. The aqueous phases flowed parallel along the fiber with the strip solution at the shell side and the feed at the bore side, unless stated otherwise. The flow velocity of feed and strip was 1.86 $m.s^{-1}$ and 0.094 $m.s^{-1}$, respectively. The temperature was kept at 25 ^oC. The concentration of the feed and strip was determined by taking 7 samples in 7 or 8 hours interval and analyzed by atomic absorption spectrometry (Spectra 10, Varian, Houten, The Netherlands). The copper flux was calculated from the slope of the copper concentration versus time.

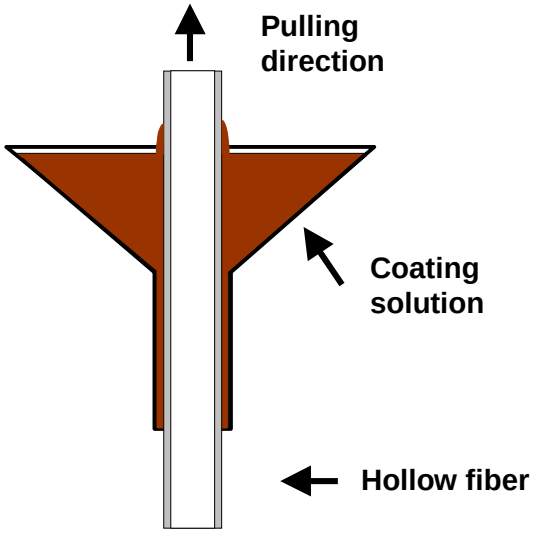

Figure 5.1 *Schematic of a dip-coating set-up for preparation of a coating layer at the outside of a hollow fiber.*

5.2.5 Scanning electron microscopy

Samples for scanning electron microscopy (SEM, JEOL JSM-T220A) were made by cryogenic breaking of fibers. All samples were allowed to dry under vacuum at 30^oC overnight before coating with a thin gold layer.

5.3 Results and discussion

5.3.1 Structure of support hollow fibers

Polysulfone and Accurel PP fibers are both hydrophobic supports and show comparable copper permeation in our system, even though the pore sizes and gas permeation of PSf membrane are much less than those of PP membranes (as seen in Figure 5.2 and Table 5.2). Polysulfone hollow fibers have smaller pores of an average size of 0.052 μm compared to 0.2 μm for the Accurel PP fibers. The PSf fiber has smaller pores at the outside than PP fibers, which means probably that the coating procedure proceeds more smoothly for PSf. Moreover, PSf has a higher surface tension, 46.6×10^{-3} N.m^{-1}, than PP (29.4×10^{-3} N.m^{-1}). Surfaces with a higher surface tension allow a solution to spread more easily and give a better film [19].

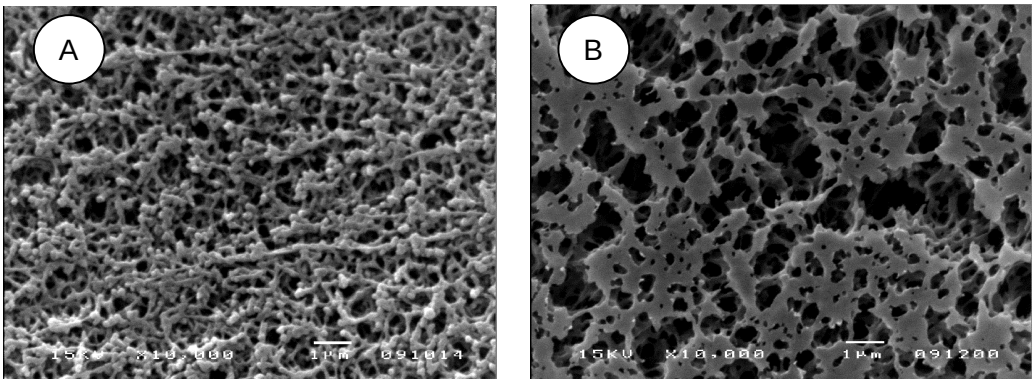

Figure 5.2 *Shell side surfaces of support hollow fibers: (A) polysulfone; (B) Accurel Q3/2 polypropylene.*

Table 5.2 *Properties of polysulfone and polypropylene hollow fibers.*

Properties	**PSf**	**Accurel PP**
Material	Polysulfone	Polypropylene
Manufacture	Tailor-made	Membrana
OD (mm)	0.9	1.0
ID (mm)	0.65	0.6
Υ (10^{-3} N.m^{-1})*	46.6	29.4
Pore size (μm)	0.052	0.2
Copper flux (10^{-9} mol.cm^{-2}.s^{-1})	5.1	5.3
Gas permeation (l.cm^{-2}.min^{-1}.bar^{-1})	0.776	1.80

* from [20]. The pore size of PSf membrane was measured by permporometry and the pore size of Accurel PP membrane was from manufacturer.

5.3.2 Selection of solvents for SPEEK

5.3.2.1 Solvent groups of SPEEK

The groups of potential solvents for SPEEK change as the sulfonation degree and the counter ions of the charged groups change [21]. The solvency stength of solvents can be expressed by a solubility parameter. This parameter is frequently considered to consist of a dispersive contribution (δ_d), a polar force contribution (δ_p) and a hydrogen bonding contribution (δ_h). Table 5.3 lists various solvents classified into four groups in terms of the polar force and hydrogen bonding contributions.

According to the rule-of-the-thumb, 'similar-like-similar', SPEEK with certain sulfonation degree can be dissolved in polar solvents belonging to Group 1 since sulfonation reaction renders the polymer polarity. Further increase in the degree of sulfonation may lead to a SPEEK soluble in solvents with higher hydrogen bonding contribution and polar contribution, such as those out of Group 2 and 4. The solvents from Group 3 do not show good solubility to SPEEK.

Table 5.3 *Classification of solvent groups for SPEEK having an ion exchange capacity larger than 1.2 meq.g^{-1} dry polymer.*

	Group 1	**Group 2**	**Group 3**	**Group 4**
Polarity	high	medium	low	high
Hydrogen bonding	low	low	low	high
Examples	NMP DMAc DMF DMSO	Acetone MEK DCM	Hexane Diethyl ether	Methanol Ethanol H_2O

NMP: N-methyl2-pyrrolidone; DMAc: dimethyl acetamide; DMF: dimethyl formamide; DMSO: dimethylsulfoxide; MEK: methyl ethyl ketone. DCM: dichloromethane.

Table 5.4 shows that SPEEK does not dissolve in solvents such as NMP when sulfonated less than 48 hours (IEC 1.21 meq.g^{-1}). SPEEK tends to dissolve in polar solvents, i.e. solvents from Group 1 and 2, if the sulfonation time is above 100 hours. This holds also for mixtures of NMP and alcohol or NMP and acetone. Upto a sulfonation time of 140 hours, SPEEK dissolves into all solvents used except water. SPEEK may even become water soluble at sulfonation times higher than 140 hours. SPEEK S-140 is used as a model polymer to demonstrate our coating concept for a high ion exchange capacity and a low resistance towards the ions.

Table 5.4 *Solubility of SPEEK with different sulfonation time.*

Polymers	**S-48**	**S-100**	**S-120**	**S-140**
Sulfonation time (hr.)	48	100	120	140
IEC (meq.g^{-1})	1.21	1.65	2.33	2.79
Sulfonation degree, SD	0.38	0.55	0.83	1.03
NMP	+	-	-	-
DMAc	+	-	-	-
NMP/Methanol*	++	-	-	-
NMP/Ethanol*	++	-	-	-
NMP/Acetone*	++	-	-	-
Methanol	+	-	-	-
Ethanol	o	+	++	-
Acetone	o	-	-	-
H_2O	o	+	+	++

* mixture ratio 50/50 wt%.

O: no change; +: swollen;
++: highly swollen; -: dissolved.

5.3.2.2 Criteria of volatility, compatibility and spreading

Not all potential solvents can be used for coating purpose because they have to meet extra criteria with respect to film formation during dip-coating: volatility, compatibility and spreading. More volatile solvents are better for drying and therefore easier coating formation (volatility criteria). Solvents from Group 1 are not suitable for preparing composite membrane using PSf as support since they dissolve PSf (criteria of solvent-polymer compatibility) and they are non-volatile. Furthermore, the coating solution system (polymer support/solvent) has to fulfill a spreading criterion: a positive spreading coefficient [22], expressed as

$$S = \gamma_{\sup port} - \gamma_{solution} - \gamma_{\sup port-solution} \qquad (2)$$

Where $\gamma_{support}$, $\gamma_{solution}$ and $\gamma_{support\text{-}solution}$ are the surface tensions of the polymer support, the coating solution and the interfacial tension between the support polymer and the coating solution, respectively (N.m^{-1}). *S* is the spreading coefficient (N.m^{-1}). The Prigogine-Marechal theory [23, 24] can be used to estimate the surface tension of the coating solution. For a solvent showing much smaller surface tension than the polymer, the solvent preferentially adsorbs at the surface; therefore, the solution surface tension is close to that of the solvent [25]. For a solvent and polymer system with similar surface tensions, a simple mixing rule gives satisfactory results.

The surface tension of SPEEK (as calculated in Appendix A) is rather high compared to that of solvents such as methanol, ethanol and acetone, and it

is quite close to the surface tension of solvents as NMP and DMAc. Therefore, in case of methanol, ethanol and acetone, the surface tension of the coating solution is approximately the surface tension of the solvent. Then the spreading equation can be expressed as

$$S = \gamma_{\sup port} - \gamma_{solvent} - \gamma_{\sup port-solvent} \quad (3)$$

The interfacial tension between support and solvent is positive and difficult to obtain with a satisfactory accuracy. We define a nominal spreading parameter $S_{nominal}$ ($N.m^{-1}$) as ,

$$S_{nominal} = \gamma_{\sup port} - \gamma_{solvent} \quad (4)$$

Consequently, for solvents as NMP and DMAc, we have

$$S_{nominal} = \gamma_{\sup port} - \gamma_{solution} \quad (5)$$

This nominal spreading parameter is not an accurate description for the physical phenomenon. However, it can be used to select potential solvents: if the parameter is negative, spreading will not occur. Neglecting the interfacial tension does not effect the final conclusion because it will reduce the nominal spreading parameter even further. We also neglect the effect of the porous structure on the spreading, i.e. the shape of the pores at the hollow fiber surface [26]. On a rough surface, i.e. membrane surface, higher contact angles are generally obtained than on a smooth surface of the same material. Therefore, a negative nominal spreading parameter based on smooth surface can guarantee no spreading on a membrane surface of the same material.

As listed in Table 5.5, negative values of the nominal spreading parameters indicate that Accurel PP is unlikely to be coated using NMP, DMAc and water as a solvent. Alcohol and acetone are the best choices while water is the worst solvent according to the spreading criteria. However, taking into account the compatibility criteria, acetone is not a good choice for PSf membrane. Alcohol, like methanol or ethanol, is probably the best solvent according to the analysis.

5.3.3 Structure and integrity of composite fibers

A SPEEK layer has a negligible resistance to the ion transport compared to the diffusion resistance [17]. The thickness of the toplayer is not as crucial as in gas separation [27] but rather the integrity. Considering various parameters, the concentration of a coating solution and the coating steps are of importance to obtain an integral coating. Figure 5.3 (A) shows the cross-section of coated PSf fibers with S-140 in methanol. A typical three-layered structure is identified as a dense coating layer, a porous support and a transitional layer in between. This transitional layer is probably a result of the penetration of the

coating solution into the open surface as shown in Figure 5.2 (A). This layer improves the adhesion of SPEEK to the PSf support membrane. The coated PP fiber, as can be seen in Figure 5.3 (B), has a dense layer of around 19 μm after applying the coating steps for four times.

Table 5.5 *Surface tension values of materials and nominal spreading constant for polymer-solvent systems. $S_{nominal}$: nominal spreading constant.*

Material	**Surface tension (10^{-3} N.m^{-1})** [19, 28]	**$S_{nominal}$ (10^{-3} N.m^{-1})**		**Polymer-solvent compatibility**	
		PSf	PP	PSf	PP
PSf	46.6	Not applicable		Not applicable	
PP	29.4				
NMP	40.1	+	-	S	NS
DMAc	33.1	++	-	S	NS
Methanol	22.6	++	+	NS	NS
Ethanol	22.8	++	+	NS	NS
Acetone	23.0	++	+	SW	NS
H_2O	72.8	--	--	NS	NS

NS: non-solvent; SW: swollen; S: solvent.
+: $0 < S_{nominal} < 10$; ++: $S_{nominal} > 10$;
-: $-10 < S_{nominal} < 0$; --: $S_{nominal} < -10$.

Figure 5.4 shows the nitrogen permeability of both PSf and PP support membranes with SPEEK as a function of the number of coatings steps. Increasing the number of coating times and the concentration of the coating solution result in defect free composite fibers for both membranes. The PSf support is much easier to dip-coat in terms of less coating procedures involved in preparation of an integral composite.

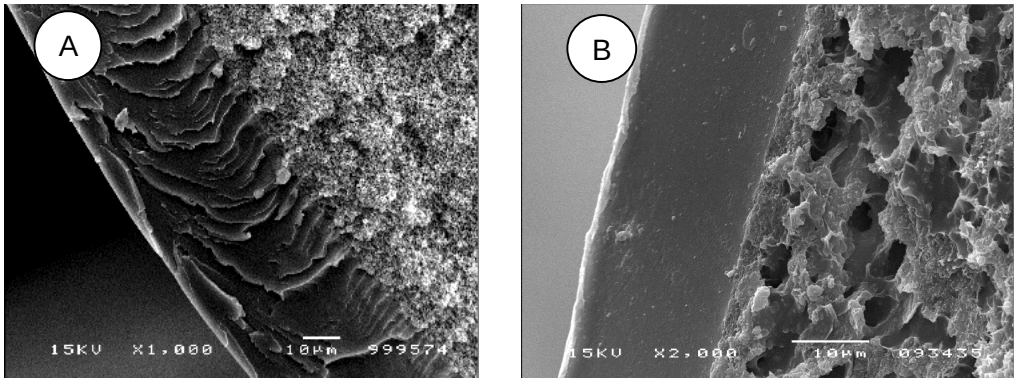

Figure 5.3 *SEM photos of the composite membranes with SPEEK coating layers at the shell side of the hollow fibers. (A) PSf support after two coating steps; (B) Accurel Q3/2 PP support after four coating steps. SPEEK coating solution: 10wt% in methanol.*

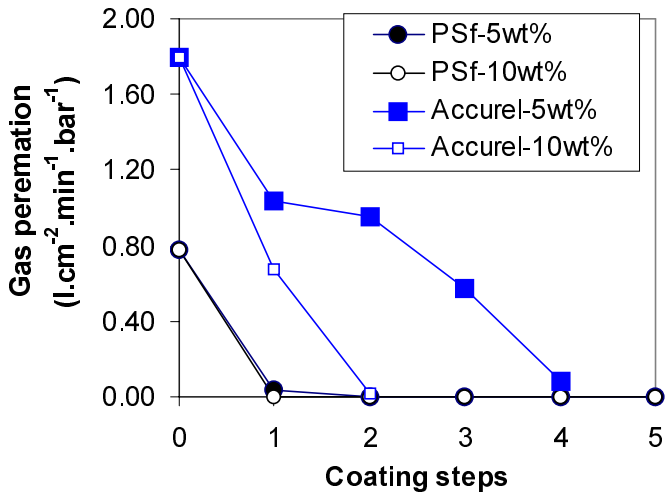

Figure 5.4 *Characterization of SPEEK coated composite hollow fibers by nitrogen gas permeation at room temperature. Accurel PP and PSf support membranes are coated with 5wt% or 10wt% SPEEK solutions in methanol.*

5.*3.4 Copper permeation and stability*

The copper flux was measured for the support membranes with and without coating as a function of time. The coated side of the composite membranes can be either in contact with the feed or the strip solutions. Compared to the composite membranes, the uncoated PSf and Accurel PP membranes are rather instable with a rapid drop of copper flux in about 200 hours to 25% of the original flux. The composite fibers show a fairly stable flux profile, particularly at time up to 200 hours. For Accurel PP support membranes, water leakage occurs as indicated by a sudden copper flux increase and the volume change of the feed and strip solutions during the course of the experiment. The results suggest that a single coating layer is not sufficient for the final aim of being stable over an extended period of months since one side of the composite membrane still directly contacts with the aqueous phase.

Very interestingly, when the coating layer faces the feed solution, both composite membranes show higher permeability than the original membranes as can be seen in Figure 5.5. However, when a strip solution contacts the coating layer, the copper flux declines. This phenomenon was reported in the lamination membrane system as well [17]. About 70% increase of copper flux was found with the feed solution at the coating side and a slight decrease with the strip solution facing the SPEEK side. Wijers et al. [17] attributed this significant increase to the pore penetration by the ion exchange layer having a lower resistance than the liquid membrane phase.

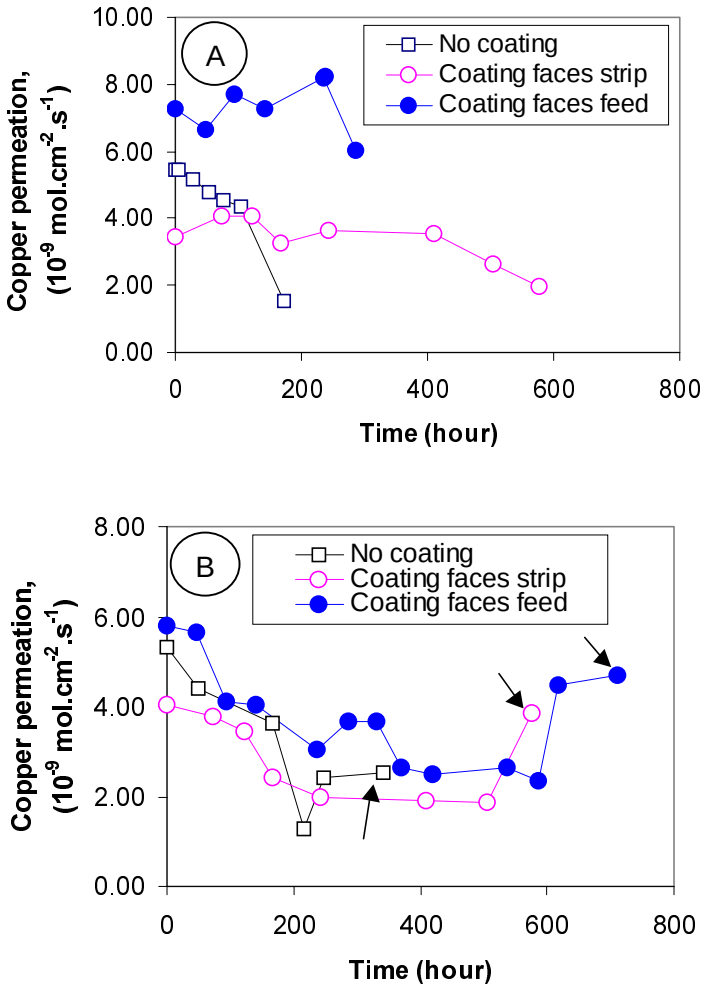

Figure 5.5 *Stability of hollow fiber membranes based on polysulfone (A) or Accurel Q3/2 polypropylene (B). The composite membranes face either feed or strip solutions.*

With the feed at the coating side, it is difficult to rationalize the increase in flux to the penetration of SPEEK into the membrane support layer. The SEM photos did not show corresponding penetration thickness of SPEEK into the support structure. Understanding of this phenomenon needs further work. Furthermore, the mass transfer coefficients for the aqueous phases are comparable for both the bore and the shell sides of the hollow fiber, as shown in Appendix B. Therefore, it can not be the reason of the difference in the initial copper flux when feed is at either the bore or shell side. On the other hand, the decrease in copper flux with the strip at shell side probably comes from the lower swelling of the SPEEK layer in a 2 M H_2SO_4 solution (as can be seen in Table 5.1).

5.3.5 Encapsulated hollow fiber membranes

To further improve the stability, a double-layer composite membrane, or encapsulated membrane, was prepared with two SPEEK layers at both the bore and shell sides and the organic phase in between. We carried out preliminary work and the initial results reveal two technical problems, which are related to the order of applying the second coating and impregnating the organic phase into the support. If applying the second coating layer after the impregnation of the organic phase, a spreading problem arises (coating-impregnating-coating). Impregnating the organic phase after preparation of the double-layered composite hollow fiber membrane is also problematic since it can not be guaranteed that the whole support structure will be wetted by the organic liquid membrane phase (coating-coating-impregnating).

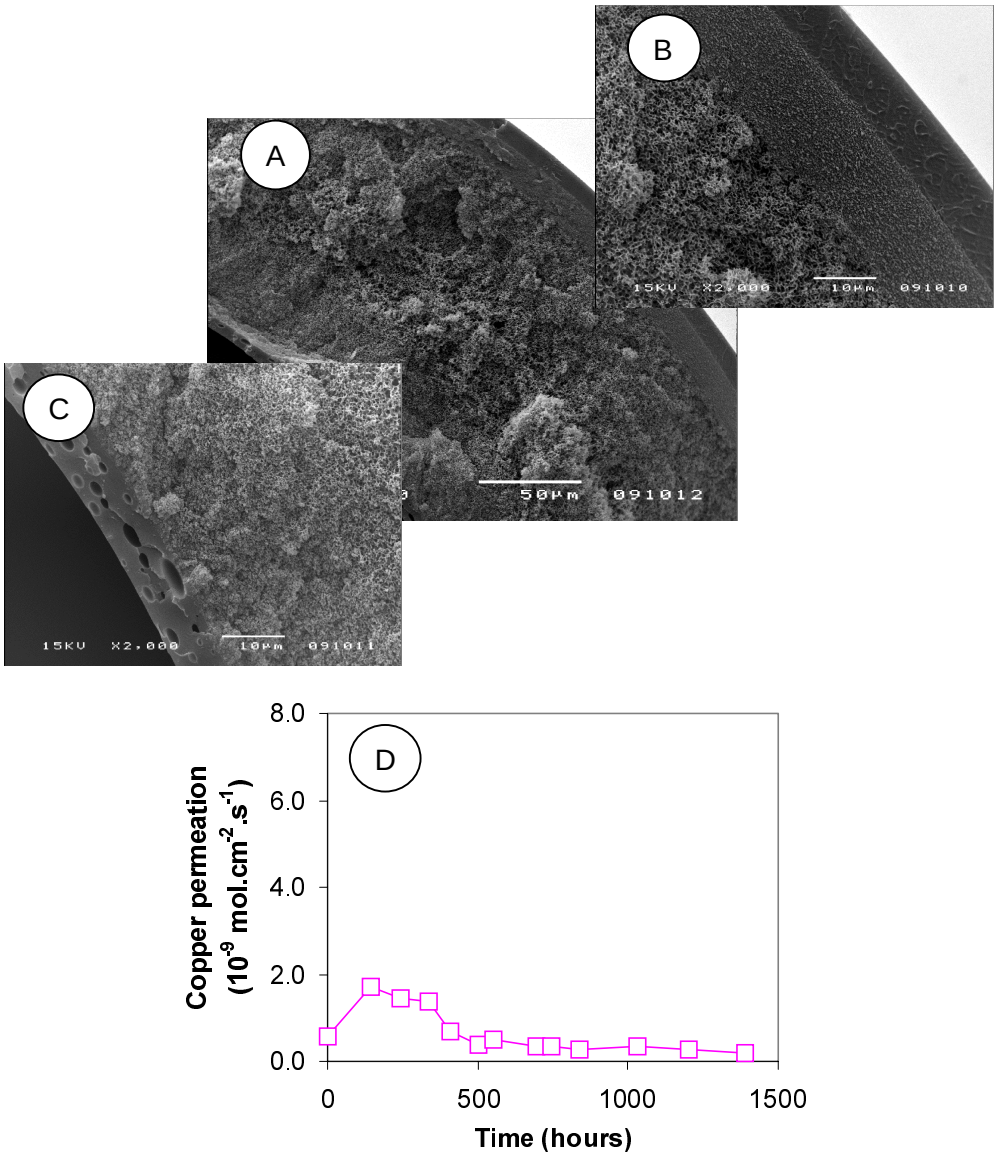

Figure 5.6 *SEM photos of the encapsulated composite hollow fiber membrane based on polysulfone support fiber (A-C) and stability of copper transport (D).*

Figure 5.6 (A-C) shows the structure of an encapsulated composite membrane, which was prepared according to a three-step procedure, “coating-impregnating-coating”. The coating layer at the outer surface (Figure 5.6 (B)) is rather dense compared to that at the bore side (Figure 5.6 (C)), which shows many holes probably due to the convective drying step during preparation. The preliminary stability result (Figure 5.6 (D)) shows a low copper flux, which could be due to the loss of the organic during the preparation procedure and the existing defects. A membrane contactor system will be a better solution in which the organic phase circulates between two composite hollow fiber modules. In this way, the organic phase in fact is encapsulated by two SPEEK coating layers, one being in the absorbing module and the other in the striping module [29].

5.4 Conclusions

Integral SPEEK coated PSf and PP hollow fibers are prepared by a systematic selection of appropriate solvents for a dip-coating process. An increase in the solubility of SPEEK in methanol, is found by increasing the sulfonation time and therefore the ion exchange capacity. An integral coating layer is prepared by controlling the coating solution concentration and the number of coating steps. These hollow fibers with hydrophilic coating on hydrophobic support show a slight increase in stability. However, these membranes are still instable due to the existence of direct contact between the organic phase and the aqueous phase. An initial research on an encapsulated composite membrane with SPEEK layers demonstrates that this is a potential solution, but further development is necessary.

5.5 Appendix A Surface tension of SPEEK

The surface tension is defined as the free energy of attraction per unit area between two semi-infinite parallel plates separated by a distance [19]. For a polymer, the surface tension is related to the cohesive energy density by Equation 6 [30]

$$\gamma = C_j \frac{\sum_i \Delta E_i^*}{(\sum_i \Delta V_i)^{2/3} m^{1/3}} \qquad (6)$$

where γ is the surface tension of the polymer and C_j is a constant related to the physical properties of the unit group. For a unit with acid groups, C_j is equal to 0.0751. m is the number of atoms in the repeating unit. The calculation is based on SPEEK with a sulfonation degree of 1 as shown in Figure 5.7. Calculated surface tension is shown in Table 5.6 as 39.8 $x10^{-3}$ $N.m^{-1}$, much higher than that of methanol, 22.6 $x10^{-3}$ $N.m^{-1}$ as can be seen in Table 5.5. The result is reasonable for the probably strong hydrogen bonding and polar interaction of SPEEK chains, which correspond to a high surface tension. The similarity

between the calculated and experimental surface tension for methanol is a side proof of the validity of the simulation.

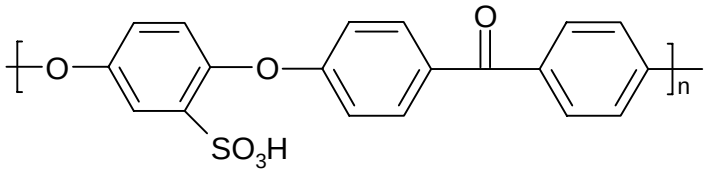

Figure 5.7 *Chemical structure of sulfonated poly(ether ether ketone)* [31].

Table 5.6 *Calculated surface tension results of SPEEK and methanol.*

Material	$\sum_i \Delta E_i^*$ **(J.mol^{-1})**	$\sum_i \Delta V_i$ **(A^3)**	$N_A \sum_i \Delta V_i$ **(cm^3.mol^{-1})**	**γ (10^{-3} N.m^{-1})**
SPEEK*	79988	297.4	179.1	39.8
Methanol	20301	36.5	22.0	24.0

*calculated with the increment method.

5.6 Appendix B Mass transfer efficiency

In this section, the mass transfer efficiency at the shell and bore sides is considered. The correlation equations from Takeuchi et al. [32] are used to calculate the mass transfer coefficient in a well-defined flow in an one fiber module.

Prior experiment results showed that a critical flow rate, which gives the maximal copper flux, is actually quite low, about 0.61 m.s^{-1}, compared to the operational flow rate, 1.86 m.s^{-1} (as can be seen in Table 5.8). Therefore, in the following part, the critical flow rate at the shell side will be calculated by choosing

$$Sh = 1.4\left(\frac{d_i}{l}\right)^{1/3} \mathrm{Re}^{1/3}\, Sc^{1/3} \qquad (7)$$

for the bore side and

$$Sh = 0.85\left(\frac{d_S}{d_O}\right)^{0.45}\left(\frac{d_e}{l}\right)^{1/4} \mathrm{Re}^{1/3}\, Sc^{1/3} \qquad (8)$$

for the shell side, where d_i and d_o are the inner and outer diameters of the hollow fiber, respectively, d_s and d_e are the inner diameter and hydraulic diameter of the module, respectively. *Re*, *Sc* and *Sh* represent the Reynolds

number, the Schmidt number and Sherwood number respectively. By setting the same mass transfer coefficients at both bore and shell sides, the concentration boundary layers for both sides are of the same value, according to film model

$$k = \frac{D_{AB}}{\delta} \tag{9}$$

where k represents the local mass transfer coefficient, D_{AB} is the diffusivity of solute A in solvent B, δ is the thickness of the stagnant boundary layer adjacent to the surface. The Reynolds number at shell side critical flow rate is calculated, so is the critical flow rate. The parameters used in the calculation are listed in Table 5.7. The copper diffusion coefficient is taken from literature [33] where the feed concentration is 4 to 20 times higher than our case. However, the diffusivity of copper ions in an aqueous phase is only a function of temperature, aqueous viscosity and some physical constants [34] and therefore, it is used in our calculation.

Table 5.7 *Parameters used in estimation of mass transfer coefficient.*

Parameters	**Value**
Inner diameter of module for shell side, d_s	= 10.5 mm
Outer diameter of the hollow fiber, d_o	= 0.9 mm
Inner diameter of the hollow fiber, d_i	= 0.65 mm
Solute diffusivity, D_{AB}	= 7.2 x 10^{-6} $cm^2 \cdot s^{-1}$ [33]
Fiber number	= 2
Length of the hollow fiber, l	= 380 mm
Liquid viscosity, η*	= 9.76 x 10^{-3} Pa.s
Liquid density, ρ*	= 0.998 $g.cm^{-3}$

* from [35]

The results listed in Table 5.8 indicate that, for a feed solution, a flow rate of 0.014 $m.s^{-1}$ (Re = 9.8) at the shell side of the fiber gives the same mass transfer coefficient as in bore side at a flow rate of 0.61 $m.s^{-1}$ (Re = 41). At this speed an optimal copper flux is obtained. In operation, the mass transfer coefficient at the shell side is higher than in the bore side. This means that the mass transfer coefficient at the shell side for the feed phase is higher than that at the bore side. Therefore, the higher flux value when the coating faces the feed solution is not from the hydrodynamic origin.

Table 5.8 *Estimation of the corresponding flow rate at the shell side of the module with the same mass transfer coefficient as bore side.*

Parameters	At minimal flow rate*		At operational flow rate		
	Bore	Shell (calc.)	Bore	Shell (calc.)	Shell (exp.)
Flow rate ($m.s^{-1}$)	0.61	0.014	1.86	0.043	0.094
Re	41	9.8	126	30	66

* Referring to the minimal flow rate at which the copper flux reaches a plateau value. Further increase of the flow rate does not significantly improve flux.

5.7 Notation and Greek Letters

d_s inner diameter of module for shell side, L
d_o outer diameter of the hollow fiber, L
d_i inner diameter of the hollow fiber, L
d_e hydraulic diameter for shell side, L (4 Cross-section area/Wetted perimeter)
D_{AB} solute difusivity, $L^2 t^{-1}$
k mass transfer coefficient in the aqueous phase, $L.t^{-1}$
l length of the hollow fiber, L
Re Reynolds number
S spreading parameter, $L t^{-2}$
Sc Schmidt number
Sh Sherwood number
v liquid flow rate, $L t^{-1}$
δ boundary layer thickness, L
μ viscosity, $ML^{-1}t^{-1}$
ρ liquid density, $M L^{-3}$
γ surface tension, $L t^{-2}$

5.8 References

[1] A. J. B. Kemperman, D. Bargeman, T. van den Boomgaard, and H. Strathmann, Stability of supported liquid membranes: state of the art, Sep. Sci. Technol., 31 (1996) 2733-2762.
[2] A. M. Neplenbroek, D. Bargeman, and C. A. Smolders, Supported liquid membranes: stabilization by gelation, J. Membrane Sci., 67 (1992) 149-165.
[3] L. Bromberg, G. Levin, and O. Kedem, Transport of metals through gelled supported liquid membranes containing carrier, J. Membrane Sci., 71 (1992) 41-50.
[4] G. Levin and L. Bromberg, Gelled membrane composed of dioctyldithiocarbamate substituted on poly(vinylchloride) and di(2-

ethylhexyl) dithiophosphoric acid, J. Appl. Polym. Sci., 48 (1993) 335-341.
[5] A. M. Neplenbroek, Stability of supported liquid membranes, Ph.D Thesis, University of Twente, Enschede, 1989.
[6] A. J. B. Kemperman, B. Damink, T. van den Boomgaard, and H. Strathmann, Stablization of supported liquid membranes by gelation with PVC, J. Appl. Polym. Sci., (1997) 1205-1215.
[7] C. Wijers, Supported liquid membranes for removal of heavy metals: permeability, selectivity and stability, Ph.D Thesis, University of Twente, Enschede, 1996.
[8] C. Clement and M. M. Hossain, Stability of a supported liquid membrane for removing hydrophobic solutes from casein hydrolysate solution, Sep. Sci. Technol., 32 (1997) 2685-2703.
[9] A. J. B. Kemperman, H. H. M. Rolevink, T. van den Boomgaard, and H. Strathmann, Stabilization of supported liquid membranes by interfacial polymerization top layers, J. Membrane Sci., 138 (1998) 43-55.
[10] M. C. Wijers, M. Wessling, and H. Strathmann, Limitation of the lifetime stabilization of supported liquid membrane by polyamides layers, Sep. Purif. Technol., 17 (1999) 147-157.
[11] Y. Wang, Y. S. Thio, and F. M. Doyle, Formation of semi-permeable polyamide skin layers on the surface of supported liquid membranes, J. Membrane Sci., 147 (1998) 109-116.
[12] X. J. Yang, A. G. Fane, J. Bi, and H. J. Griesser, Stabilization of supported liquid membranes by plasma polymerization surface coating, J. Membrane Sci., 168 (2000) 29-37.
[13] O. Kedem and L. Bromberg, Ion-exchange membranes in extraction processes, J. Membrane Sci., 78 (1993) 255-264.
[14] V. S. Kislik and A. M. Eyal, Hybrid liquid membrane (HLM) and supported liquid membrane (SLM) based transport of titanium, J. Membrane Sci., 111 (1996) 271-281.
[15] V. S. Kislik and A. M. Eyal, Hybrid liquid membrane (HLM) system in separation technologies, J. Membrane Sci., 111 (1996) 259-272.
[16] R. Wodzki and G. Sionkowski, Recovery and concentration of metal ions. II multimembrane hybrid system, Sep. Sci. Technol., 30 (1995) 2763-2778.
[17] M. C. Wijers, M. Jin, M. Wessling, and H. Strathmann, Supported liquid membranes modification with sulphonated poly(ether ether ketone): permeability, selectivity and stability, J. Membrane Sci., 147 (1998) 117-130.
[18] T. He, M. H. V. Mulder, and M. Wessling, Permeation and stability of polysulfone hollow fibers for supported liquid membranes, To be published.
[19] S. Wu, Polymer Interface and Adhesion, Marcel Dekker, Inc., New York, 1982.
[20] J. Brandrup, E. H. Immergut, and E. A. Grulke, Polymer Handbook, Fourth Edition, John Wiley & Sons Inc., New York, 1999.

[21] X. Jin, M. T. Bishop, T. S. Ellis, and F. E. Karasz, A sulfonated poly(aryl ether ketone), British Polym. J., 17 (1985) 4-10.
[22] L. H. Lee, Fundamentals of adhesion, Plenum Press, New York, 1991.
[23] I. Prigogine and J. Marechal, The influence of difference in molecular size on the surface tension of solutions. IV, J. Colloid Sci., 7 (1952) 122-127.
[24] K. S. Siow and D. Patterson, Surface thermodynamics of polymer solutions, J. Phys. Chem., 77 (1973) 356-365.
[25] G. B. Tanny, The surface tension of polymer solutions and asymmetric membrane formation, J. App. Polym. Sci., 18 (1974) 2149-2163.
[26] A. C. M. Franken, J. A. M. Nolten, D. Bargeman, and C. A. Smolders, Wetting criteria for the applicability of membrane distillation, J. Membrane Sci., 33 (1987) 315-328.
[27] S.-G. Li, G. H. Koops, M. H. V. Mulder, T. van den Boomgaard, and C. A. Smolders, Wet spinning of integrally skinned hollow fiber membranes by a modified dual-bath coagulation method using a triple orifice spinneret, J. Membrane Sci., 94 (1994) 329-340.
[28] D. R. Lide, Handbook of organic solvents, CRC Press, Inc., Boca Raton, 1995.
[29] T. He, L. A. M. Versteeg, M. H. V. Mulder, and M. Wessling, Selection and modeling of a new type of composite hollow fiber membrane in a membrane contactor, To be published.
[30] A. A. Askadskii, Physical properties of polymers: prediction and control, Gordon and Breach Publishers, Moscow,Vol. 2, 1996.
[31] C. Bailly, D. J. Williams, F. Karasz, and W. J. MacKnight, The sodium salts of sulphonated poly(aryl ether ether ketone) (PEEK): preparation and characterization, Polymer, 28 (1987) 1009-1016.
[32] H. Takeuchi, K. Takahashi, and M. Nakano, Mass transfer in single oil-containing microporous hollow fiber contactors, Ind. Eng. Chem. Res., 29 (1990) 1471-1476.
[33] A. K. Guha, C. H. Yun, R. Basu, and K. Sirkar, Heavy metal removal and recovery by contained liquid membrane permeator, AIChE J., 40 (1994) 1223-1237.
[34] R. M. C. Viegas, M. Rodriguez, S. Luque, J. R. Alvarez, I. M. Coelhoso, and J. P. S. G. Crespo, Mass transfer correlations in membrane extraction: analysis of Wilson-plot methodology, J. Membrane Sci., 145 (1998) 129-142.
[35] B. P. Whim and P. G. Johnson, Directory of solvents, Chapman & Hall, London, 1996.

Ethanol, if by no means useful for the coating purpose, is much more appropriate to be a solvent for the coating polymer than to be a pore-filling agent.

People who make nice membrane cook well. An excellent cook has great potential to make fabulous membranes.

Chapter 6 Composite hollow fiber membranes in membrane contactor application

Abstract

This chapter discusses the application of a novel composite hollow fiber membrane with a sulfonated poly (ether ether ketone) layer in membrane contactor systems. A membrane contactor configuration is selected and applied for copper transport. Stability experiments for more than two and a half months demonstrate that the new concept of using composite membranes is a practical and feasible approach. A resistance model is developed to estimate the stable copper flux of the membrane contactor based on supported liquid membrane (SLM) experiments of the uncoated and composite membranes. Feasibility of the model is proved for both the polysulfone and the polypropylene contactor systems. According to the model, an improvement in flux can be realized by using two thin, dense ion exchange hollow fibers.

6.1 Introduction

A membrane contactor can achieve liquid/liquid mass transfer without dispersion of one compound in the other, which makes it energetically efficient and economically attractive. It overcomes many disadvantages of the conventional extraction process as well, i.e. dispersion and coalescence, emulsification, insufficient density difference between organic and aqueous phases, difficulty in scale-up, etc. [1-3].

Based on the hydrodynamics of the organic phase, two different types of liquid membrane can be distinguished:

- A liquid membrane in which the organic phase is stagnant [4-7];
- A liquid membrane in which the organic phase circulates [8-12].

A stagnant type has a large mass transfer resistance because the organic liquid layer is thick and stationary [10]. A membrane contactor can also be classified according to the nature of the support material into either a hydrophilic or a hydrophobic contactor. The choice of the support matrix depends completely on the nature of the organic phase. An aqueous membrane liquid or polar organic phase requires a hydrophilic type and a nonpolar, hydrophobic extractant requires a hydrophobic support [4].

Compared to a supported liquid membrane, a membrane contactor shows a long life-time because of the large amount of organic phase. However, the loss of organic extractant is still a potential obstacle for the introduction of membrane contactors on an industrial scale. Our aim in this paper is to increase the life-time of the supported liquid membrane to a few months, suitable for an industrial application.

Recently, a new concept of using a hydrophilic/hydrophobic composite membrane was investigated and showed promising result [13]. In this work, an ion exchange polymer was laminated on top of an Accurel polypropylene flat membrane to prevent loss of organic phase diffusing out of the support membrane. The other research combinign ion exchange membranes with a liquid membrane was mainly focusing on the permeation [14]. A successful and practical technology has been developed to manufacture a composite hollow fiber membrane with a cation exchange coating at the outside of a hydrophobic support, showing a more stable copper flux profile [15]. This chapter reports on a new investigation on the novel composite hollow fiber membrane in a membrane contactor configuration. A simple resistance model predicts the ion flux of the contactor, which is comparable to the experimental results. The model has been developed to select the potential composite membrane for a membrane contactor by a few SLM experiments.

6.2 Experimental

6.2.1 Materials and membranes

Polysulfone (PSf) hollow fibers were prepared in our lab at University of Twente as described in [16]. Polypropylene (PP) fibers (Accurel Q3/2 or Q6/2) were obtained from Membrana, Germany (formerly AKZO Nobel Membrana). Sulfonated poly (ether ether ketone) (SPEEK) and the composite membrane were prepared following the same procedure as described in chapter 5 with a coating layer at the outside of the fiber.

Copper sulfate pentahydrate, $CuSO_4.5H_2O$ (cryst. extra pure) and concentrated sulfuric acid (96-98%, analytical grade) were purchased from Merck. Dodecane with a purity of 99% was purchased from Janssen Chimica. The solvents are of analytical grade and used without further purification. LIX84-I, as carrier in copper transport, was purchased from Henkel KgaA, Germany as a mining chemical grade. Ultrapure water (MilliQ, Millipore) was used to prepare feed and strip solutions.

6.2.2 Determination of pore size and porosity

The pore size of the membranes was determined by permporometry for the PSf membrane [17]. The porosity was determined with a pycnometer (Accupyc 1330, from ®Micromeritics Instrument Corporation). Firstly, the density of polysulfone, ρ_{PSf}, was measured by the pycnometer. Then the nominal density of the hollow fiber, ρ_{nom} was obtained from the mass and the volume of the fiber. Finally, the porosity of a fiber, ϕ was obtained from

$$\phi = (1 - \frac{\rho_{nom}}{\rho_{PSf}}) \times 100 \qquad (1)$$

The density measurements were within an error of 2% compared to literature data.

6.2.3 Breakthrough pressure

The breakthrough pressure is defined as the minimal gas pressure used to displace the organic solution inside the porous support membrane immersed in an aqueous media from the bore side. A fiber of 10 cm was potted into a polyethylene tube (Length of 4 cm and diameter of 6 mm) at one end, where the gas pressure was applied, and the other end was blocked with a hot melt polyethylene as shown in Figure 6.1. By slowly adjusting the pressure with a micro-valve (Praxair) at a speed of 0.1 $bar.s^{-1}$, the hollow fiber pre-filled with organic was pressurized from the bore side. The actual pressure was recorded

by a digital barometer (Eurothermo). The hollow fiber was immersed into a water bath for an accurate observation of the organic at the breakthrough pressure.

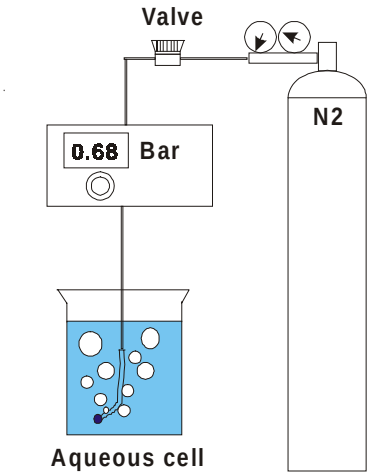

Figure 6.1 *Setup for breakthrough pressure experiments.*

6.2.4 Copper permeation measurements

The setup to determine the copper permeability was the same as reported in reference [16]. Two types of membrane contactor systems are shown in Figure 6.2. Both systems consist of two separate modules in which the organic phase circulates at the shell side (Figure 6.2 (a)) or at the bore side of the modules (Figure 6.2 (b)). The composite hollow fiber membranes were prepared as described previously and the final membranes consisted of a SPEEK coating layer at the outside of the fiber [15]. The effective surface area of the module with a single fiber was 3.5×10^{-4} m^2 for the PSf support and 3.8×10^{-4} m^2 for the PP support membranes. All connecting tubing were Norprene® from Masterflex® 6404-16 (Cole-Parmer Instrument Co., USA). The total volume of the organic phase was 20 ml and the flow rate inside the tubing was 2.4 $l.hr^{-1}$. Fresh aqueous solutions were introduced before taking samples. All experiments were carried out at 25°C. For the large bench-scale modules, both feed and strip phases were 2 liters and the organic phase was 0.170 liter.

6.3 Results and discussion

6.3.1 Stability of supported liquid membranes

A supported liquid membrane is an unstable system because of the loss of the organic liquid from the support membrane, although a hydrophilic coating layer is situated at the outside of the hollow fiber membranes. The

results are summarized in Figure 6.3. Nevertheless, a composite hollow fiber membrane is more stable than a membrane without a coating layer. The composite membranes show a lower initial copper flux, which is caused by the low swelling of the SPEEK layer in the strip phase. When the feed phase faces the coating layer, higher initial fluxes are obtained with a similar life-time [15].

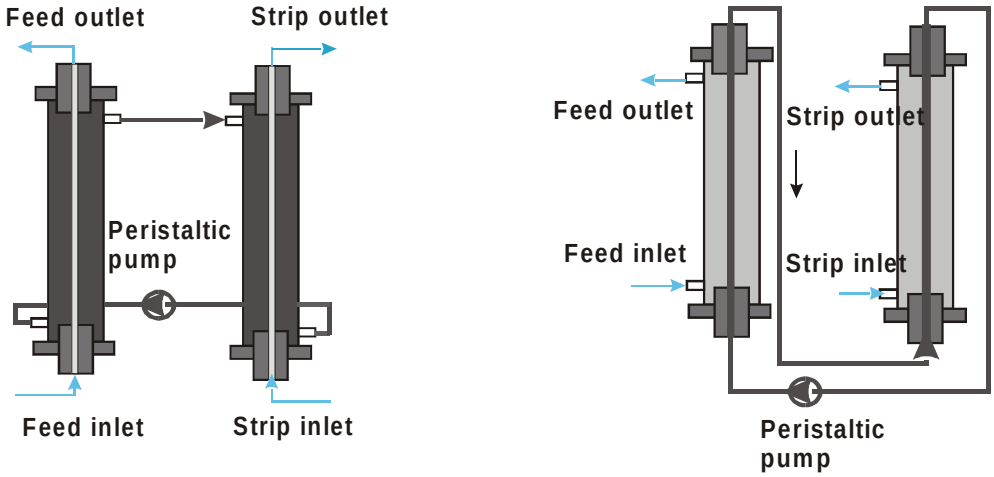

Figure 6.2 *Flow configuration of membrane contactor modules. (a) organic phase at shell side; (b) aqueous phase at shell side.*

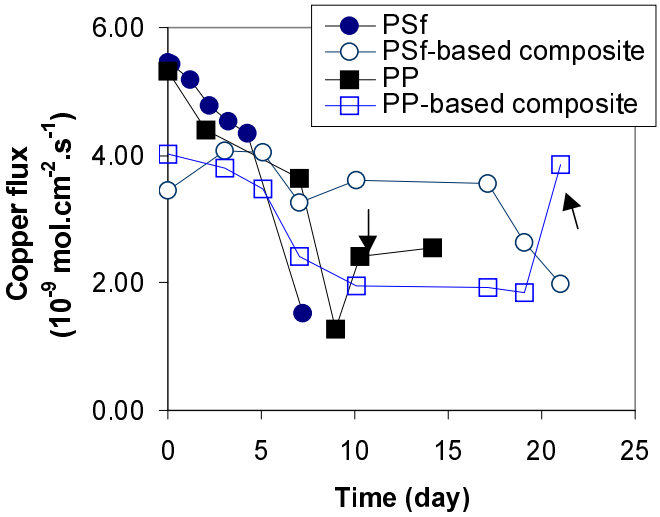

Figure 6.3 *Copper flux and stability of a polysulfone and a polypropylene support membrane with and without a SPEEK coating layer at the outside layer. The ion exchange layer is in contact with the strip phase. Arrows refer to leakage.*

6.3.2 Selection of membrane contactor configuration

Membrane modules based on uncoated hollow fibers may suffer from liquid breakthrough if the absolute pressure at one side of the fiber (generally at the bore side) exceeds the maximum breakthrough pressure. These maximum

pressures are listed in Table 6.1. It is low for a membrane with large pores, such as the Accurel PP membrane. This explains the leakage in our experiment for PP membranes with a flow rate of 1.86 $m.s^{-1}$ at the bore side for a contactor system as in Figure 6.2 (a). At this flow rate, the pressure at the inlet of the hollow fiber is about 0.95 bar, far above its break through pressure of 0.69 bar. For polysulfone membranes, no breakthrough is observed due to the smaller pore size. Nevertheless, we still need to prevent a direct contact between the organic phase and aqueous phases.

For composite hollow fiber membranes, the suitable membrane contactor system is as depicted in Figure 6.2 (b), in which the organic circulates through the bore side of the fibers. If the aqueous phase circulates in the bore side, a water transport may happen because the average absolute pressure here is almost 1.5 bar, compared to atmosphere pressure on the shell side. A pressure difference of 0.5 bar might be a sufficient driving force for water permeation across the hydrophilic coating. Having the organic phase at the bore side, we expect much less transport for the organic phase, caused by the pressure difference owing to the hydrophilic coating layer. Therefore, a much more stable system is obtained using the configuration shown in Figure 6.2 (b).

Table 6.1 *Specifications of PP and PSf hollow fiber membranes.*

Terms	**PSf**	**Accurel PP Q3/2**
Inner diameter (mm)	0.65	0.6
Out diameter (mm)	0.9	1.0
Average pore size (μm)	0.052	0.2*
Skin layer	Asymmetric, inner skin	Symmetric
Initial copper flux (10^{-9} $mol.cm^{-2}.s^{-1}$)	5.1	5.3
Breakthrough pressure (bar)	>1.4	0.69

* According to manufacturer.

Two membrane contactor systems are tested based on composite PSf and Accurel PP hollow fiber membranes, as shown in Figure 6.4. The flux curves basically consist of two regions: a transition period and a stable period. The transition period is probably caused by saturation of the organic phase with copper: the membrane surface area is small compared to the large amount of organic phase. We expect less transition time if the ratio of the membrane area to the volume of organic phase is larger.

Both systems show a stable copper flux during the experimental period. To our knowledge, this is the first data reported in literature demonstrating a stable operation of a membrane contactor for liquid-liquid extraction over an extended period of 75 days. The last 8 data points amount to an average flux for PSf based contactor of 2.2 $x10^{-9}$ $mol.cm^{-2}.s^{-1}$ and 2.4 $x10^{-9}$ $mol.cm^{-2}.s^{-1}$ for Accurel PP based system.

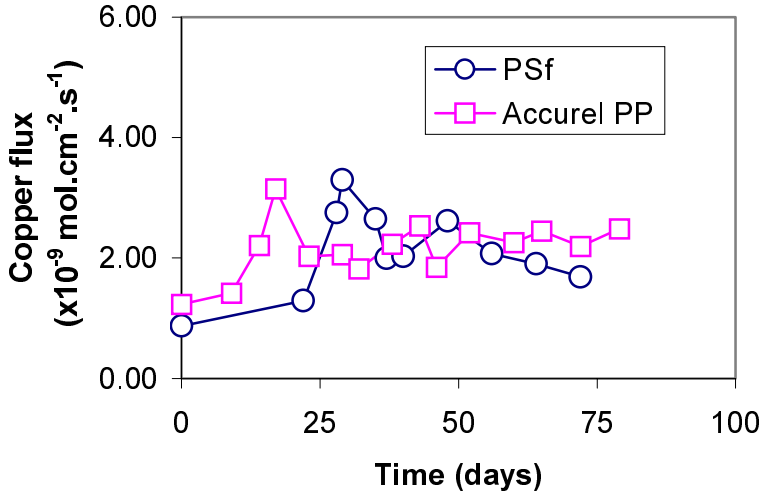

Figure 6.4 *Stability of the membrane contactor systems for composite hollow fiber membranes based on PSf and Accurel PP membrane.*

6.4 Modeling

6.4.1 Resistance model based on a double-layer composite membrane

To describe the transport, at first, a composite hollow fiber membrane composed of two coating layers is taken as a model, as shown in Figure 6.5 (a). It can be related to the contactor system as shown below. Ionic transport across the membrane consists of a series of steps (as seen in Figure 6.5 (b)).

The following assumptions are used to describe the mass transfer in a steady state:

1. Extraction reactions are fast enough that the diffusion inside the membrane support layer is the rate-limiting step.
2. Two ion exchange coatings are situated at the outside and inner side of the hollow fiber.
3. There is no influence of the interface curvature on the solute distribution coefficient, rate of solute transfer, and interfacial area.
4. The transport of ions through the membrane support filled with organic phase is described by means of a membrane transfer coefficient, K_m based on the effective area of the membrane.
5. The aqueous and organic boundary layer resistance may be combined with the membrane resistance as one-dimensional series of diffusion resistance [18].
6. The distribution coefficient *m* is a constant.
7. The concentration distribution at the interfaces between aqueous phase and ion exchange coating is based on Donnan exclusion effects. This is included in the total resistance of the coating layer.

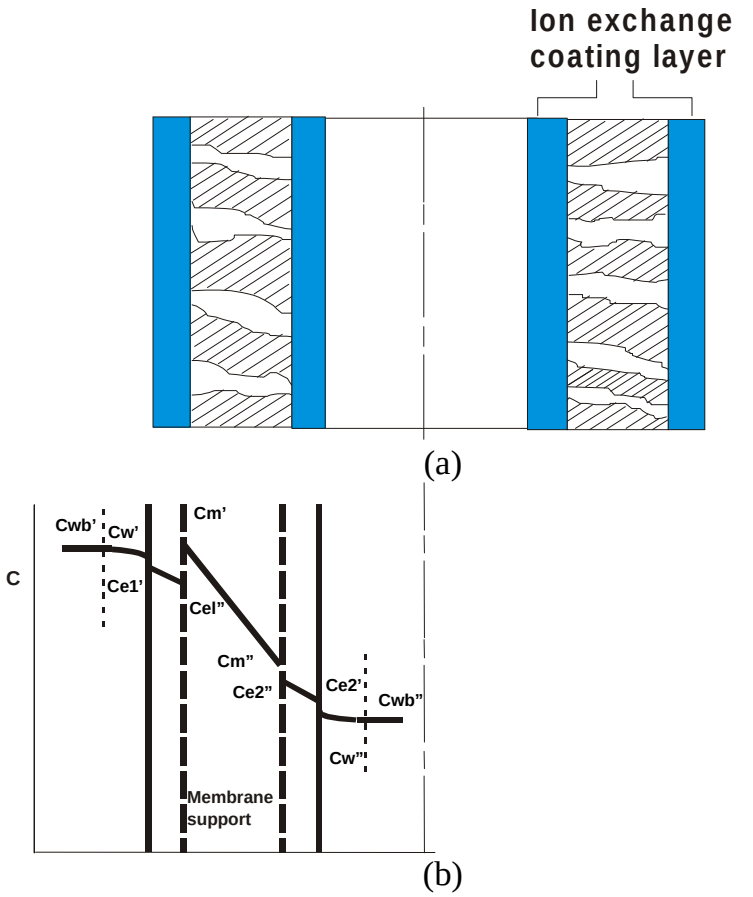

Figure 6.5 *Solute concentration profiles for extraction of ions with a composite hollow fiber membrane. (a) specifications of the hollow fiber; dense layers refer to the hydrophilic coating; (b) concentration profiles.*

A relation between the transport resistance or the overall mass transfer coefficients and all other transfer coefficients can be obtained as

$$\frac{1}{K_w d_{in}} = \frac{1}{K'_{wb} d_{out}} + \frac{1}{K_{e1} d_{e1}} + \frac{1}{m K_m d_m} + \frac{1}{K_{e2} d_{e2}} + \frac{1}{K''_{wb} d_{in}} \qquad (2)$$

K_w is the overall mass transfer coefficient based on the aqueous phases. K_{wb}', K_m, K_{wb}'' are the local mass transfer coefficients for the first aqueous phase, the membrane matrix and the second aqueous phase, respectively. K_{e1} and K_{e2} are the local mass transfer coefficients for the first and the second ion exchange coating layers. d_{in}, d_{out}, d_{e1}, d_{e2} and d_m represent the dimensions of the hollow fiber. m is the solute distribution coefficient.

6.4.2 Simplification of the model

The mass transfer relationship is obtained for a hollow fiber SLM system, either without coating or with only one coating layer using Equation 2.

For uncoated hollow fibers, $\frac{1}{K_{e1}d_{e1}}$ and $\frac{1}{K_{e2}d_{e2}}$ do not exist and the overall mass transfer coefficient is given as

$$\frac{1}{K_w d_{in}} = \frac{1}{K'_{wb} d_{out}} + \frac{1}{mK_m d_m} + \frac{1}{K''_{wb} d_{in}} \tag{3}$$

For a composite hollow fiber membrane with an outside coating only, the total resistance to mass transfer is given as

$$\frac{1}{K_w d_{in}} = \frac{1}{K'_{wb} d_{out}} + \frac{1}{K_{e1} d_{e1}} + \frac{1}{mK_m d_m} + \frac{1}{K''_{wb} d_{in}} \tag{4}$$

For a membrane coated at the inside, Equation 2 reads

$$\frac{1}{K_w d_{in}} = \frac{1}{K'_{wb} d_{out}} + \frac{1}{mK_m d_m} + \frac{1}{K_{e2} d_{e2}} + \frac{1}{K''_{wb} d_{in}} \tag{5}$$

Moreover, by assuming negligible resistances at the aqueous boundary layers (both at feed and strip side) compared to the diffusion resistance, Equations 3, 4 and 5 can be expressed as

$$\frac{1}{K_w d_{in}} \approx \frac{1}{mK_m d_m} \tag{6}$$

$$\frac{1}{K_w d_{in}} \approx \frac{1}{K_{e1} d_{e1}} + \frac{1}{mK_m d_m} \tag{7}$$

$$\frac{1}{K_w d_{in}} \approx \frac{1}{mK_m d_m} + \frac{1}{K_{e2} d_{e2}} \tag{8}$$

Hence, we can estimate the individual mass transfer coefficients separately. Neglecting any liquid phase boundary layer can be rationalized by the optimized flow rates for both aqueous phases.

The mass transfer in a membrane contactor is the same as described before except an additional mass transfer resistance occurs from the transport of the organic phase from one module to the other. This can be accounted for a mass transfer coefficient K_o. For a membrane contactor consisting of two composite hollow fiber membranes, the overall mass transfer relationship can be given as

$$\frac{1}{K_w d_{in}} = \frac{1}{K_{e1} d_{e1}} + \frac{1}{mK_m d_m} + \frac{1}{K_o} + \frac{1}{mK_m d_m} + \frac{1}{K_{e2} d_{e2}} \tag{9}$$

where two resistances from two coating layers ($\frac{1}{K_{e1}d_{e1}}$ and $\frac{1}{K_{e2}d_{e2}}$) are included as well as the porous supports ($\frac{1}{mK_m d_m}$) and the transportation of the organic phase between the two modules ($\frac{1}{K_0}$). If the flow rate of the organic phase is zero, an infinite resistance exists and no ions will be transferred from one module to the other. However, by assuming an optimal organic phase flow rate in the bore side of the hollow fiber, the transport resistance between two modules can be neglected, as

$$\frac{1}{K_o} \approx 0 \tag{10}$$

This assumption is evaluated by comparing the transport time through different parts. It is found that Equation 10 is valid for the flow rate of organic phase used in our case. Thus, we have

$$\frac{1}{K_w d_{in}} = \frac{1}{K_{e1}d_{e1}} + \frac{2}{mK_m d_m} + \frac{1}{K_{e2}d_{e2}} \tag{11}$$

This equation represents the maximum transport capacity of a contactor system with two hollow fiber modules. The model needs only three bench-scale experiments for the parameter evaluation, i.e. a transport of a fiber without coating, transport of a fiber with a coating facing the feed phase and with a coating facing the strip phase. All these can be obtained from experiments in a SLM operation mode.

6.4.3 Results

Chapter 5 describes the performance of SLMs with and without coatings in contact with the feed or strip side. From these experiments, the mass transfer resistance can be obtained. As seen in Table 6.2, the predicted values for both PSf and PP membranes are quite comparable to the experimental values. It confirms the feasibility of the resistance model in the description of the transport process of a membrane contactor.

According to the model, a higher contactor flux can be obtained by improving the initial copper flux as SLM, as seen in Figure 6.6. A PSf membrane is taken as an example with an original flux of 5.1 $x10^{-9}$ $mol.cm^{-2}.s^{-1}$. By increasing the copper flux of the membrane at the feed side of the contactor, the overall contactor flux can be improved up to 3 $x10^{-9}$ $mol.cm^{-2}.s^{-1}$. However, by improving the flux at the strip side, the overall contactor flux increases to a much higher value. This implies that the transport-limiting step is at the strip side, caused by the low swelling of the stabilization layer in the concentrated acid. In order to obtain a productive membrane contactor, all

transport resistance needs to be minimized. In fact, the ideal membrane contactor system would comprise of two thin, dense ion exchange hollow fibers.

Table 6.2 *Comparison of predicted and experimental permeation of membrane contactors based on composite PSf and Accurel PP Q3/2 hollow fiber membranes.*

Terms			PSf	Accurel PP
Copper fluxes (10^{-9} mol.cm^{-2}.s^{-1})	SLMs*	uncoated membrane	5.1	5.3
		Coating at feed	7.2	5.8
		Coating at strip	3.4	4.0
	Contactors	Prediction	2.3	2.4
		Experimental	2.2	2.4

* From Chapter 5. Coating at feed: the composite membrane with feed facing the coating layer; Coating at strip: the composite membrane with strip facing the coating layer.

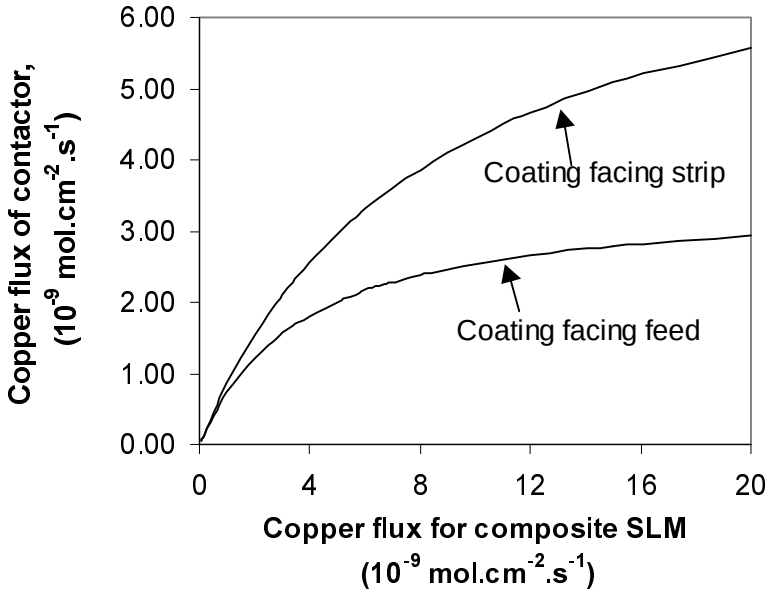

Figure 6.6 *Modeling flux of contactors by changing copper flux in SLM with coated polysulfone hollow fiber membranes.*

6.5 Scale-up of the membrane contactor

A larger bench-scale process is developed with Accurel Q6/2 polypropylene membranes as support and a SPEEK coating at the outside surface (Figure 6.7). All specifications are listed in Table 6.3. A larger fiber diameter (Q6/2 instead of Q3/2) is used for the following reasons:

- Firstly, it shows less dimensional increase caused by organic phase than a smaller fiber; therefore, better hydrodynamic transport can be achieved for the feed and the strip phases.
- Secondly, the small fiber is difficult to coat according to our experience [15].

A flux of 1.8-1.9 $x10^{-2}$ $mol.m^{-2}.hr^{-1}$ (0.47-0.53 $x10^{-9}$ $mol.cm^{-2}.s^{-1}$) is obtained in the extraction of the copper. The value is low compared to the fluxes shown before. We attribute this to the thick membrane matrix layer for copper transport. It is also a side proof that decreasing the thickness of the support can increase the performance of the membrane contactor.

Table 6.3 *Specifications of the large bench scale modules for membrane contactor operation.*

Dimension of the composite hollow fibers	Outside diameter (mm)	3.0
	Inner diameter (mm)	1.8
Specifications of membrane contactor	Effective length (cm)	22
	Number of fibers	30
	Effective surface area (m^2)	0.062
	Volume of feed and strip (liter)	2.0
	Volume of organic phase (liter)	0.170
Flow rate ($l.hr^{-1}$)	Feed	93.6
	Strip	93.6
	Organic phase	29
Copper permeation (10^{-2} $mol.m^{-2}.hr^{-1}$)		1.8-1.9

The composite membranes used are based on Accurel Q6/2 PP fibers. The SPEEK coating is performed at 10wt% SPEEK in methanol for five coating steps.

6.6 Conclusions

In this chapter, a membrane contactor system has been described for the copper transport using a novel hollow fiber membrane with a cation exchange coating layer. Stability and permeation results demonstrate that long-term operation has been realized in a bench-scale process. A resistance model has been developed to estimate the copper flux of the membrane contactor based on the initial SLM permeability.

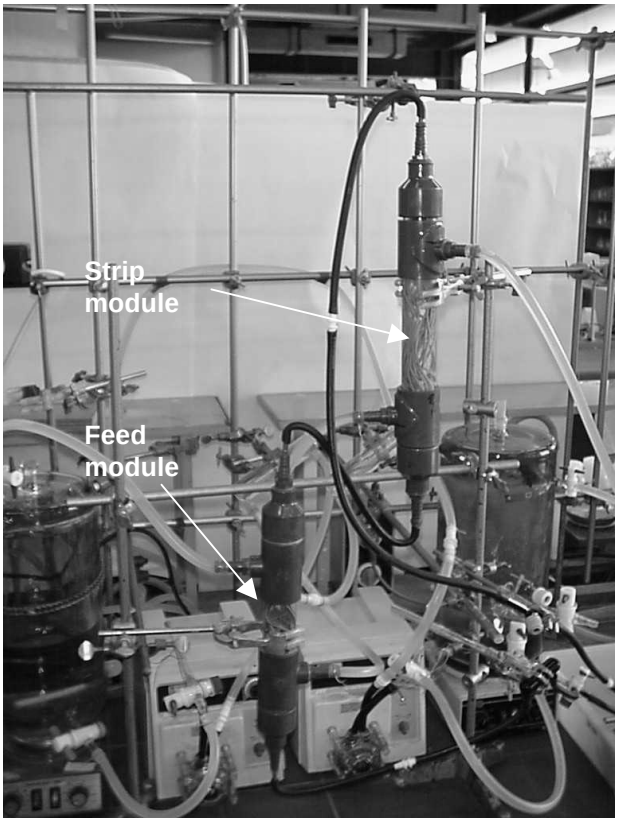

Figure 6.7 *Photo of large bench-scale modules based on Accurel Q6/2 PP support membranes.*

The model agrees well with experimental results for membrane contactors based on support membrane of PSf and the PP. According to the model, an improvement in flux is expected using a membrane contactor system composed of two thin dense ion exchange hollow fibers.

6.7 Notation

$C_{wb}^{'}$, $C_{wb}^{''}$	ion concentration in two bulk aqueous phases, mol.L^{-3}
$C_{w}^{'}$, $C_{w}^{''}$	ion concentration at two interfaces between aqueous and coating layers, mol.L^{-3}
$C_{e1}^{'}$, $C_{e1}^{''}$	ion concentration in the first ion exchange coating at aqueous and organic sides, mol.L^{-3}
$C_{e2}^{'}$, $C_{e2}^{''}$	ion concentration in the second ion exchange coating at aqueous and organic sides, mol.L^{-3}
$C_{m}^{'}$, $C_{m}^{''}$	concentration of ion-organic complex in the organic phase at two aqueous and organic interfaces respectively, mol.L^{-3}
d_{in}	inner diameter of the composite fiber membrane, L
d_{out}	Outer diameter of the composite fiber membrane, L
d_{e1}	effective diameter of the first coating layer, L
d_{e2}	effective diameter of the second coating layer, L
d_{m}	effective diameter of the liquid membrane layer, L

K_w	overall mass transfer coefficient based on aqueous phase, $L.t^{-1}$
K_m ,	membrane mass transfer coefficient for ions, $L.t^{-1}$
K_{wb}	local mass transfer coefficient in the first aqueous phase, $L.t^{-1}$
K_{e1}	mass transfer coefficient when coating at the shell side, $L.t^{-1}$
K_{e2}	mass transfer coefficient when coating at the lumen side, $L.t^{-1}$
K_{wb} "	local mass transfer coefficient in the second aqueous phase, $L.t^{-1}$
K_o	mass transfer coefficient from transport of the organic phase from feed module to strip module, $L.t^{-1}$
m	solute distribution coefficient: ratio of organic phase solution concentration to aqueous phase solute or solution concentration in ion exchange materials.

6.8 References

[1] B. W. Reed, M. J. Semmens, and E. Cussler, Membrane contactors, in R. D. Noble and S. A. Stern, ed., Membrane Separations Technology. Principles and Applications, Elsevier Science B.V., Amsterdam, 1995, p467-498.

[2] K. Sirkar, Membrane separation technologies: current developments, Chem. Eng. Comm., 157 (1997) 145-184.

[3] A. Gabelman and S. T. Hwang, Hollow fiber membrane contactors, J. Membrane Sci., 159 (1999) 61-106.

[4] A. Sengupta, R. Basu, R. Prasad, and K. K. Sirkar, Separation of liquid solutions by contained liquid membranes, Sep. Sci. Technol., 23 (1988) 1735-1751.

[5] A. K. Guha, C. H. Yun, R. Basu, and K. Sirkar, Heavy metal removal and recovery by contained liquid membrane permeator, AIChE J., 40 (1994) 1223-1237.

[6] D. K. Mandal, A. K. Guha, and K. K. Sirkar, Isomer separation by a hollow fiber contained liquid membrane permeator, J. Membrane Sci., 144 (1998) 13-24.

[7] R. Basu and K. K. Sirkar, Hollow fiber contained liquid membrane of citric acid, AIChE J., 37 (1991) 383-393.

[8] M. Teramato, N. Tohno, N. Ohnishi, and H. Matsuyama, Development of a spiral-type flowing liquid membrane module with high stability and its application to the recovery of Chromium and Zinc, Sep. Sci. Technol., 24 (1989) 981-999.

[9] M. Teramoto, H. Matsuyama, and T. Yonehara, Selective facilitated transport of benzene across supported and flowing liquid membranes containing silver nitrate as carrier, J. Membrane Sci., 50 (1990) 269-284.

[10] M. Teramoto, H. Matsuyama, T. Yamashiro, and S. Okamoto, Separation of ethylene from ethane by a flowing liquid membrane using silver nitrate as a carrier, J. Membrane Sci., 45 (1989) 115-136.

[11] S. Schlosser and I. Rothova, A new type of hollow-fiber pertractor, Sep. Sci. Technol., 29 (1994) 765-780.

[12] I. M. Coelhoso, P. Silvestre, R. M. C. Viegas, J. P. S. G. Crespo, and M. J. T. Carrondo, Membrane-based solvent extraction and stripping of lactate in hollow-fiber contactors, J. Membrane Sci., 134 (1997) 19-32.
[13] M. C. Wijers, M. Jin, M. Wessling, and H. Strathmann, Supported liquid membranes modification with sulphonated poly(ether ether ketone): permeability, selectivity and stability, J. Membrane Sci., 147 (1998) 117-130.
[14] O. Kedem and L. Bromberg, Ion-exchange membranes in extraction processes, J. Membrane Sci., 78 (1993) 255-264.
[15] T. He, M. H. V. Mulder, and M. Wessling, Composite hollow fiber membranes as supported liquid membranes, Chapter 5.
[16] T. He, M. H. V. Mulder, and M. Wessling, Permeation and stability of polysulfone hollow fibers for supported liquid membranes, Chapter 3.
[17] Y. Liu, G. H. Koops, and H. Strathmann, Morphology controlled PES hollow fibers by the addition of PEG in dope and lumen solutions, Sep. Purif. Technol., To be published.
[18] R. Prasad and K. K. Sirkar, Membrane-based solvent extraction, in W. S. W. Ho and K. K. Sirkar, ed., Membrane Handbook, Van Nostrand Reinhold, New York, 1992.

One monk carries water by himself. Two monks lift water together. Three monks have no water to drink since no body takes responsibility.
(Chinese parable)

Chapter 7 Nanofiltration membranes by coating polyethersulfone hollow fibers with sulfonated poly (ether ether ketone) (SPEEK)

Abstract

We report a new type of nanofiltration membrane based on coating of a sulfonated poly (ether ether ketone) layer on top of a polyethersulfone or polysulfone support. The membrane is characterized by rejection measurements of a dextran mixture, salts and dyes. Due to its negative charge, the coating layer shows a retention in the order of Na_2SO_4 > NaCl > $MgCl_2$. In addition, the composite membranes show a 97 to 100% retention to negatively charged organic dyes with a molecular weight of about 450 $g.mol^{-1}$. The rejection results can be improved by increasing the coating thickness and the polymer concentration in the coating solution. Moreover, penetration of SPEEK into the support prevents it from free swelling, thus increases the fixed charge density and the retention. The Donnan-steric-pore-model is used to describe the membrane properties.

7.1 Introduction

Nanofiltration (NF) covers the filtration spectrum between ultrafiltration and reverse osmosis. The unique feature of nanofiltration is the separation of mono and bivalent ions as well as a high rejection for organic compounds with a molecular weight from 100 to 500 $g.mol^{-1}$ [1, 2]. Even though the transport mechanism is not yet fully understood, the applications expand rapidly [2]. Most of the approaches for manufacturing nanofiltration membranes can be found in Petersen's extensive review article [3]. In general, these membranes are prepared in two subsequent steps. Nanofiltration membranes can be prepared in a one step process by immersion precipitation process (including co-extrusion) as well [4, 5] as can be seen in Table 7.1.

In terms of the fabrication characters, three different approaches can be used to prepare nanofiltration membranes (Table 7.1). Immersion precipitation process generally prepares membranes with distinct pores at nanometer range. The membranes show low rejection to inorganic salts but high rejection to organic dyes. Coating of a dense layer can achieve a broad range of rejection properties dependent on the coating material used. This coating layer normally swells at the operation condition, which is completely different from its dry state. It is because of the change of the structure at the operation conditions, which contributes the nanofiltration properties. Among chemically controlled cross-linked polymer coating techniques, interfacial polymerization (IP) is the most successful and important example. The membranes prepared by the last two approaches, most of the time, are regarded as a porous support with a dense active layer.

The further understanding of the transport mechanism in recent years [5-22], combined with earlier research work [23-30], reveals a contradictory description of the active layer in nanofiltration membranes. Basically, a dense skin layer is assumed by the Torell-Meyer-Sievers model (TMC) and the hybrid model. On the contrary, the Space-charge model and the Donnan-steric-pore-model (DSPM) are based on a porous skin layer [12, 16]. These models all has been successfully applied in prediction the electrolyte rejection by NF membranes in aqueous solutions. In a recent paper of Bowen et al. [9], well-formed pores at the surface of commercial membrane by IP technique were observed by atomic force microscopy (AFM), which supported validity of the DSPM model. The other support was an immersion type of membrane which possessed well-defined pores and high real rejection [5]. This membrane showed high permeation as well. For the NF membrane prepared by coating, no pores can be detected at a dry state. However, at the swollen state, pores might be existed, which is still in lack of thorough investigation.

In this chapter, we address the formation of nanofiltration membranes by coating of sulfonated polymers. The membrane belongs to the second category as listed in Table 7.1. The dense skin layer swells in aqueous solutions and the swelling degree is a function of the sulfonation degree. The sulfonation time determines the sulfonation degree as well as the ion exchange capacity and the

fixed charge density. Sulfonated polymers, i.e. sulfonated polysulfone [31], sulfonated polyethersulfone [32, 33], sulfonated poly(2,6-dimethyl-1,4-phenylene oxide) [34] have been investigated by several researchers. These studies were focused on a flat membrane support. In this chapter, hollow fiber support membranes are used and a chemically stable material, sulfonated poly (ether ether ketone) (SPEEK), is applied as a coating material [35]. SPEEK can also have a much higher ion exchange capacity compared to sulfonated polysulfone or sulfonated polyethersulfone without dissolving in water. SPEEK is much more chemically stable than most of the current nanofiltration membranes as well, which are based on polyamide. Furthermore, commercial membranes, such as the NTR 7450 series from Nitto Denko based on sulfonated polyethersulfone, involve a tedious synthetic work [32].

Table 7.1 *Category of polymeric nanofiltration membrane in terms of fabrication and structure.*

Approaches	**Membrane structure**	**Properties**	**Examples**
Immersion precipitation	Porous of nano-pores	Low rejection to inorganic ions but high to organic ions	Co-extruded SPES/PSf hollow fiber membrane; SPEEK/PSf blend membrane
Coating	Dense in dry state, but swollen in wet state	Rejection controlled by substitution degree	Sulfonated polysulfone, sulfonated polyethersulfone
Cross-linked polymer coating	Slightly swollen in aqueous solutions	Rejection controlled by monomers, reaction conditions	Interfacial polymerised polymer, cross-linked PVA coating

The swelling of SPEEK at high ion exchange capacity may form a hydrogel-like structure with extended meshes, where the water clusters form the effective pores. By adjusting the ion exchange capacity of the coating material, the swelling can be changed and hence the mesh size and the fixed charge density, resulting in tunable separation properties. The DSPM model is used to predict the rejection properties of the SPEEK coated membrane by incorporating the pore size measured experimentally.

7.2 Experimental

7.2.1 Materials and membranes

Poly (ether ether ketone) powder (Victrex PEEK 450PF, Mw 102000 g.mol-1, specific density 1.34 $kg.l^{-1}$) was purchased from ICI. AG grade methanol was obtained from Merck. Ultrapure water was from a MilliQ water

purification unit (Millipore Corp.). AG grade sodium sulfate (Na_2SO_4), sodium chloride (NaCl) and magnesium chloride ($MgCl_2$) were purchased from Merck. Two dyes were used: procion blue (Mw 840.12 $g.mol^{-1}$, negatively charged, λ_{max} 607 nm, from Chimica) and sunset yellow (Mw 452.38 $g.mol^{-1}$, negatively charged, λ_{max} 482 nm, from Aldrich).

SPEEK was prepared and characterized following the same procedure as described in former work [36]. Polyethersulfone (PES) and polysulfone (PSf) porous membranes were prepared in our laboratory with the properties as listed in Table 7.2.

Table 7.2 *Properties of the support membranes used in this experiment.*

Material	**PES**	**PSf**
ID/OD (mm)	0.60/1.3	0.65/0.9
Skin layer	Inside	Inside
Pore radius (nm)*	10	26
Pure water permeability ($l.m^{-2}.hr^{-1}.bar^{-1}$)	1500	540

* determined by permporometry [37].

7.2.2 Coating procedure of SPEEK onto support membranes

Methanol was used as solvent for SPEEK. Two types of SPEEK were selected because of their difference in water uptake as can be seen in Table 7.3. The solutions were filtered with a 15 μm filter before degassing, and then applied at the inner surface of the hollow fiber using the equipment shown in Figure 7.1. The solution was raised from the bottom to the top of the fiber by an air bulb. After observing the solution at the top of the fiber, the solution was allowed to remain inside the fiber for 3 seconds and drained from the bottom of the fiber by gravity. Immediately after the drainage, the membrane was dried with flowing nitrogen gas from a gas cylinder for 24 hours. The membranes were coded with three preparation parameters as material-concentration-coating steps. For example, membrane 120-1.0-1 represents the coating of the SPEEK sulfonated for 120 hours (S-120) at a polymer concentration of 1wt% for one coating step.

Table 7.3 *Water uptake of SPEEK at 25^oC.*

SPEEK	Swelling (wt%)
S-120	50
S-140	440

S-120 indicates that the sulfonation time is 120 hours.

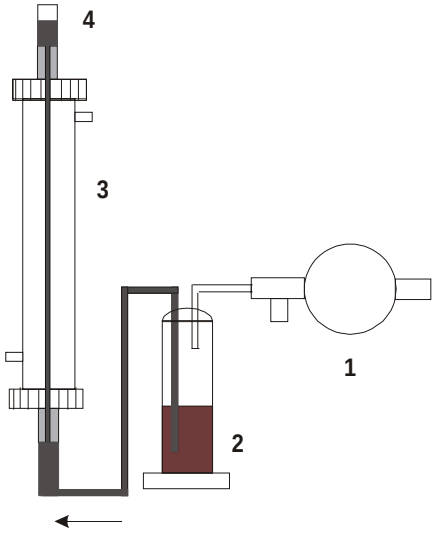

Figure 7.1 *Coating setup. 1, rubber bulb; 2, solution cell; 3, membrane module; 4, overflow indicator.*

7.2.3 Characterization of composite membrane

Two hollow fibers with an effective length of 20 cm were mounted onto a permeation setup as shown in Figure 7.2. A pressure difference of 0.2 bar between the inlet and outlet of the module gave a flow velocity inside the fiber of 0.48 $m.s^{-1}$. The average working pressure was set to 2.0 bar absolute. The rejection of dextrans by the membrane was determined with a feed solution of ultrapure water with 0.3wt% dextran (Mw 71400 $g.mol^{-1}$, polydispersity 4.7, Sigma Chemicals, Sigma D-3759) and 0.03wt% ethylene glycol as internal gel permeation chromatography (GPC)-standard. Both retentate and permeate were analyzed by GPC (Polymer Standards Service, PSS GmbH). The specifications of the GPC was as follows: GPC columns, PSS Suprema 1000 and PSS Suprema 30; detector: Shodex RI 71 differential refractometer (Shodex); software: WINGPC 6 GPC software (Polymer Standards Service); eluent, 0.05 M $NaNO_3$ in ultrapure water (MilliQ), flow = 1.0 $ml.min^{-1}$; Sieve Curve Determination using PSS WINGPC Software. The molecular weight cut-off (MWCO) is defined as the dextran molecular weight which the membrane shows 90% rejection. The molecular radius, r_s (m), was calculated by using the Stokes-Einstein equation,

$$r_s = \frac{kT}{6\pi\mu D} \qquad (1)$$

D is the diffusivity of the dextran in water; T is the temperature; μ is the viscosity of the water. By fitting experimental results as reported in literature for several organic solutes [38], an empirical relationship was obtained as

$$r_s = (0.182 \times \ln M_w - 0.577) \times 10^{-9} \quad (2)$$

where M_w is the molecular weight of the dextran.

For salt and organic dye rejection, a concentration at 500 ppm was used. A conductivity meter (Model LF 537, Wissenschaftliche-Technische Werkstätten, Germany) was used to measure the salt concentrations in the feed and permeate solutions. UV/VIS Scanning Spectrophotometer (PU8720, Philips) was used to measure the dye concentration. The observed rejection is calculated as

$$R = 1 - \frac{C_p}{C_f} \quad (3)$$

in which C_p and C_f are the permeate and feed concentration in the bulk, respectively.

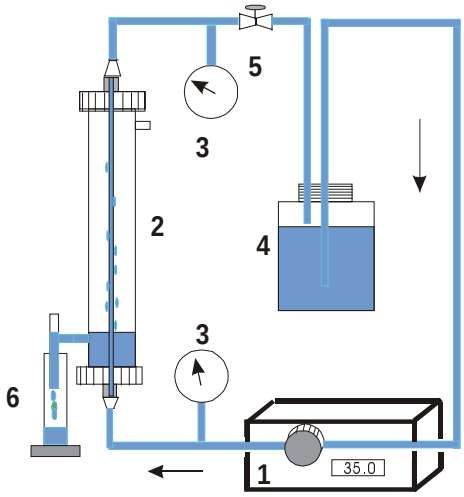

Figure 7.2 *Schematic of permeation setup. 1, pump; 2, module; 3, manometer; 4, feed tank; 5, valve; 6, permeate.*

7.2.4 Scanning electron microscopy

Samples for scanning electron microscopy (SEM, JEOL JSM-T220A) were prepared by cryogenic breaking of the fresh wet fibers. Samples were allowed to dry under vacuum at 30°C overnight and coated with a thin gold layer. A field emission scanning electron microscopy (FESEM, JSM 5600 LV) was used to characterize the inner surface of the PES membrane.

7.3 Results and discussion

7.3.1 Structure of composite membranes

The coating thickness is a function of the polymer concentration in the coating solution. Figure 7.3 shows that the coating thickness increases with increasing SPEEK concentration. A sharp increase of the thickness is observed in the region of 1.5 to 3wt%, which probably originates from pore penetration of SPEEK into the pores of the support membrane. At lower polymer concentration, the penetration of the polymer solution into the support layer may occur. At higher concentration, this may not occur due to the higher viscosity of the coating solution. As can be seen in Figure 7.4, a sharp interface between coating polymer and the support is obtained for a concentration of 5wt%; at 0.5wt%, the dense coating layer is basically soaked into the skin of the support membrane.

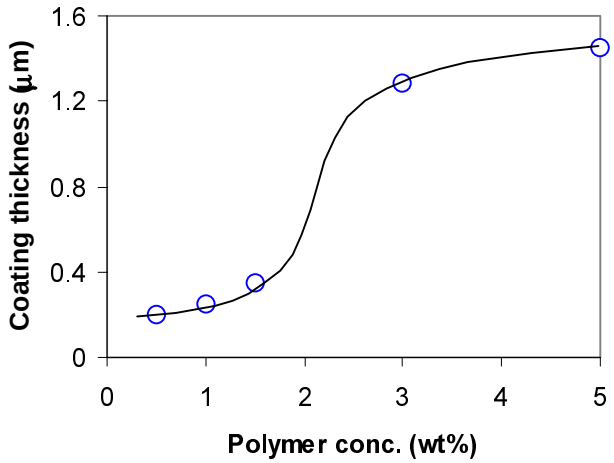

Figure 7.3 *Effect of the coating solution concentration of SPEEK S-120 on the coating layer thickness. Support membrane: PES.*

Whether the polymer penetrates into the porous structure depends on several parameters, i.e. SPEEK concentration, solvent, pore size of the support, and drying techniques. With the selected solvent and drying technique, the coating polymer concentration and the pore size of the support membrane may be varied. At a concentration higher than the association concentration [39], the penetration of coating material inside the support structure is much less than at lower concentration. Consequently, a much thicker coating can be obtained when less penetration occurs. However, when the pore size of the support membrane increases, the penetration of the coating polymer is expected even at a higher concentration. This will be elucidated in the later discussion.

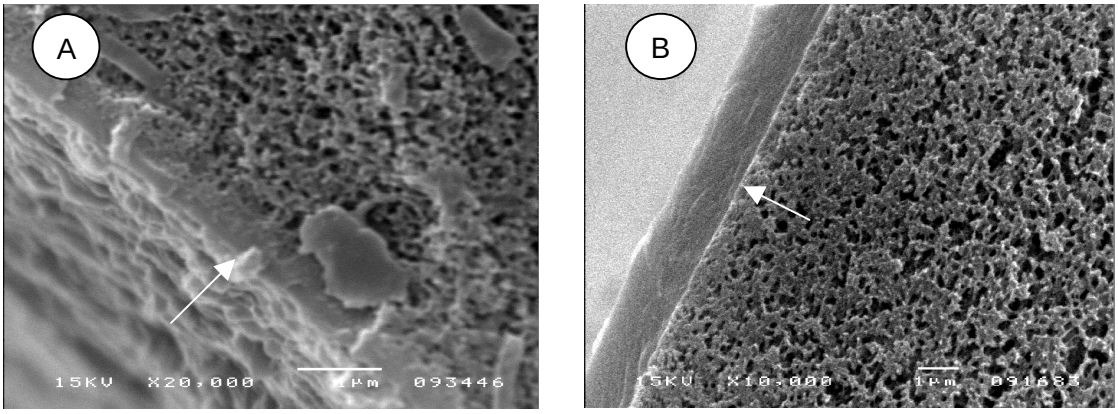

Figure 7.4 *SEM photos of composite membranes with a SPEEK layer of S-120. (A) 0.5wt%; (B) 5.0wt%. Arrows refer to the coating layers.*

7.3.2 Pore size of composite membranes

SPEEK is a highly swollen material in water as indicated by the water uptake. It acts as a physically cross-linked network as well. A highly swollen material contains meshes which can incorporate and separate macromolecules with different size [40]. The mesh size depends on the size of the chain between the consecutive cross-links, the activity of the water at the environment and crystallinity of the material. As an amorphous material with a sulfonation degree higher than 9 % [41], the swelling of SPEEK is affected mostly by the -$SO_3^-H^+$on the backbone of the polymer chains. Increase of the mesh size can be achieved by increasing the sulfonation time and consequently increase the swelling. A large difference in swelling between S-120 and S-140 indicates that two polymers may have a significant difference in mesh size at swollen state, hence, in molecular weight cutoff (MWCO).

Table 7.4 shows the MWCO values ranging from 5000 to 35000 Dalton, which correspond to a mesh radius in the scale of 0.9 to 1.3 nm, being similar to that of a microporous hydrogel [40]. The mesh radius is much smaller than the support membrane, which has an average pore radius of 10 nm (as can be seen in Table 7.2). Since the membrane shows high flux (as can be seen in Table 7.4), a convective transport predominates the overall transport rather than diffusive transport. This high flux is an indirect proof of the existence of the mesh-like pores.

The SPEEK concentration in the coating solution also affects the membrane MWCO. For a coating concentration of 0.5 to 5.0wt%, the molecular weight cutoff ranges from 7400 $g.mol^{-1}$ to 22000 $g.mol^{-1}$ and then decreases to about 5000 $g.mol^{-1}$ (see Table 7.4). This observation itself is already surprising since the ion exchange coating is normally regarded as a dense layer.

Table 7.4 *Coating thickness[a] and molecular weight cutoff values of the SPEEK coated membranes.*

Sulfonation time	SPEEK conc. (wt%)	Coating thickness (μm)	MWCO	Stoke Radius (nm)	PWP[b]
120	0.5	0.19	5300 7400	0.98 1.04	20-30
	1.0	0.22	9400 11000 22000	1.09 1.12 1.24	20-40
	3.0	1.3	5300	0.98	2-8
	5.0	1.5	5000	0.97	0.8-1
140	1.0	0.22	35000	1.33	40

[a] coating thickness is estimated from the SEM images by neglecting the penetration of SPEEK into the substructure. Gross error estimated to be within 10%; [b] Pure water permeation, $l.m^{-2}.hr^{-1}.bar^{-1}$.

The MWCO for the membrane prepared with a 0.5wt% solution is similar to that of a 5wt% solution. Combining the SEM photos in Figure 7.4, this could be caused by the partial penetration of the polymer confined by the porous structure, leading to a decrease in swelling, or the "pore" size. To understand the decrease of the MWCO from 22000 to 5000 $g.mol^{-1}$, we believe that the dextran molecules easily partition into the swollen coating layer. With the convective flow of water through the coating, the dextran is dragged through the network by disentanglement and stretching. The retention of the macromolecular dextran is a complex function of polymer network structure, degree of swelling and membrane thickness. At low fluxes (thick membrane), drag forces are considered to be low and disentanglement occurs to a less extent. The macromolecular dextran remains in its original coil-like conformation, resulting in a higher retention. This can be found for coating concentration of 3 and 5wt%. Moreover, at higher ion exchange capacity, i.e. S-140, the swelling degree increases, generating a larger "pore" diameter and a higher flux. The latter causes strong disentanglement and drag forces inducing an even larger MWCO.

7.3.3 Nanofiltration properties of composite membranes

The change of swelling degree and the coating thickness influence the separation performance of the composite membrane. The pore penetration of the coating material affects the pore size as well. In this section, we will discuss

these parameters with several examples in terms of the ion separation properties.

7.3.3.1 Effect of swelling degree

For both membranes 120-1.0-1 and 140-1.0-1, the same order of salt rejection is obtained (Figure 7.5)

$$Na_2SO_4 > NaCl > MgCl_2$$

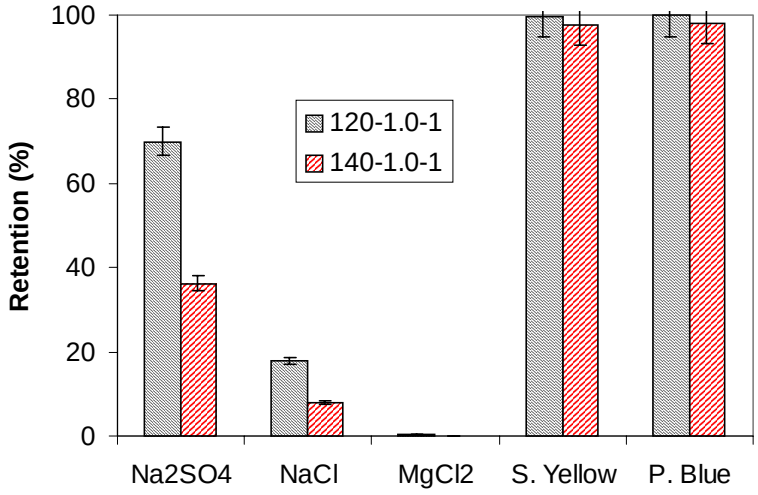

Figure 7.5 *Effect of different coating polymers on the retention of the membranes. 120-1.0-1 means a membrane prepared by a coating polymer S-120 at concentration of 1.0wt% by one step coating. Support membrane: PES.*

This sequence is based on the Donnan exclusion mechanism for negatively charged membranes [42]. In addition, Membrane 120-1.0-1 shows a rejection of 70% for Na_2SO_4 and almost 100% for sunset yellow (Mw 452.38 g.mol^{-1}) and procion blue (840.12 g.mol^{-1}), which are negatively charged organic dyes. Since S-140 shows a higher swelling value and a lower fixed charge density, a lower salt rejection is observed for membrane 140-1.0-1: 36% for Na_2SO_4. However, the rejection for sunset yellow and procion blue remains high up to 98%. This can be explained by a synergistic effect of steric hindrance and Donnan exclusion [12].

7.3.3.2 Effect of number of coating steps

A coating solution of S-140 (1.0 wt%) is used to investigate the effect of the coating steps. Figure 7.6 (B) shows a thicker coating layer for two coating steps and a more condensed penetrating layer into the support structure than the membrane prepared with one coating step (Figure 7.6 (A)). As seen in Figure 7.6 (C), the rejection of Na_2SO_4 increases from 36% to 79% when the number of coating steps increases from one to two. For NaCl, the rejection increases from 8% to 23%. The dye molecules show the same rejection

behavior independent on the coating steps. The water permeability of membrane 140-1.0-2 is much lower than that of membrane 140-1.0-1; a value of 40 $l.m^{-2}.hr^{-1}.bar^{-1}$ is obtained for the former membrane but only 5-8 $l.m^{-2}.hr^{-1}.bar^{-1}$ for the latter membrane having a thicker coating layer. This might be caused by increased penetration and thicker coating layer.

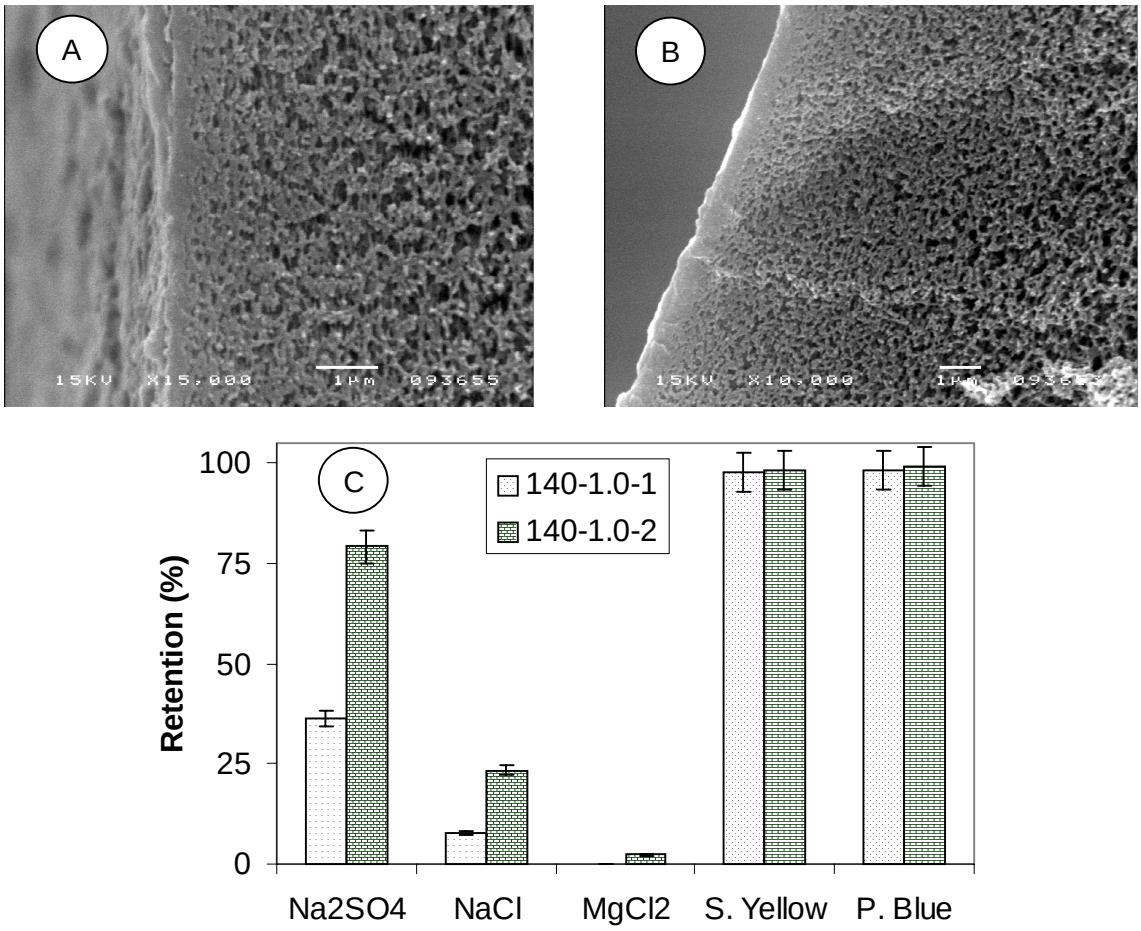

Figure 7.6 *Effect of number of coating steps on the retention of the membrane. Membrane code: 140-1.0-1 means a membrane prepared by a coating polymer S-140 at concentration of 1.0 wt% by one step coating. 140-1.0-2 means two step coating procedures. Support membrane: PES.*

7.3.3.3 *Effect of polymer concentration*

The effect of the polymer concentration in the coating solution is shown in Figure 7.7. The retention is hardly affected by the coating concentration. We have no conclusive support, but believe that the penetration into the support increases the fixed charge density counteracting a low rejection associated with a thin layer.

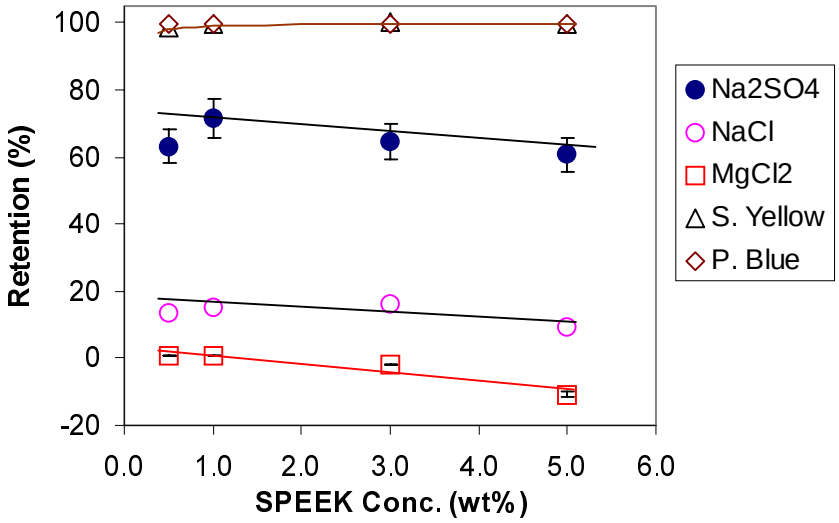

Figure 7.7 *Effect of coating polymer concentration on the retention of the membranes. Support membrane, PES; coating solution: S-120 in methanol.*

7.3.4 Proof of pore-penetration mechanism

In order to demonstrate the difference in pore penetration, a coating solution of SPEEK of 5wt% is used since it does not show a clear penetration for PES support with small pores (Figure 7.8 (A) and (C)).

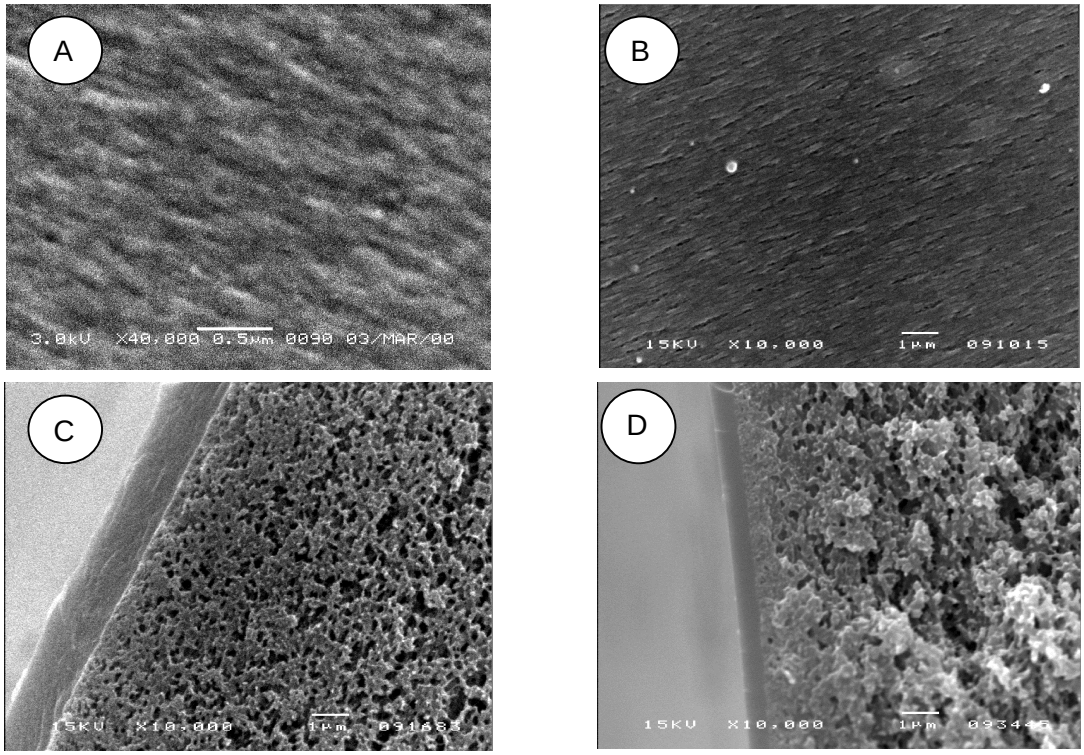

Figure 7.8 *SEM pictures of the surface structure of PES and PSf hollow fiber membranes and the inner skin layers of composite membranes. (A) Inner surface of PES membrane (FESEM); (B) Inner surface of PSf membranes; (C) Skin layer of composite PES membrane; (D) Skin layer of composite PSf membranes. Coating solution: S-120 at 5wt%.*

However, the solution penetrates into a PSf support membrane, which has bigger pores, as can be seen in Figure 7.8 (B) and (D). Under exactly the same coating conditions, a coating thickness of 1.5 µm is obtained for the PES membrane, compared to a thickness of only 0.5 µm for the PSf membrane. In case of the PSf support, pore penetration is visible from the interface. Consequently, the effect of the pore penetration is shown with the rejection results in Figure 7.9. A thicker coating layer based on the PES membrane gives higher water permeation and lower rejections than a thinner coated membrane based on the PSf membrane. A confined polymer network inside a pore shows decrease in swelling because of the constraint. Thus, the fixed charge density increases and the pore size decreases, which explains a higher rejection and a lower flux for a much thinner coated membrane.

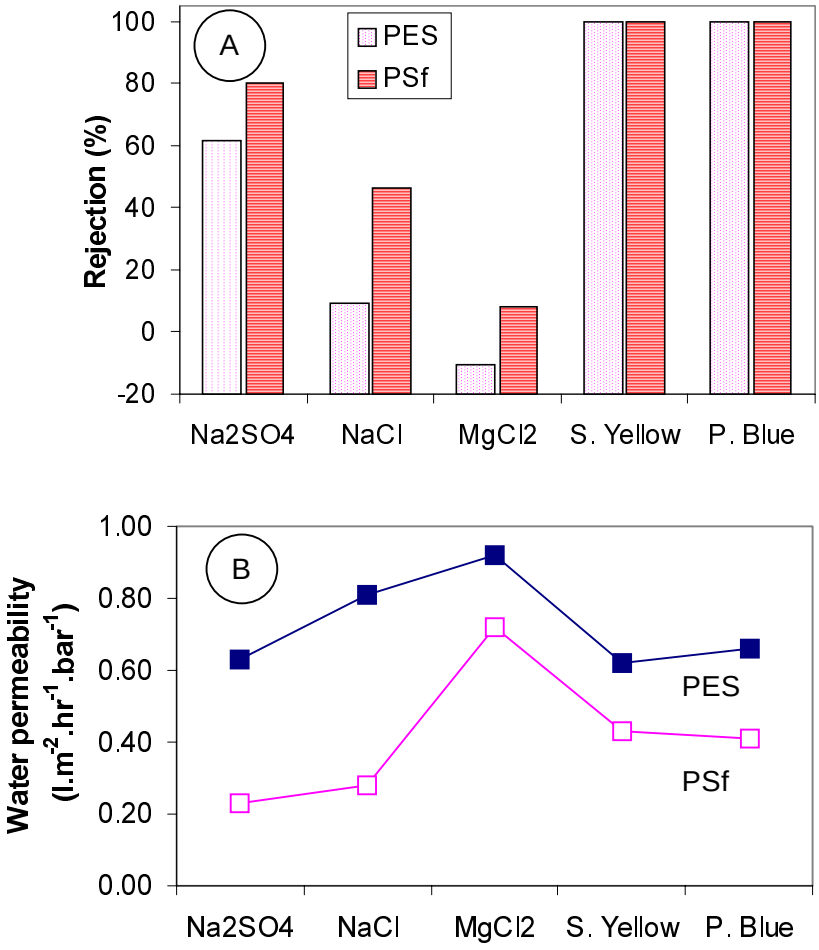

Figure 7.9 *Effect of support structure on membrane retention and permeation. Coating solution concentration: S-120 at 5wt%.*

7.3.5 Modeling

In order to give a complete view of the separation properties for ions of the new nanofiltration membrane, the DSPM model is used [12] to fit the

experimental values (for a description of the model refer to Appendix). Following the same procedure as described in literature [5, 8-12], the membrane properties, effective pore radius (through dextran rejection values), effective coating thickness and effective charge density are obtained for each membrane. Based on the membrane parameters, a prediction is made for three different ions as shown in Figure 7.10.

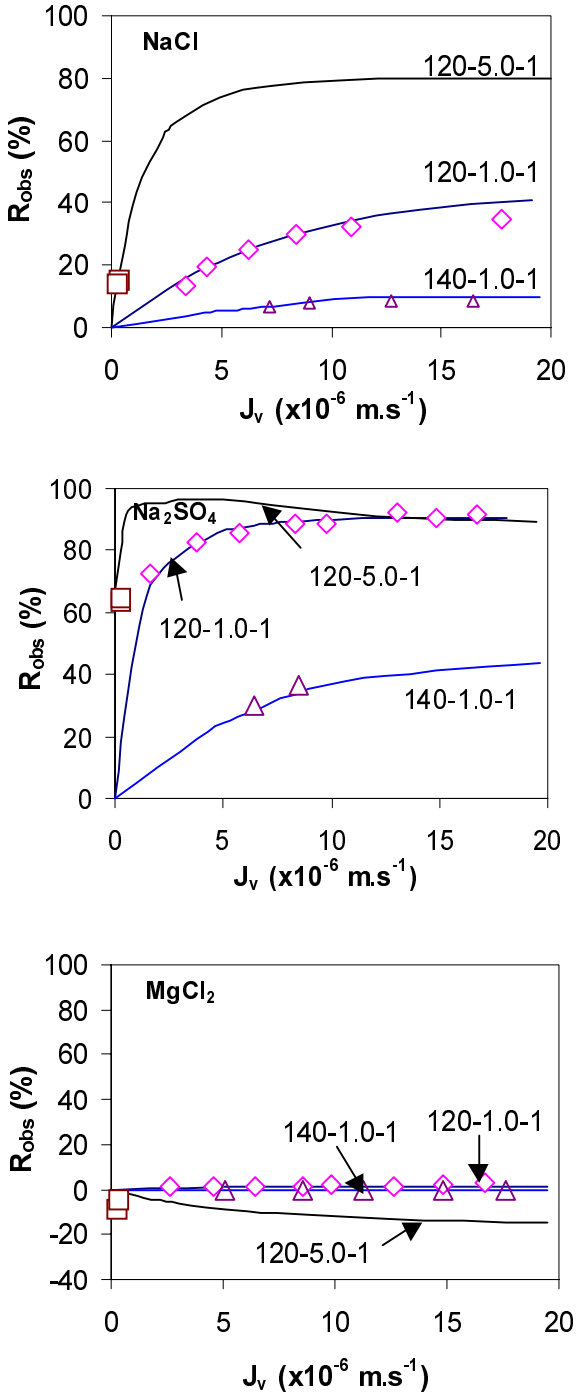

Figure 7.10 *Prediction of salt rejection based on DSPM model. Data points are experimental data and the lines are calculated results.*

Three typical membranes are selected based on the permeability in an order of 140-1.0-1 > 120-1.0-1 > 120-5.0-1. An opposite effect is obtained for the rejection of NaCl and Na_2SO_4 at relatively low flux regimes. For separation of Na_2SO_4, a quite similar rejection value is obtained for membrane 120-1.0-1 and 120-5.0-1. This is probably because of a more strong concentration polarization for membrane 120-5.0-1 than the other membrane. Since the permeability of membrane 120-5.0-1 is much lower than membrane 120-1.0-1, a higher salt concentration at the membrane is obtained at the same flux. This leads to a lower rejection [12]. For $MgCl_2$, the SPEEK layer shows no rejection for membrane 120-1.0-1 and 140-1.0-1 and negative rejection for membrane 120-5.0-1. Therefore, these high flux membranes, i.e membrane 140-1.0-1 and 120-1.0-1, could be good candidates for water softening. A broad range of rejection values for NaCl and Na_2SO_4 can be achieved by adjusting the ion exchange capacity of the coating material and the coating solution concentration.

7.4 Conclusions

A new type of nanofiltration membrane has been prepared by coating a sulfonated poly (ether ether ketone) layer on top of a polyethersulfone or polysulfone support. The membrane is characterized by rejection measurements of dextran mixture, salts and dyes. The negative charges at the coating layer shows a retention in the order of Na_2SO_4 > NaCl > $MgCl_2$. In addition, the composite membranes show a 97 to 100% retention to negatively charged organic dyes with a molecular weight of about 450 Dalton. The rejection can be improved by an increase in the coating thickness, the polymer concentration in the coating solution and the pore size of the support membranes. The penetration of SPEEK into the support can be used to prepare high retention membranes. The DSPM model fits well to the experimental values and is very useful in describing the membrane properties.

7.5 Appendix

The extended Nernst-Planck equation can describe the transport of multicomponent systems inside porous membranes. It represents transport due to diffusion, electrical potential gradient and convection. The equations can be written as

$$j_i = -D_{i,p}\left(\frac{dc_i}{dx} + \frac{Z_i c_i F}{RT}\frac{d\psi_m}{dx}\right) + K_{i,c} c_i J_v \qquad (3)$$

Where

$$D_{i,p} = K_{i,d} D_{i,\infty} \qquad (4)$$

j_i is the flux of solute i, and $D_{i,p}$ is the hindered diffusion coefficient corrected from the bulk diffusion coefficient, $D_{i,\infty}$ by the diffusion hindrance factor $K_{i,d}$. j_v is the solvent flux and $K_{i,c}$ the convective hindrance factor. The equation does not include the influence of the pressure on diffusion and specific ion membrane matrix interaction on $D_{i,p}$.

For uncharged solutes, no electrostatic term is in Equation 3; thus the solute flux can be expressed as

$$j_i = -D_{i,p}\frac{dc_i}{dx} + K_{i,c}c_i V \tag{5}$$

To obtain an expression for the rejection of the solute, Equation 5 is integrated across the membrane. The Hagen-Poiseuille equation gives the relationship between the pure waterflux and the applied pressure across the membrane:

$$J_w = \frac{r_p \Delta P}{8\mu(\Delta x / A_k)} \tag{6}$$

r_p is extracted from the MWCO and hence the value for $\Delta x/A_k$ can be calculated.

For charged solutes, the concentration at the interface can be determined using the following equilibrium conditions which will be taken as a combination of the Donnan and steric effects,

$$(\frac{c_i}{C_i}) = \phi \exp(-\frac{z_i F}{RT}\Delta\psi_D) \tag{7}$$

The term ϕ is the steric partitioning term to account for the steric effects on the entrance to the membrane, and can be described as

$$\phi = (1-\lambda)^2 \tag{8}$$

where λ is the ratio of the solute to the pore radius. The activity coefficients for both bulk solution and inside the membrane are also taken to be 1 based on relatively a low salt concentration in bulk and the difficulty to know the activity coefficient in membrane.

Once r_p and $\Delta x/A_k$ are obtained, the rejection data of NaCl can be used to estimate the effective charge density X_d,of the membrane at the specific concentration. Since there is strong concentration polarization in a hollow fiber configuration, the concentration next to the membrane is a function of the flux. X_d is specific for the concentration. Therefore, it is a function of the flux as well. The exact calculating procedure can be found in literature [5-22].

7.6 List of symbols

A_k	porosity of the membrane
c_i	concentration in the membrane, mol.L^{-3}
C_i	bulk solution concentration, mol.L^{-3}
$D_{i,p}$	hindered diffusivity, $L^2.t^{-1}$
$D_{i,\infty}$	bulk diffusivity, $L^2.t^{-1}$
F	Faraday constant, C.mol^{-1}
j_i	ion flux, mol.$L^{-2}.t^{-1}$
J_w	water flux (based on membrane area), $L.t^{-1}$
$K_{i,c}$	hindrance factor for convection
$K_{i,d}$	hindrance factor for diffusion
ΔP	applied pressure difference, $ML.t^{-2}$
r_p	effective pore radius, L
R	gas constant, $ML^2.t^{-2}.T$
T	absolute temperature, T
x	distance normal to membrane, L
Δx	effective membrane thickness, L
X	effective membrane charge density, mol.L^{-3}
z_i	valence of ion
ϕ	steric partitioning term
μ	viscosity of solution, $ML.t^{-1}$
ψ	electric potential in axial direction (V)
$\Delta\psi_D$	Donnan potential (V)

7.7 References

[1] P. Eriksson, Nanofiltration extends the range of membrane filtration, Environmental Prog., 7 (1988) 58-62.

[2] L. P. Raman, M. Cheryan, and N. Rajagopalan, Consider nanofiltration for membrane separations, Chem. Eng. Prog., 90 (1994) 68-74.

[3] R. J. Petersen, Composite reverse osmosis and nanofiltration membranes, J. Membrane Sci., 83 (1993) 81-150.

[4] T. He, M. H. V. Mulder, M. Wessling, and H. Strathmann, Preparation of composite hollow fiber membranes. Co-extrusion of dense hydrophilic coating onto porous hydrophobic support structures, Chapter 4, submitted to J. Membrane Sci.

[5] W. R. Bowen, T. A. Doneva, and H. B. Yin, Polysulfone-sulfonated poly (ether ether) ketone blend membranes: systematic synthesis and characterization, J. Membrane Sci., 181 (2001) 253-263.

[6] H. C. van der Horst, J. M. K. Timmer, T. Robbersten, and J. Leenders, Use of nanofiltration for concentration and demineralization in the dairy industry: model for mass transport, J. Membrane Sci., 104 (1995) 205-218.

[7] G. M. Rio, R. Joulie, S. J. Sarrade, and M. Carles, Investigation of ion separation by microporous nanofiltration membranes, AIChE J., 42 (1996) 2521-2528.
[8] W. R. Bowen and H. Mukhtar, Characterization and prediction of separation performance of nanofiltration membranes, J. Membrane Sci., 112 (1996) 263-274.
[9] W. R. Bowen, A. W. Mohammad, and N. Hilal, Characterisation of nanofiltration membranes for predictive purposed-use of salts, uncharged soluted and atomic force microscopy, J. Membrane Sci., 126 (1997) 91-105.
[10] W. R. Bowen and A. W. Mohammad, Characterizaton and prediction of nanofiltration membrane performance -a general assessment, Trans. IChemE, 76 (1998) 885-893.
[11] W. R. Bowen and A. W. Mohammad, A theoretical basis for specifying nanofiltration membranes-dye/salt/water streams, Desalination, 117 (1998) 257-264.
[12] W. R. Bowen and A. W. Mohammad, Diafiltration by nanofiltration: prediction and optimization, AIChE J., 44 (1998) 1799-1812.
[13] R. Levenstein, D. Hasson, and R. Semiat, Utilization of the Donnan effect improving electrolyte separation with nanofiltration membranes, J. Membrane. Sci., 116 (1996) 77-92.
[14] C. Bardor, E. Gaubert, and A. E. Yaroshchuk, Unusual mutual influence of electrolytes during pressure-driven transport of their mictures across charged porous membranes, J. Membrane. Sci., 103 (1995) 11-17.
[15] X. Xu and H. G. Spencer, Dye-salt separation by nanofiltration using weak acid polyelectrolyte membranes, Desalination, 114 (1997) 129-137.
[16] X. L. Wang, T. Tsuru, M. Togoh, S. Nakao, and S. Kimura, Electrolyte transport through nanofiltration membranes by the space-charge model and the comparison with Teorell-Meyer-Sievers model, J. Membrane. Sci., 103 (1995) 117-133.
[17] X. L. Wang, T. Tsuru, M. Togoh, S. Nakao, and S. Kimura, Evaluation of pore structure and electrical properties of nanofiltration membranes, J. Chem. Eng. Japan, 28 (1995) 186-192.
[18] Y. Garba, S. Taha, N. Gondrexon, and G. Dorange, Ion transport modelling through nanofiltration membranes, J. Membrane. Sci., 160 (1999) 187-200.
[19] K. Mehiguene, Y. Garba, S. Taha, N. Gondrexon, and G. Dorange, Influence of operating conditions on the retention of copper and cadmium in aqueous solutions by nanofiltration: experimental results and modelling, Sep. Purif. Technol., 15 (1999) 181-187.
[20] A. E. Yaroshchuk, Asymptotic behavior in the pressure-driven separation of ions of different mobilities in charged porous membranes, J. Membrane. Sci., 167 (2000) 163-185.
[21] M. S. Hall, V. M. Starov, and D. R. Lloyd, Reverse osmosis of multicomponent electrolyte solutions. Part I. Theoretical development, J. Membrane. Sci., 128 (1997) 23-37.

[22] G. Hagmeyer and R. Gimbel, Modelling the salt rejection of nanofiltration membranes for ternary ion mixture and for single salts at different pH values, Desalination, 117 (1998) 247-256.
[23] M. Perry and C. Linder, Intermediate reverse osmosis ultrafiltration (RO UF) membranes for concentration and desalting of low molecular weight organic solutes, Desalination, 71 (1989) 233-245.
[24] P. Schirg and F. Widmer, Characterisation of nanofiltration membranes for the separation of aqueous dye-salt solutions, Desalination, 89 (1992) 89-107.
[25] I. Jitsuhara and S. Kimura, Rejection of inorganic salts by charged ultrafiltration membranes made of sulfonated polysulfone, J. Chem. Eng. Japan, 16 (1983) 394-399.
[26] I. Jitsuhara and S. Kimura, Structure and properties of charged ultrafiltration membrane made of sulfonated polysulfone, J. Chem. Eng. Japan, 16 (1983) 389-393.
[27] T. Tsuru, S. Nakao, and S. Kimura, Calculation of ion rejection by extended Nernst-Planck equation with charged reverse osmosis membranes for single and mixed electrolyte solutions, J. Chem. Eng. Japan, 24 (1991) 511-517.
[28] T. Tsuru, S. Nakao, and S. Kimura, Reverse osmosis of single mixed electrolyte with charged membranes: experiment and analysis, J. Chem. Eng. Japan, 2 (1991) 518-524.
[29] D. Bhattacharyya, J. M. McMCarthy, and R. B. Grieves, Charged membrane ultrafiltration of inorganic ions in single and multi-salt systems, AIChE J., 20 (1974) 1206-1212.
[30] K. S. Spiegler and O. Kedem, Thermodynamics of hyperfiltration (Reverse Osmosis) criteria for efficient membranes, Desalination, 1 (1966) 311-326.
[31] Y. Matsumoto, S. Masao, and Y. Suzuki, Preparation of composite UF membranes of sulfonated polysulfone coated on ceramics, J. Membrane Sci., 158 (1999) 55-62.
[32] K. Ikeda, S. Yamamoto, and H. Ito, JP61200817, 1986.
[33] K. Ikeda, T. Nakano, H. Ito, and S. Yamamoto, New composite charged reverse osmosis membrane, Desalination, 68 (1988) 109-119.
[34] K. Kim, G. Chowdhurry, and T. Matsuura, Low pressure reverse osmosis performances of sulfonated poly(2,6-dimethyl-1,4-phenylene oxide) thin film composite membranes: effect of coating conditions and molecular weight of polymer, J. Membrane Sci., 179 (2000) 43-52.
[35] M. T. Bishop, F. E. Karasz, and P. S. Russo, Solubility and properties of a poly(aryl ether ether ketone) in strong acids, Macromolecules, 18 (1985) 86-93.
[36] T. He, M. H. V. Mulder, and M. Wessling, Composite hollow fiber membranes as supported liquid membranes, Chapter 5.
[37] Y. Liu, G. H. Koops, and H. Strathmann, Morphology controlled PES hollow fibers by the addition of PEG in dope and lumen solutions, Sep. Purif. Technol., To be published.

[38] S. Nakao and S. Kimura, Analysis of solutes rejection in ultrafiltration, J. Chem. Eng. Japan, 14 (1981) 32-37.
[39] H. Fujita, Polymer solutions, Elsevier, Amsterdam, 1990.
[40] N. A. Peppas, Hydrogels in medicine and pharmacy, CRC Press, Inc., Boca Raton, Florida,Vol. I Fundamentals, 1986.
[41] C. Bailly, D. J. Williams, F. Karasz, and W. J. MacKnight, The sodium salts of sulphonated poly(aryl ether ether ketone) (PEEK): preparation and characterization, Polymer, 28 (1987) 1009-1016.
[42] J. M. M. Peeters, M. H. V. Mulder, and H. Strathmann, Retention measurements of nanofiltration membranes with electrolyte solutions, J. Membrane Sci., 145 (1998) 199-209.

Chapter 8 Swelling behavior of a polymer network in anisotropic and isotropic confinement

Abstract

Swelling of a polymer network in an anisotropic confinement leads to an anisotropic swelling. This article discusses the characteristics of an anisotropic swelling compared to an isotropic confinement. Effect of the E-modulus and the solvent-polymer interaction parameter are investigated by means of the extension ratios in the radial and longitudinal directions.

8.1 Introduction

A confinement such as a porous support controls the swelling properties of a polymer system immobilized inside the pores. This suppressed swelling alters the physical properties such as the transport resistance or the concentration of the chemical functionality (ion exchange groups) per volume polymer. A plasma-grafted filled-type of membrane, which showed swelling control more efficiently than cross-linking, has been prepared by filling a support membrane based on crystalline polyethylene with poly(methyl acrylate) [1]. A model based on Flory-Huggins's theory was developed, using the elastic energy from the tie segment binded to crystals as the swelling constraint [2]. Another similar work has been carried out by photografting poly(4-vinylpyridine) onto a polypropylene or polyethylene microfiltration membrane support [3]. The swelling value of the cross-linked polyelectrolyte inside the isotropic pores is largely suppressed due to the rigidity of the support matrix. This research is based on an assumption of isotropic confinement. However, a more general case is an anisotropic constraint.

An example of an anisotropic constraint is a cylinder-type matrix structure. Assuming a support membrane consisting of cylindrical pores, the penetrated polymer must have the same shape of being a rod or a disc, depending on the ratio of the length and the radius. More specifically, the pore size of the porous support generally used is in the ultrafiltration region with a pore size in the range a few to ten nanometers. However, the penetration thickness of the coating can be 100 nm or more. By defining a rod having a length to radius ratio higher than 10, the penetrated polymer is rod alike. We are also aware of the fact that the real membrane pore geometry in the support is much more complex, but the cylindrical description represents an ideal situation and will not alter the physical essence.

In this chapter, the effect of an anisotropic confinement on the swelling behavior of a polymer network is described. The difference between isotropic and anisotropic behaviors is studied in terms of the extension ratio and polymer concentration at equilibrium. Flory-Rehner's swelling theory [4] of a polymer network is used as the basic model, which includes a mixing energy term and an elastic contribution from the network itself. In addition, a constraint is introduced by the elastic energy, the E-modulus, of the matrix as the third term.

8.2 Models

8.2.1 Description of swelling process

At equilibrium, the elastic energy exerted by the network counter-balances the entropy and enthalpy contribution. Therefore, the change of the total free energy can be expressed as a sum of the change of free energy of mixing, an elastic free energy term related to the expansion of the network

structure and an external energy contribution. Furthermore, at equilibrium, the total free energy of the system is at a minimum value, so is the change of the free energy. This can be understood by following the actual swelling process. The free energy decreases by adding the solvent molecules into the polymer structure until an equilibrium state has been reached. Hence the first derivative of the free energy towards the number of solvent molecules is negative. Bearing in mind that an equilibrium state is a stable state, the second derivative of the free enthalpy is negative as well. Therefore, the change in free enthalpy against the number of solvent molecules is a monotonically decreasing function until equilibrium, where a minimal value is reached.

We assume:

1. A rod-shaped polymer network is confined in a cylindrical channel with an elastic wall;
2. The rod has a length to diameter ratio higher than 10, i.e. $\delta_0 / r_0 > 10$;
3. The external structure shows ideal elasticity with an E-modulus, or the energy density, of K;
4. The expansion process is reversible and the energy exerts on the swollen polymer is the same as that dissipates through the swelling process.
5. The total volume of a swollen polymer network is the sum of the volume of the original polymer and the solvent. Hence, we assume constant partial molar volumes.

The change in total free energy of the system can be expressed as

$$\Delta G_{total} = \Delta G_m + \Delta G_{el} + \Delta G_{ext} \tag{1}$$

where ΔG_m is the free energy of mixing according to Flory-Rehner's swelling theory and can be expressed as

$$\Delta G_m = RT(n_1 \ln \phi_1 + \chi n_1 \phi_2) \tag{2}$$

in which

$$\phi_1 = \frac{n_1 v_1}{n_1 v_1 + V_0} \text{ and } \phi_2 = \frac{V_0}{n_1 v_1 + V_0} \tag{3}$$

where n_1 and n_2 are the numbers of moles of solvent and of polymer chains, respectively; ϕ_1 and ϕ_2 are the volume fractions of the solvent and the polymer, respectively; χ is the Flory-Huggins interaction parameter. R and T are the gas constant and temperature. V_0 is the volume of the polymer at the original state and can be described as $n_2 v_2$, where n_2 and v_2 are the number of moles and molar volume of the polymer chains. ΔG_{el} and ΔG_{ext} are the elastic energy of the network upon extension and the external energy from the constraint.

In case of a deformed network in three dimensions (x,y,z), the entropy change involved in deformation is described as [4]

$$\Delta S_{el} = -\frac{Rn_2}{2}\left[\alpha_x^2 + \alpha_y^2 + \alpha_z^2 - 3 - \ln(\alpha_x \alpha_y \alpha_z)\right] \quad (4)$$

Following a coordination transformation of (x,y,z) to (r,θ,z), the free energy can be expressed as

$$\Delta G_{el} = -T\Delta S_{el} = \frac{RTn_2}{2}\left[2\alpha^2 + \beta^2 - 3 - \ln(\alpha^2 \beta)\right] \quad (5)$$

in which α and β are the extension ratios in the radial and longitudinal directions, respectively, defined as

$$\alpha = \frac{r}{r_0} \text{ and } \beta = \frac{\delta}{\delta_0} \quad (6)$$

r and δ are the radius and length of the network at swollen state, r_0 and δ_0 are the radius and length of the polymer at the original state.

8.2.2 Elastic-R model

Figure 8.1 schematically describes the anisotropic change after swelling of a polymer network structure inside an elastic channel.

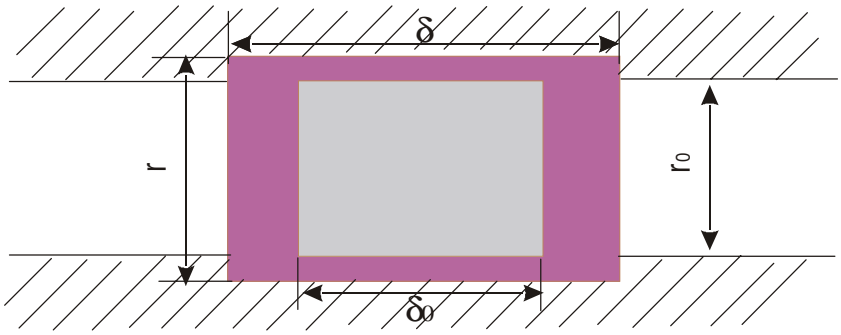

Figure 8.1 *Schematic of the Elastic-R model.*

Since the external energy term originates from the elastic deformation of the support matrix, the actual volume change of the matrix in the channel is required, which can be expressed as

$$\Delta V = \pi r^2 \delta - \pi r_0^2 \delta = \pi r_0^2 \delta_0 (\alpha^2 \beta - \beta) \quad (7)$$

Therefore, the free energy contribution can be described as

$$\Delta G_{ext} = \pi r_0^2 \delta_0 K(\alpha^2 \beta - \beta) = V_0 K(\alpha^2 \beta - \beta) \quad (8)$$

hence the total free energy change is obtained by combing Equation 2, 5 and 8

$$\Delta G_{total} = RT\left[n_1 \ln \phi_1 + n_1\phi_2\chi + \frac{n_2}{2}\left(2\alpha^2 + \beta^2 - 3 - \ln(\alpha^2\beta)\right) + \frac{V_0 K}{RT}(\alpha^2\beta - \beta)\right] \tag{9}$$

Defining V being the volume of the swollen polymer, and according to assumption 5,

$$V = n_1 v_1 + V_0 \tag{10}$$

in which V_0 is the polymer volume in the initial state. Hence, the relationship between the α, β and n_1 can be expressed as

$$\phi_2 = \frac{V_0}{V} = \frac{V_0}{n_1 v_1 + V_0} = \frac{\pi r_0^2 \delta_0}{\pi r^2 \delta} = \frac{1}{\alpha^2\beta} \tag{11}$$

therefore,

$$\alpha^2 = \frac{1}{\beta}(1 + \frac{n_1 v_1}{V_0}) \tag{12}$$

From the relationship given above, it may be concluded that the change in free energy is a function of two independent variables, the solvent concentration, n_1, and one of the extension ratios, α or β. For the simplicity in derivation procedure, β is taken as a variable together with n_1. Hence, according to Equation 9 and 12, the description of the change of free enthalpy can be rearranged as

$$\Delta G_{total} = RT\left[n_1 \ln \phi_1 + n_1\phi_2\chi + \frac{n_2}{2}\left(\frac{2}{\beta}(1 + \frac{n_1 v_1}{V_0}) + \beta^2 - 3 - \ln(1 + \frac{n_1 v_1}{V_0})\right) + \frac{KV_0}{RT}(1 + \frac{n_1 v_1}{V_0} - \beta)\right] \tag{13}$$

Consequently, the derivatives of the free energy towards n_1 and β can be obtained as

$$\left(\frac{\partial \Delta G_{total}}{\partial n_1}\right)_{T,P,\beta} = RT\left[\ln \phi_1 + \phi_2 + \chi\phi_2^2 + \frac{v_1}{v_2}(\frac{1}{\beta} - \frac{\phi_2}{2}) + \frac{Kv_1}{RT}\right] \tag{14}$$

and

$$\left(\frac{\partial \Delta G_{total}}{\partial \beta}\right)_{T,P,n_1} = -\frac{n_2}{\beta^2}\left(\frac{V_0 + n_1 v_1}{V_0} - \beta^3\right) - \frac{KV_0}{RT} = -\frac{n_2}{\beta^2}\left(\frac{V_0 + n_1 v_1}{V_0} - \beta^3 + \frac{Kv_2}{RT}\beta^2\right) \tag{15}$$

To obtain the above formula, two derivatives are used

$$\frac{\partial \phi_1}{\partial n_1} = \frac{\phi_1 \phi_2}{n_1} \text{ and } \frac{\partial \phi_2}{\partial n_1} = -\frac{\phi_1 \phi_2}{n_1} \tag{16}$$

At a swelling equilibrium, the change in free energy is at a minimum, consequently,

$$\left(\frac{\partial \Delta G_{tatal}}{\partial n_1}\right)_{T,P,\beta} = 0 \tag{17}$$

$$\left(\frac{\partial \Delta G_{total}}{\partial \beta}\right)_{T,P,n_1} = 0 \tag{18}$$

Thus, two equations are obtained

$$\ln \phi_1 + \phi_2 + \chi \phi_2^2 + \frac{v_1}{v_2}\left(\frac{1}{\beta} - \frac{\phi_2}{2}\right) + \frac{Kv_1}{RT} = 0 \tag{19}$$

and

$$\frac{V_0 + n_1 v_1}{V_0} - \beta^3 + \frac{Kv_2}{RT}\beta^2 = 0 \tag{20}$$

8.2.3 Elastic-R-L model

Assuming the polymer network is completely confined by an elastic matrix in both radial and longitudinal directions, the isotropic change for the matrix can be expressed as

$$\Delta V = \pi r^2 \delta - \pi r_0^2 \delta_0 = \pi r_0^2 \delta_0 (\alpha^2 \beta - 1) \tag{21}$$

Therefore, the free energy contribution can be described as

$$\Delta G_{ext} = \pi r_0^2 \delta_0 K(\alpha^2 \beta - 1) = V_0 K(\alpha^2 \beta - 1) \tag{22}$$

Combining Equation 2, 5 and 22, the change in free energy can be expressed as

$$\Delta G_{total} = RT\left[n_1 \ln\phi_1 + n_1\phi_2\chi + \frac{n_2}{2}\left(2\alpha^2 + \beta^2 - 3 - \ln(\alpha^2\beta\right) + \frac{V_0 K}{RT}(\alpha^2\beta - 1)\right] \quad (23)$$

Following Equation18 by applying Equations 12 and 16, two equations are obtained

$$\ln\phi_1 + \phi_2 + \chi\phi_2^2 + \frac{v_1}{v_2}(\frac{1}{\beta} - \frac{\phi_2}{2}) + \frac{Kv_1}{RT} = 0 \quad (24)$$

and

$$\frac{V_0 + n_1 v_1}{V_0} - \beta^3 = 0 \quad (25)$$

8.2.4 Free swelling model

A free swelling is a special case where the external constraint is zero. Thus, by leaving out the parts related to the K value in Equations 19 and 20, a description for the free swelling is obtained as

$$\ln\phi_1 + \phi_2 + \chi\phi_2^2 + \frac{v_1}{v_2}(\frac{1}{\beta} - \frac{\phi_2}{2}) = 0 \quad (26)$$

and

$$\frac{V_0 + n_1 v_1}{V_0} - \beta^3 = 0 \quad (27)$$

8.3 Results and discussion

8.3.1 Effect of confinement

Compared to the free swelling model and the Elastic-R model, the Elastic-R-L model shows the strongest constraint, which effectively decreases the swelling of the network as can be seen in Figure 8.2 (B). Over the entire range of molar volume ratio v_1/v_2, the polymer volume fraction ϕ_2 is larger than for the other two cases (free swelling and radial confinement). Although the external confinement has a rather low E-modulus, 0.2 Mpa, the dramatic change in swelling indicates that the support structure can be very useful in controlling the final swelling structure. The difference is more pronounced when the polymer chain length between two cross-linking points is longer, i.e. a ratio of v_1/v_2 less than 0.001.

Because of the anisotropic confinement, the extension ratio in the longitudinal direction is always higher than that in the radial direction as can be seen in Figure 8.2 (A). The physical meaning of this is that the polymer network preferably extends in the longitudinal direction rather than in the radial

direction because there is more restraint in the radial direction than at the other direction. Both extension ratios become almost equal when the molar volume ratio is high, i.e. $v_1/v_2 > 0.06$. However, the difference between the two increases with decreasing the molar volume ratio v_1/v_2. After passing through the maximum, the extension ratio, α, in radial direction decreases because this gives the lowest free enthalpy according to thermodynamics. On the other hand, since the restriction of Elastic-R model is only in the radial direction, the swelling extensions are in between the free swelling state and the Elastic-R-L model at a molar volume ratio $v_1/v_2 > 0.0004$.

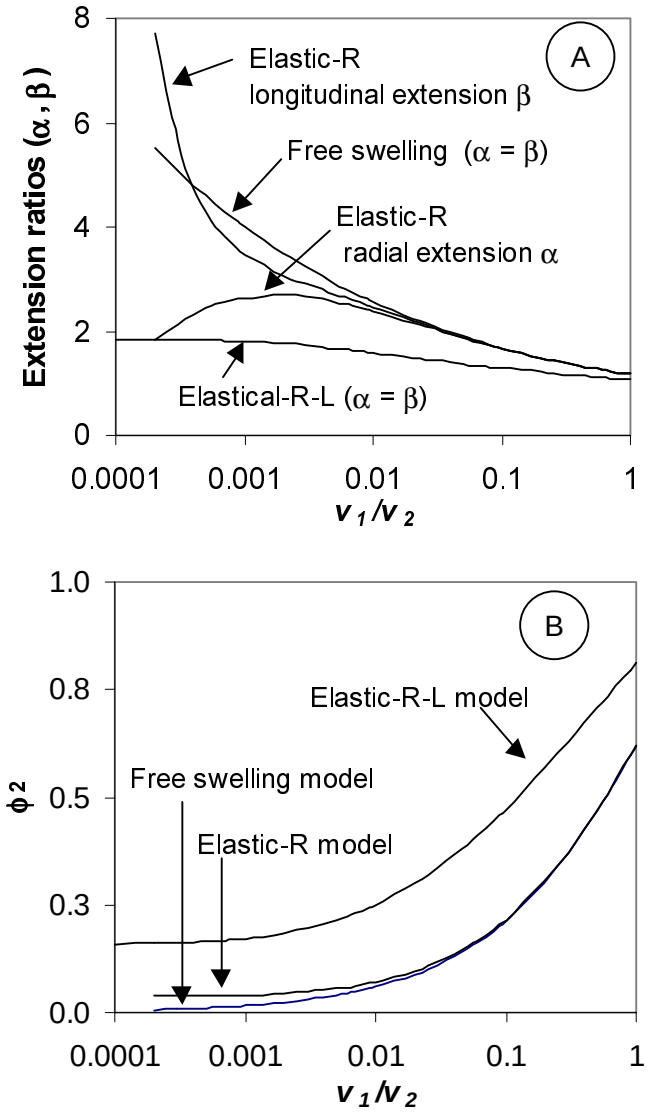

Figure 8.2 *Extension ratio of polymer network (A) and polymer concentration (B) (volume concentration) in swollen state as a function of the molar volume ratio. K = 0.2 MPa; χ= -0.5.*

8.3.2 Effect of E-Modulus of external matrix

For the Elastic-R model, an E-modulus of 0.2 to 1 MPa is chosen based on the consideration of the elastic limit as described in section 8.3.4. This is

realistic for a rubbery matrix at relatively low elongation [4]. As can be seen in Figure 8.3, the extension ratio of a network can be adjusted by changing the E-modulus of the external matrix. When the external matrix has a higher E-modulus, the extension ratio at radial direction is higher but the extension ratio at the longitudinal direction is lower as well as a higher polymer concentration at equilibrium.

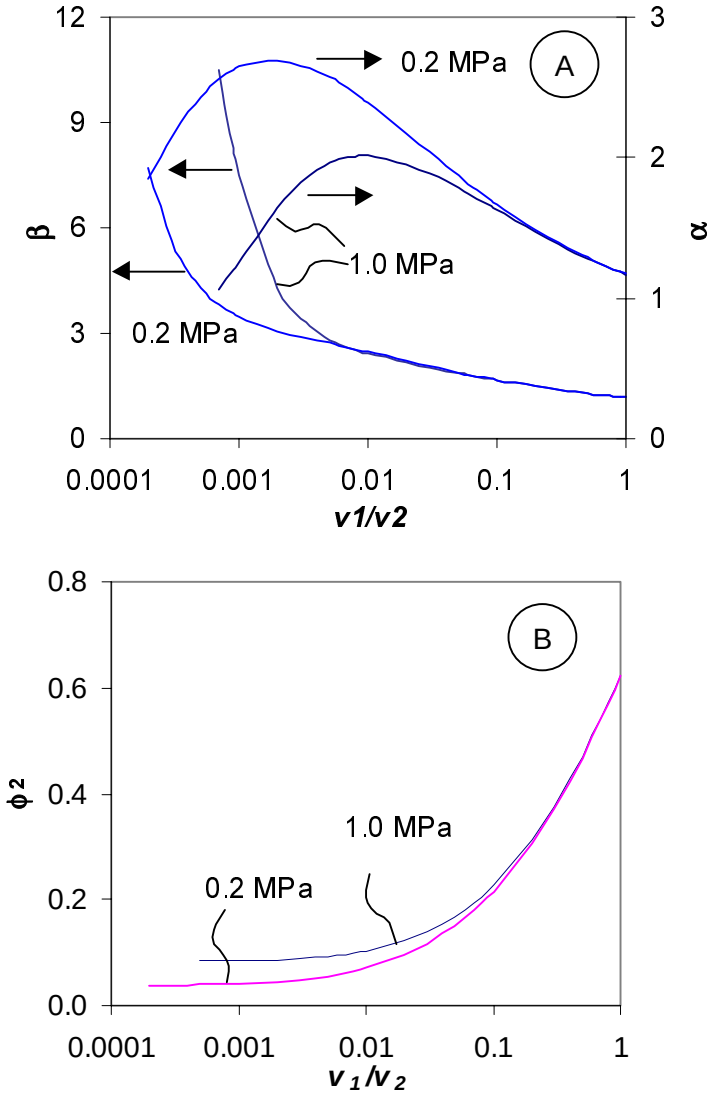

Figure 8.3 *Asymmetric extension (A) and polymer concentration (B) as a function of the molar volume ratio. Model: Elastic-R model, χ = -0.5.*

8.3.3 Effect of polymer-solvent interaction parameter

The polymer-solvent interaction parameter, χ, is another important parameter in the swelling process. In a sorption process, increasing of χ generally represents lower sorption of the solvent. A decrease of the radial and the longitudinal extension ratios results from a higher polymer-solvent

interaction parameter as can be seen in Figure 8.4. A better solvent is characterized by a higher extension ratio for both radial and longitudinal directions.

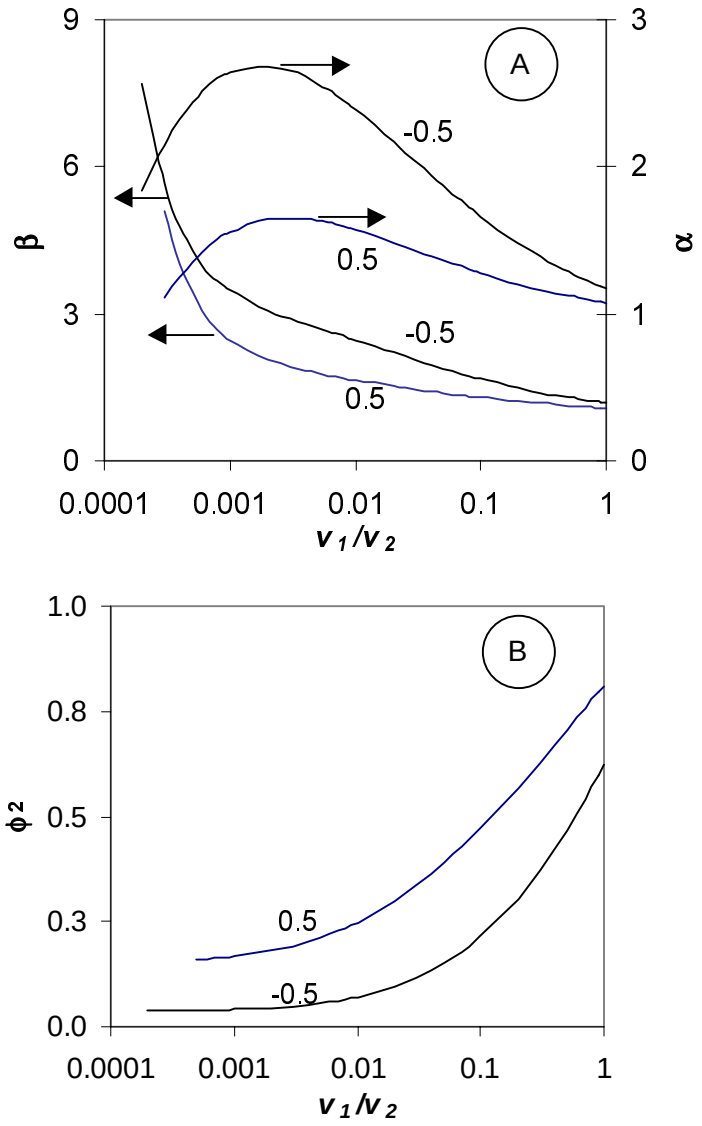

Figure 8.4 *Asymmetric extension (A) and polymer concentration (B) as a function of the molar volume ratio. Model: Elastic-R model, K = 0.2 MPa. The numbers in figures represent values for the interaction parameter.*

8.3.4 Restriction of Elastic-R model: Elastic limitation

Anisotropic constraints have a specific effect on the swelling of a polymer network. The characteristic of this anisotropy is that the extension ratio in the radial and longitudinal directions are not the same. A maximum value at the radial extension ratio is obtained as well when decreasing the molar volume ratio of solvent and polymer chain. However, since the decrease in molar ratio results in a decrease of the α value, α may become less than 1 at a

certain point, which is not possible. The Elastic-R model implicates that in case α being unity, no interaction takes place with the external matrix and only the longitudinal direction extends.

At the point where the α is equal to 1, the relation between the polymer concentration and β can be described as

$$\beta = \frac{1}{\phi_2} \tag{28}$$

Combined with Equation 20 and 28, we obtain

$$\beta^2 - \frac{Kv_2}{RT}\beta - 1 = 0 \tag{29}$$

Solving the above equation, the relation between β, v_2 and K is given as

$$\beta = \frac{Kv_2}{2RT} + \sqrt{\left(\frac{Kv_2}{2RT}\right)^2 + 1} \tag{30}$$

The negative value is omitted. This equation gives the maximal extension ratio in longitudinal direction at which the Elastic-R model is still valid. Above this value, the network obeys a linear extension in the longitudinal direction only. From Equation 28, the following limits can be obtained as

$$\left(\frac{Kv_2}{2RT}\right)^2 >> 1, \text{ then } \beta \approx \frac{Kv_2}{RT} \tag{31}$$

$$\left(\frac{Kv_2}{2RT}\right)^2 << 1, \text{ then } \beta \approx \frac{Kv_2}{2RT} + 1 \tag{32}$$

A simple estimation of this theory in a realistic situation can be made using an E-modulus of 10^8 N.m^{-2} and a molar volume of a polymer chain of 10^{-2} m^3.mol^{-1} at T=300 K. The value of Kv_2/RT is equal to 401, which is much higher than 1. Therefore, the present model actually indicates that a typical glassy polymeric matrix does not behave as an elastic constraint but a rigid channel. However, this model is based on a very simple and strong assumption, for example assumption 1,3 and 5, which may not be valid in a real situation. The model described in this paper basically provides a new approach to predict the swelling control in a confinement. In a further research, we expect a better description after incorporating the partial molar volume and the non-ideality of elasticity into the model for both the solvent and the polymer network.

8.3.5 Effect of E-modulus based on isotropic constraint

By adjusting the elastic properties of the confining matrix, the swelling behavior of a polymer inside the matrix will be different. Figure 8.5 shows the extension ratio and the polymer concentration in the swollen polymer inside a support structure with a broad E-modulus, taking a isotropic confinement based on the Elastic-R-L model. This E-modulus range in the calculation is rather realistic for a glassy porous matrix, which normally has a E-modulus at the scale of 100 MPa. A dramatic phenomenon is that the extension ratio decreases rapidly with an increase of the E-modulus. The polymer concentration increases dramatically up to about 70%. Under a constraint, the swelling can be effectively suppressed.

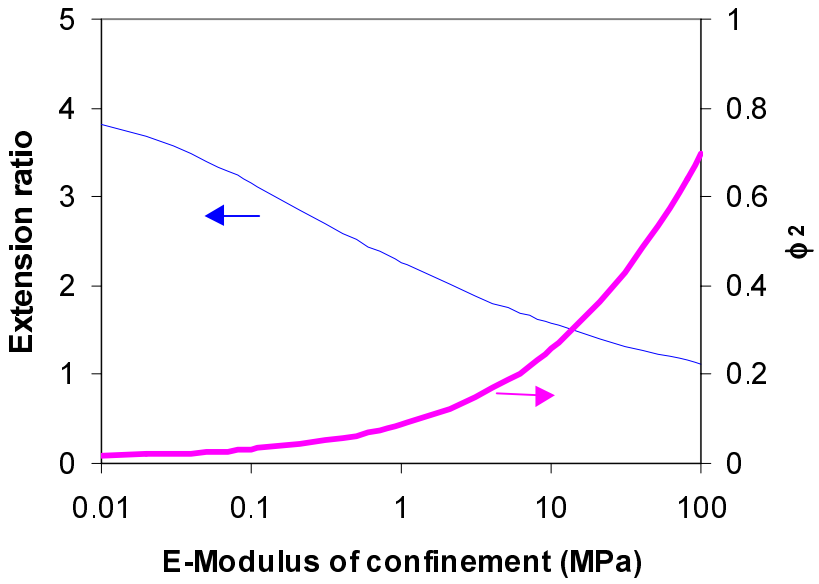

Figure 8.5 *Effect of the E-modulus of the confinement structure on the swelling properties of the polymer network. Model: Elastic-R-L model;* χ*=-0.5;* $v_1=18.02x10^{-6}\ m^3.mol^{-1}$; $v_1/v_2=10^{-3}$.

8.4 Conclusions

The isotropic and anisotropic confinement on the swelling of a network structure has been investigated in terms of the extension ratios in longitudinal and radial directions. The modeling quantifies the anisotropy in swelling of the network by external constraints. Extension ratios in radial and longitudinal directions strongly depend on the E-modulus of the external matrix and the solvent polymer interaction parameter. Decreasing the molar volume ratio results in a maximum in the extension ratio at the radial direction.

8.5 Appendix

As the volume fraction of the solvent inside the polymer network changes, the physical and transport properties of the polymer/solvent mixture changes as well. In previous chapter on the nanofiltration properties of composite membranes comprising an ion exchange layer and a porous support, we hypothesized that the fixed charge density of sulfonic acid groups may depend on the environment in which the polymer absorbs water. The fixed charge density is given by the amount of ionic groups per volume of the swollen polymer. Free and confined swelling influences the latter and hence the fixed charge density decrease as the polymer in confined.

The model developed can quantify the effect of the confinement on the swelling degree as shown in Figure 8.6. The ratio of fixed charge density in a confined polymer and a free swelling polymer is plotted as the function of the E-modulus of the confining matrix. A drastic increase of the fixed charge density is found by increase of the E-modulus of the support matrix structure based on Elastic-R-L model. The effect of increase in fixed charge density is more pronounced when the interaction of the polymer and the solvent is negative, or a better interaction between the polymer chains and the solvent.

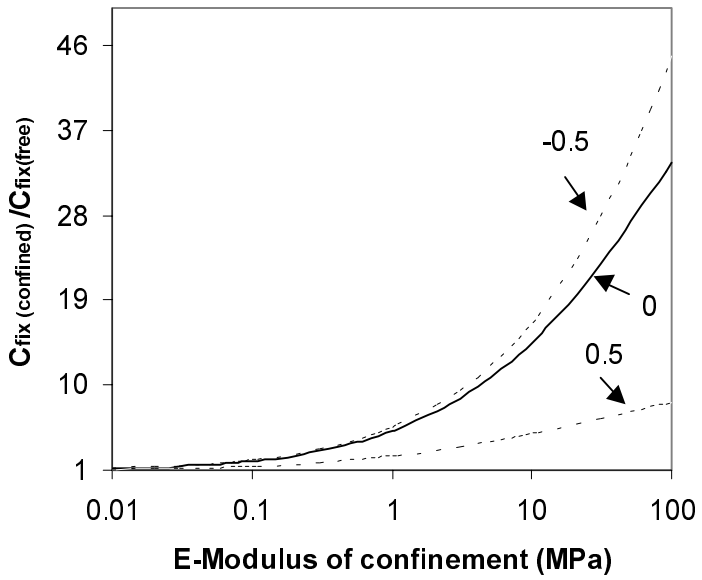

Figure 8.6 Effect of E-modulus on the ratio of fixed charged density at a confined state and at a free state. The numbers indicated in the figure are the polymer-solvent interaction parameters. Model: Elastic-R-L model, v_1=18.02 x10^{-6} m^3.mol^{-1}; v_1/v_2= 10^{-3}.

8.6 Notation

n_1 number of moles of the solvent; mol
n_2 number of moles of polymer chains; mol
r_0 original diameter of the polymer; m
r diameter of the swollen polymer; m
δ_0; original length of the polymer; m
δ length of the swollen polymer; m
ϕ_1 volume fraction of the solvent
ϕ_2 volume fraction of the polymer
v_1 molar volume of the solvent molecules; $m^3.mol^{-1}$
v_2 molar volume of the polymer chains; $m^3.mol^{-1}$
K E-modulus of the external matrix, Pa or $J.m^{-3}$
V_0 volume of the polymer at initial state, m^3
V volume of the polymer at swollen state, m^3
χ Flory-Huggins interaction parameter
R gas constant, $J.mol^{-1}.K^{-1}$
T temperature, K
α extension ratio in radial direction
β extension ratio in longitudinal direction

8.7 References

[1] T. Yamaguchi, S. Nakao, and S. Kimura, Plasma-graft filling polymerisation: preparation of a new type pervaporation membrane for organic liquid mixture, Macromolecules, 24 (1991) 5522-5527.
[2] T. Yamaguchi, S. Nakao, and S. Kimura, Swelling behavior of the filling-type membrane, J. Polym. Sci. Part B: Polym. Phys., 35 (1997) 469-477.
[3] A. M. Mika, R. F. Childs, J. M. Dickson, B. E. McCarry, and D. R. Gagnon, A new class of polyelectrolyte-filled microfiltration membranes with environmentally controlled porosity, J. Membrane Sci., 108 (1995) 37-56.
[4] P. J. Flory, Principles of Polymer Chemistry, Cornell University Press, Ithaca, New York, 1953.

Summary

Supported liquid membranes are of particular interest owing to the combination of extraction and stripping into a single step, the reduction of solvent usage and the achievement of very high enrichment factors. However, the industrial application of SLMs is not realized yet due to the short life-time. Chapter 1 summarizes the historical development of the stabilization techniques and introduces a concept to prepare a composite hollow fiber membrane with an ion exchange coating on a hydrophobic support by co-extrusion and dip-coating.

Chapter 2 describes the application of a triple-orifice spinneret in the preparation of microfiltration membranes with a highly porous surface. Dilution solvents, i.e. NMP and NMP/acetone (50/50wt%), have been used as the external liquids during spinning. A polymer solution close to the cloud point does not show significant improvement in permeability since the surface pores are open enough and not the controlling parameter for transport. However, a porous surface can be obtained for a polymer solution far from cloud point forming a dense skin layer but an open substructure, such as blending solution of PSf and PVP.

In Chapter 3, a new type of polysulfone hollow fiber has been prepared and used as the support for SLMs. The effect of polymer concentration, amount of the additive and the NMP content in the bore liquid are investigated in terms of copper flux. Gas and pure water permeability, the porosity and pore size of the membrane are used as characterization methods. To obtain a suitable support membrane, the polysulfone content should be less than 22wt%, preferably 17wt% and the amount of additive, DegOH, is preferably 30.6wt%. It has been shown that a further decrease of the polymer content does not necessarily increase the porosity of the substructure and therefore does not increase the copper permeability. The amount of NMP in the bore liquid is optimized at 75wt%. A higher NMP content does not show a higher copper flux. The stability of the polysulfone membranes is similar to the commercial Accurel polypropylene membrane.

In Chapter 4, a SPES composite hollow fiber membranes are successfully prepared by co-extrusion of SPES solutions onto polysulfone solutions. In terms of mechanical and adhesion properties, the SPES concentration in the coating solution is of key importance to obtain an integral composite membrane. A transition from nodular to cellular structure is observed when the SPES concentration changes from 20 to 35wt% and this corresponds to an improvement in mechanical properties. Adhesion of the coating to the PSf support is also improved by increasing the SPES concentration of the coating solutions. At dry state, the composite hollow fiber shows an extremely low copper ion transport in supported liquid membrane system and no selectivity for He/N_2, He/CO_2 and N_2/CO_2 in gas separation. At wet state, the membrane shows low inorganic salt retention and high retention for charged organic dye molecules. The concept of a co-extruded membrane with an ion exchange functionality in the coating layer shows high potential to

be used as a nanofiltration membrane as well as a tight hydrophilic ultrafiltration membrane.

Chapter 5 discusses the preparation of a SPEEK coated PSf or PP hollow fiber by a systematic selection of appropriate solvents for a dip-coating process. An increasing in the solubility of SPEEK in methanol, is found by increasing the sulfonation time and therefore the ion exchange capacity. An integral coating layer is prepared by controlling the coating solution concentration and the number of coating steps. These hollow fibers with hydrophilic coating on hydrophobic support show a slight increase in stability in SLMS. However, they are still instable due to the existence of direct contact between the organic phase and the aqueous phase. An initial research on an encapsulated composite membrane with SPEEK layers demonstrates that it is a potential solution, but further development is necessary.

In Chapter 6, a membrane contactor system has been described for the copper transport using the novel composite hollow fiber membranes described in Chapter 5. Stability and permeation results demonstrate that long-term operation has been realized in a bench-scale process. A resistance model has been developed to estimate the copper flux of the membrane contactor based on the initial SLM permeability. The model agrees well with experimental results for membrane contactors based on support membrane of PSf and the PP. According to the model, an improvement in flux is expected using a membrane contactor system composed of two thin dense ion exchange hollow fibers.

The potential of the composite hollow fiber membranes has been explored in pressure driven processes, e.g. nanofiltration as well, in Chapter 7. High MWCO for dextran is observed indicating the existence of the pores or meshes inside the SPEEK coating layer. Due to the negative charges in the coating layer, the membranes show a retention in the order of Na_2SO_4 > NaCl > $MgCl_2$. In addition, a 97 to 100% retention has been obtained for negatively charged organic dyes with a molecular weight of about 450 $g.mol^{-1}$. The rejection can be improved by an increase in the coating thickness, the polymer concentration in the coating solution and the pore size of the support membranes. The penetration of SPEEK into the support results in a high retention membrane due to the increase in the fixed charge density caused by the decrease in the swelling of the SPEEK. The Donnan-steric-pore-model fits well to the experimental values and is very useful in describing the transport of our membranes.

In Chapter 8, a theoretical model is developed to describe the isotropic and anisotropic confinement on the swelling of a polymer network. The model quantifies the anisotropy in swelling of the network by external constraints. Extension ratios in radial and longitudinal directions strongly depend on the E-modulus of the external matrix and the solvent polymer interaction parameter. As an example, substantial increase in the fixed charge density is observed by increase in the E-modulus of a confinement, giving a solid theoretical support to the hypothesis in Chapter 7.

Samenvatting

Geïmmobiliseerde vloeistofmembranen (supported liquid membranes, SLMs) zijn zeer interessant vanwege de mogelijkheid het extractie- en stripproces te combineren in een stap, de reductie van het gebruik van oplosmiddel en de zeer hoge verrijkingsfactoren die mogelijk zijn. Toepassing van SLMs op industriële schaal is echter nog niet mogelijk vanwege de korte levensduur.

In hoofdstuk 1 wordt de historische ontwikkeling van stabilisatie-technieken samengevat. Daarnaast wordt het concept van de bereiding van composiet holle vezel membranen geïntroduceerd, waarbij een ionen-uitwisselende coating door middel van co-extrusie en dipcoating op een hydrofobe drager wordt aangebracht.

Hoofdstuk 2 beschrijft het gebruik van een zogenaamde ‘triple-orifice’ spinneret bij de bereiding van sterk poreuze oppervlakken. Verdunde oplosmiddelen, dat wil zeggen NMP en NMP/aceton (50%/50%) zijn bij het spinnen aan de buitenzijde gebruikt als vloeistof . Een polymeeroplossing die zich dicht bij het cloud-point bevindt vertoont geen significante verbetering in permeabiliteit omdat de oppervlakteporiën voldoende open zijn en geen bepalende factor zijn voor transport. Een poreus opppervlak kan echter wel verkregen worden door gebruik te maken van een polymeeroplossing die zich ver beneden het cloud-point bevindt, zoals een blend-oplossing van PSf en PVP. Deze vormt een dichte laag maar heeft een open substructuur.

In hoofdstuk 3 is een nieuw type polysulfon holle vezel gemaakt en gebruikt als drager voor SLMs. Het effect van de polymeerconcentratie, de hoeveelheid van het additief en het NMP-gehalte in de vloeistof aan de binnenkant van de spinneret zijn onderzocht in relatie tot de koperflux. De gas- en waterpermeabiliteit, the porositeit en de poriegrootte van het membraan zijn gebruikt als karakteriseringsmethoden. Om een geschikt dragermembraan te bereiden moet het polysulfongehalte minder dan 22 gew.% zijn. De hoeveelheid additief in de oplossing moet bij voorkeur groot zijn, tot 30,6 gew.%. Er is aangetoond dat een verdere verlaging van het polymeergehalte niet noodzakelijkerwijs de porositeit van de substructuur en daarmee de koperpermeabiliteit verhoogd. De hoeveelheid NMP in de vloeistof in het inwendige van de spinneret is optimaal bij 75 gew.%. Hogere NMP-concentraties leveren geen hogere flux op. De stabiliteit van de polysulfonmembranen is gelijk aan die van het commercieel verkrijgbare Accurel polyproyleen membraan.

In hoofdstuk 4 worden succesvol integrale SPES composiet holle vezel membranen bereid door middel van co-extrusie van SPES-oplossingen op polysulfon-oplossingen. Met betrekking tot de mechanische en adhesie-eigenschappen speelt de SPES-concentratie in de coatingoplossing een belangrijke rol in het verkrijgen van een goed composietmembraan.
Een nodulaire tot cellulaire structuur wordt waargenomen als de SPES-concentratie verandert van 20 naar 35 gew.%. Dit komt overeen met een verbetering in de mechanische eigenschappen. Adhesie van de coatinglaag aan

de PSf-drager wordt eveneens verbeterd door de SPES-concentratie van de coatingoplossing te verhogen. De composiet holle vezel heeft in het supported liquid membrane syteem een extreem lage koper-ionenflux en bij gasscheiding geen selectiviteit voor He/N_2, He/CO_2, en N_2/CO_2. Het membraan heeft een lage retentie voor anorganische zouten en een hoge retentie voor geladen organische kleurstoffen. Het concept van co-extrusie met een ionen-uitwisselende functionaliteit in de coatinglaag kan mogelijkerwijs zowel toegepast worden als nanofiltratie membraan en als dicht hydrofiel ultrafiltratie membraan.

Hoofdstuk 5 bediscussieerd de bereiding van met SPEEK gecoate PSf en PP holle vezel membranen met behulp van dipcoating middels een systematische selectie van geschikte oplosmiddelen. Een verhoging van de oplosbaarheid van SPEEK in methanol wordt gevonden bij toenemende sulfoneringstijd en daarmee toenemende ionen-uitwisselingscapaciteit. Een integrale coatinglaag kan bereid worden door de concentratie van de coatingoplossing en de hoeveelheid coatingstappen te controleren. Deze holle vezels met een hydrofiele coatinglaag op een hydrofobe drager hebben een licht verhoogde stabiliteit. Ze zijn echter nog steeds instabiel door het directe contact tussen de organische en de waterige fase. Een eerste onderzoek naar ‘encapsulated’ composiet membranen met SPEEK lagen toont dat dit een mogelijke oplossing is, hoewel verder onderzoek noodzakelijk is.

In hoofdstuk 6 wordt een membraan-contactorsysteem voor kopertransport beschreven, waarbij gebruik wordt gemaakt van de nieuwe composiet holle vezel membranen die beschreven zijn in hoofdstuk 5. Stabiliteits- en permeatieresultaten laten zien dat lange duur toepassing op kleinere schaal mogelijk is. Er is op basis van de initiële SLM permeabiliteit een weerstandsmodel ontwikkeld om de koperflux van de membraancontactor af te schatten. Gebaseerd op dragermembranen van PSf en PP komt het model goed overeen met de experimentele resultaten van membraancontactoren. Volgens het model valt er een verbetering van de flux te verwachten als een membraancontactorsysteem gebruikt wordt dat bestaat uit twee dunne ion-uitwisselende holle vezels.

De potentiële mogelijkheid van composiet holle vezel membranen is verder onderzocht in drukgedreven processen, zoals bijvoorbeeld nanofiltratie. In hoofdstuk 7 zijn de met SPEEK gecoate polyethersulfon of polysulfon membranen gekarakteriseerd middels retentiemetingen van dextranmengsels, zouten en kleurstoffen. Vanwege de negatieve lading in de coatinglaag vertonen de membranen een afnemende retentie in de volgorde Na_2SO_4 >NaCl > $MgCl_2$. Daarnaast bedraagt de retentie 97 tot 100% voor negatief geladen organische kleurstoffen met een molecuulgewicht rond 450 $g.mol^{-1}$. De retentie kan verbeterd worden door verhoging van de dikte van de coatinglaag, de polymeerconcentratie in de coatingoplossing en de poriegrootte van de dragermembranen. De penetratie van SPEEK in de drager leidt tot een membraan met een hoge retentie als gevolg van een toename in de dichtheid van de gefixeerde lading. Deze toename in de ladingsdichtheid wordt veroorzaakt door een afname van de zwelling van SPEEK. Het Donnan-model

voor sterische poriën komt goed overeen met de experimentele waardes en is zeer geschikt voor het beschrijven van het transport van onze membranen.

In hoofdstuk 8 is een theoretisch model ontwikkeld voor de beschrijving van de isotrope en anisotrope beperkingen met betrekking tot zwelling van een polymeernetwerk. Het model kwantificeerd de anisotrope zwelling van het netwerk onder invloed van externe beperkingen. Uitzettingsratio's in radiale en longitudinale richtingen zijn sterk afhankelijk van de E-modulus van de externe matrix en de polymeer-oplosmiddel interactieparameter. Als voorbeeld kan genoemd worden de substantiële toename in de dichtheid van de gefixeerde lading die waargenomen wordt bij verhoging van de E-modulus van een externe matrix, wat leidt tot een solide theoretische basis voor de hypothese van hoofdstuk 7.

Resume

Tao He, born in Meishan, October 20, 1971

09/1990-06/1994	Bachelor of Engineering at Chengdu University of Science and Technology, Chengdu, P.R. China Production of potassium sulfate from potassium chloride and sodium sulfate Supervisors: Dr. C.F. Jiang and Prof. Y.G. Shu
09/1994-06/1995	Course study at Graduate School of Chinese Academy of Sciences, Beijing, P.R. China
07/1995-06/1997	Master of Science in Chemical Engineering at Dalian Institute of Chemical Physics, Dalian, P.R.China Preparation of polyethersulfone microfiltration membranes with organic nonsolvent additives Supervisor: Prof. C.Z. Jiang
09/1997-09/2001	Ph.D. in Chemical Engineering at University of Twente, Enschede, The Netherlands Supervisors: Prof.dr.ing. M.Wessling, Prof.dr.ing. H. Strathmann and Prof.dr.ing. M.H.V. Mulder